water

*Review*

# Review of Experimental Investigations of Dam-Break Flows over Fixed Bottom

**Francesca Aureli [1], Andrea Maranzoni [1,*], Gabriella Petaccia [2] and Sandra Soares-Frazão [3]**

[1] Department of Engineering and Architecture, University of Parma, 43124 Parma, Italy
[2] Department of Civil Engineering and Architecture, University of Pavia, 27100 Pavia, Italy
[3] Institute of Mechanics, Materials and Civil Engineering, Université Catholique de Louvain, 1348 Louvain-la-Neuve, Belgium
* Correspondence: andrea.maranzoni@unipr.it

**Abstract:** Laboratory experiments of dam-break flows are extensively used in investigations of geophysical flows involving flood waves, to provide insight into relevant aspects of the physics of the process and collect experimental data for validating numerical models. A dam-break flow is a typical example of a highly unsteady free surface flow with high reproducibility. Indeed, dam-break experiments can be repeated several times under the same test conditions obtaining large amounts of different types of data (possibly using various measuring techniques) that can be combined in a single rich dataset. Moreover, laboratory tests on dam-break flows are widely considered a valuable benchmark for the validation of numerical models, since field data from historical events are scarce, sparse, and highly uncertain. However, no systematic review of laboratory investigations of dam-break flows and existing related datasets are available in the literature to provide a comprehensive overview of the test conditions considered, the measuring techniques used, and the experimental data collected. This review article aims to fill this gap, focusing on laboratory tests in schematic and idealized setups with a fixed, non-erodible bed. In particular, this review aims to help researchers and modelers to: (a) select the most appropriate laboratory tests for validating their numerical models; (b) facilitate access to databases by indicating relevant bibliographic references; (c) identify specific challenging aspects worthy of further experimental research; and (d) support the development of new or improved technologies for the mitigation of the impact of dam-break flood waves. The references reviewed are organized into tables according to the purposes of the laboratory investigation, and comprehensive information is provided on test conditions, datasets, and data accessibility. Finally, suggestions for future experimental research on dam-break flows are provided.

**Keywords:** dam-break flow; experimental tests; datasets; validation of numerical models; review



**Citation:** Aureli, F.; Maranzoni, A.; Petaccia, G.; Soares-Frazão, S. Review of Experimental Investigations of Dam-Break Flows over Fixed Bottom. *Water* **2023**, *15*, 1229. https://doi.org/10.3390/w15061229

Academic Editor: Giuseppe Pezzinga

Received: 19 February 2023
Revised: 12 March 2023
Accepted: 14 March 2023
Published: 21 March 2023



## 1. Introduction

The technique of suddenly removing a gate placed between a reservoir storing a mass of water initially at rest and a downstream area is extensively used to generate unsteady free surface flows in experimental investigations of a variety of geophysical phenomena involving flood waves, such as dam-break floods and tsunamis. Despite active research (both theoretical and numerical) in this field in the last decades, physical modelling remains a widely used approach to provide insight into the features of the flow and collect valuable data for validating numerical models.

A dam-break flow is a typical (albeit extreme) example of an unsteady and rapidly varying flow. It is characterized by rapid and abrupt flow depth and velocity changes and by the presence of wetting and drying fronts. Hence, a dam-break flow is usually considered a stringent and probative validation test for numerical models. Indeed, it can be assumed that a numerical model able to cope with dam-break flows will also be able to simulate accurately less severe, slower floods.

Physical modelling in laboratory conditions on schematic, idealized geometries allows "for assessment within a controlled environment, enabling the isolation of individual processes and close study of their effect on the modelled system. The complexities of modelled systems are reduced to what is practical and feasible to model in a physical scale environment" [1]. Dam-break flow experiments are then relatively 'easy' to perform on the laboratory scale, since a small quiescent water volume must be released without the need to set up complex recirculation systems and regulation devices. In addition, dam-break flows are highly reproducible in controlled laboratory conditions, which allows experimental runs to be repeated several times under the same test conditions to collect a large amount of data of different types and merge them to form a complete database. This ease of implementation has fostered the investigation of various scenarios and situations characterized by different geometries and the presence of singularities and obstacles of various shapes. Therefore, even though laboratory setups do not reproduce, in general, the complexity of real situations in which various singularities and complex flow features simultaneously occur, conducting multiple idealized experiments focusing on specific singular features allows for an in-depth investigation of possible realistic flow conditions.

The physical quantities relevant to describe the process can be acquired with high accuracy in the laboratory via advanced and sophisticated measuring techniques. In particular, the advances in measuring techniques in the last two decades, especially the non-intrusive ones, have considerably enlarged the types of data that can be collected, and have improved their accuracy (e.g., [2–4]). Conversely, recovering reliable and accurate validation data from historical documents on real dam-breaks is unlikely because such catastrophic events are, fortunately, rare and seldom well documented [5]. Moreover, laboratory dam-break tests on scale physical models with real topography (which sometimes combine the real topography with an idealized situation [6]), are sporadic [5,7,8] although recent examples can be found in the literature [9].

Due to the advantages previously mentioned, a large number of laboratory tests on dam-break flows were performed in the past, and high-quality datasets are now available to the scientific community. However, a systematic review of laboratory investigations of dam-break flows, which provides a comprehensive overview of the test conditions, measuring techniques and available datasets, is missing in the literature. Only fragmentary or partial information is reported in some documents (e.g., [10–12]). Therefore, this review attempts to fill this gap, focusing on experiments conducted in schematic, idealized laboratory setups with a fixed, non-erodible bottom. It covers a period from the beginning of the 1900s (when the noteworthy early experiments on dam-break waves were performed) until the end of 2022. In particular, this review aims at helping researchers and dam-break modelers: (a) to select the most appropriate laboratory test cases for validating their numerical models; (b) to facilitate access to datasets and reference material through the indication of relevant bibliographic references; (c) to identify specific aspects regarding dam-break flows worthy of further insight and future research; and (d) to support the development of improved technologies to mitigate the impact of dam-break flood waves.

This review is limited to investigations with flood waves or bores generated by a typical dam-break mechanism, characterized by the total removal of a gate, and releasing the liquid mass stored behind. Investigations using different wave generation mechanisms (based on piston- or pumping-type wave makers, vertical release systems, and underflow gates) have not been considered. Furthermore, experiments on dam-break flows over an erodible bed with sediment transport, gravity currents, granular flows, and debris flows are not considered here in order not to overextend the scope of the review. Each of these topics would deserve a specific review (e.g., [3]) due to the relevance of the related applications and the amount of experimental research carried out.

## 2. State of the Art Experimental Investigations of Dam-Break Flows

Typical setups for dam-break flow studies are illustrated in Figure 1. Figure 1a shows an experimental facility for the simulation of a total dam-break, consisting of a rectangular flume equipped with a sluice gate, which can be suddenly removed to release a mass of quiescent water behind it. In the beautiful historical photo taken during Dressler's experiments in the 1950s [13], the wall of water released by the gate removal can be appreciated. The side walls of the flume are typically transparent to allow direct observation of the phenomenon and the use of image processing techniques. Figure 1b shows a typical laboratory setup for the study of partial dam-break phenomena. It consists of a tank in which a portion acting as a reservoir is separated from a floodable area through a partition wall, in which a sluice gate is located. In the case shown in the picture, the bottom of the tank (made of opalescent material) is backlit in order to apply a colorimetric technique based on light absorption to measure the free surface [14].

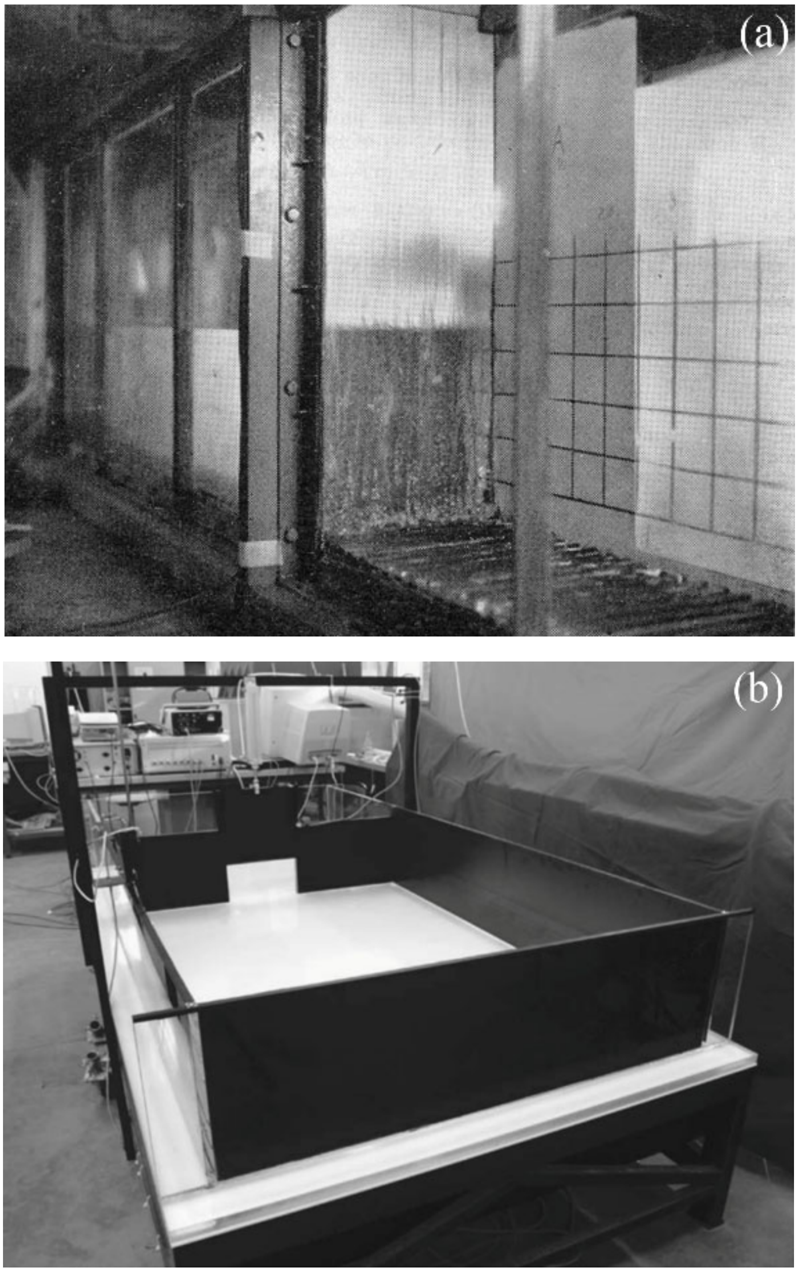


**Figure 1.** Pictures of typical experimental facilities for dam-break flow investigations. (**a**) Total dam-break in a rectangular channel (reprinted with permission from Ref. [13]; courtesy of International Association of Hydrological Sciences). (**b**) Prismatic tank for partial dam-break experiments (reprinted with permission from Ref. [14]).

References retrieved in the literature review are classified according to the objectives of the experimental investigation and organized into different tables.

Table 1 reports basic investigations of the physical characteristics of dam-break flows in straight (typically rectangular) channels or spreading on a plane. Such investigations mainly aim to explore the fundamental aspects and features of dam-break wave generation and propagation. Most reported cases concern smooth horizontal channels, but some studies also consider sloping channels or rough beds. Figure 1 shows typical laboratory setups for the study of total and partial dam-break flows.

Table 2 includes laboratory investigations of dam-break waves through geometric singularities (channel constrictions, bottom sills, curves or bends, etc.) to examine the effect of geometric elements and transition structures on the flow.

Table 3 lists experimental investigations of the dam-break wave impact against isolated obstacles, such as walls or vertical columns of various shapes. The disturbance induced on the flow by the presence of the obstacle is mainly analyzed in such experiments. Sometimes, the wave impact dynamics and the hydrodynamic load on the structure are also investigated.

Table 4 shows laboratory investigations of dam-break floods in idealized urban areas aiming to offer insights and an advanced understanding of urban flooding resulting from a dam-break event. In this field, the problem can be considered an extension of that presented in Table 3, since multiple obstacles are placed in the floodable area to reproduce a structured urban layout where more complex flow processes occur.

Table 5 reports experimental investigations concerning the propagation of tsunami bores (generated by a gate removal) in the swash zone. Such studies typically analyze the run-up over an adverse slope or the effect of coastal protective structures. Although a tsunami bore cannot strictly be considered a dam-break wave, these two wave types have many affinities, so tsunami bores are sometimes generated in the laboratory through the sudden removal of a gate. This review includes only investigations which use this technique to simulate a tsunami bore.

Table 6 lists experimental investigations of green water events in ships or offshore structures. In naval and maritime engineering, a 'green water' event is related to the presence of water on the deck of a ship or platform due to high waves exceeding the freeboard. Only the studies in which the wave overtopping onto the deck is produced by the sudden removal of a gate are considered in this review.

Table 7 includes experimental investigations and databases of dam-break waves of non-Newtonian liquids. Such phenomena are commonly observed in nature as well as in many industrial processes.

Table 8 shows laboratory investigations of dam-breaks in cascade reservoirs formed by multiple dams placed in sequence along a channel. In this case, a dam-break flood hazard assessment should consider that the collapse of the upstream dam could cause a flood wave involving the downstream dams, potentially inducing their overtopping or failure in a domino effect. Cascade reservoirs ensure flood hazard mitigation depending on their filling level and mutual distance.

Table 9 reports experimental investigations of dike-break-induced flows on a lateral floodplain. The break of a lateral structure produces significantly different effects compared to the collapse of a frontal one. Indeed, the flooding resulting from a dike-break is asymmetric, characterized by a long-term evolution, and is strongly influenced by the flow conditions in the main channel.

Finally, Table 10 contains details of experimental studies on the catastrophic failure of storage tanks with consequent potential overtopping of secondary containment systems (such as dikes or bunds). Such an application is of considerable interest in the industry when cylindrical tanks are used to store hazardous liquids whose sudden release could cause catastrophic effects.

Studies investigating multiple topics of those previously mentioned and potentially falling into many categories appear in all relevant tables for clarity.

Each table consists of 11 columns, which contain the information described below.

Column 1 provides the references in which the experimental investigations are presented and described.

Column 2 indicates the test conditions and the main characteristics of the dam-break flows investigated. In particular, this column specifies whether the dam-break is total or partial and whether the downstream channel is initially dry or wet. Moreover, it reports the types and dimensions of the singularities or obstacles interacting with the dam-break wave.

Column 3 describes the geometric configurations of the laboratory facilities and provides their main dimensions and roughness conditions.

Column 4 indicates the initial conditions of the experimental tests, namely the water depth behind the dam and the downstream water depth in wet bed conditions.

Column 5 reports the breach width, which can be different from the channel width in the event of a partial dam-break.

Columns 6 and 7 indicate the laboratory and the year in which the experiments were performed, respectively.

Column 8 gives the physical quantities measured, and Column 9 lists the measurement techniques and devices used.

Column 10 indicates whether experimental databases are freely available and downloadable in digital format.

Finally, Column 11 informs whether the experimental data were used to validate the dam-break numerical models in the original reference. In particular, this column specifies the types of numerical models used (among the many existing dam-break and flooding models reported, e.g., in [15–18]) and the value of the roughness coefficient set in the numerical simulations, if available. The knowledge of the roughness values proposed in the related references facilitates modelers, who can thus avoid laborious calibrations of this model parameter. In drafting Column 11, we have neglected the use of the data to develop and validate theoretical approaches or analytical solutions. Moreover, we have not investigated the subsequent use that other modelers may have made of the various databases in subsequent numerical studies.

**Table 1.** Basic experimental investigations of fundamental dam-break wave physical characteristics.

| (1) Reference | (2) Dam-Break Type | (3) Setup Characteristics [1] | (4) Initial Conditions [2] | (5) Breach Width | (6) Laboratory | (7) Year | (8) Measured Data | (9) Measuring Technique [3] | (10) Data [4] | (11) Numerical Simulation [5] |
|---|---|---|---|---|---|---|---|---|---|---|
| Schoklitsch [19] | Total;<br>dry bottom | Rectangular channel<br>Exp. (a) $L$ = 26 m, $W$ = 0.6 m<br>Exp. (b) $L$ = 150 m, $W$ = 1.3 m<br>$Lr$ > 8 m, $S$ = 0; smooth | (a) $h_u$ < 0.25 m<br>(b) $h_u$ < 1 m | (a) 0.6 m<br>(b) 1.3 m | Technischen Hochschule,<br>Graz, Austria | 1917 | Wave profiles; depth at the dam section as a function of $h_u$ | Metal plates covered with washable colored stripes quickly dipped and lifted | ✗ | |
| Trifonov [20,21] | Total;<br>dry bottom | Rectangular channel<br>$L$ = 30 m, $W$ = 0.4 m<br>$Lr$ = N.A., $S$ = 0.004; smooth | $h_u$ = 0.3, 0.4 m | 0.4 m | Research Institute of Hydraulic Engineering,<br>Leningrad, Russia | 1933 | Wave profiles | N.A. | ✗ | |
| Eguiazaroff [22] | Total<br>(partial opening of the gate with different velocities) | Rectangular channel<br>$L$ = 30 m, $W$ = N.A.<br>$Lr$ = N.A., $S$ = 0;<br>smooth and rough | $h_u$ = 0.3 m | N.A. | Hydro-electric Laboratory,<br>Leningrad, Russia | 1935 | Negative wave:<br>free surface profiles at selected times;<br>flow depth time series at six locations<br>Positive wave:<br>wave front celerity; free surface profiles at selected times | Electric chronograph;<br>floating flow level recorder | ✗ | ($\gamma$ = 0.056 m$^{1/2}$,<br>$\gamma$ = 0.4 m$^{1/2}$) |
| Levin [7] | Total;<br>dry and wet bottom | Rectangular, triangular, and trapezoidal channels<br>$L$ = N.A., $W$ = N.A.<br>$Lr$ = N.A., $S$ = 0;<br>smooth and rough | $h_d/h_u$ = 0–0.75 | N.A. | Belgrade<br>Polytechnic, Serbia | 1952 | Flow depth at the dam site and at some representative sections of the wave profile | N.A. | ✗ | 1D<br>SWE<br>(graphical method)<br>($n$ = 0.007 s m$^{-1/3}$,<br>$n$ = 0.026 s m$^{-1/3}$) |
| Martin and Moyce [23] | Collapse of a liquid column;<br>dry bottom | Tank<br>$L$ > 3 $Lr$, $W$ = 0.057 m,<br>$Lr$ = 0.057 m, $S$ = 0; smooth | $h_u$ = 0.114, 0.057 m | 0.057 m | N.A. | 1952 | Wave front position; stage hydrographs | Video camera<br>(300 fps) | ✗ | |
| Dressler [13] | Total;<br>dry bottom | Rectangular channel<br>$L$ = 65 m, $W$ = 0.225 m<br>$Lr$ = N.A., $S$ = 0; rough<br>(3 roughness values) | $h_u$ = 0.22, 0.11, 0.055 m | 0.225 m | US Bureau<br>Standard, USA | 1954 | Front positions,<br>water depth profiles | Video cameras<br>(1800 fps) | ✗ | – |
| WES [24] | Total;<br>dry bottom | Rectangular channel<br>$L$ = 121.92 m, $W$ = 1.22 m<br>$Lr$ = 60.96 m, $S$ = 0.005; smooth | $h_u$ = 0.3048 m | 0.07–1.22 m | Vicksburg,<br>Mississippi, USA | 1960 | Stage and discharge hydrographs | Video cameras<br>(16 mm movies,<br>8–12 fps) | ✗ | ($n$ = 0.009 s ft$^{-1/3}$) |
| WES [25] | Total;<br>dry bottom | Rectangular channel<br>$L$ = 121.92 m, $W$ = 1.22 m<br>$Lr$ = 60.96 m, $S$ = 0.005; rough | $h_u$ = 0.09, 0.18, 0.30 m | 0.18–1.22 m | Vicksburg,<br>Mississippi, USA | 1961 | Stage and discharge hydrographs | Video cameras<br>(16 mm movies,<br>8–12 fps) | ✗ | (0.04 < $n$ < 0.12 s ft$^{-1/3}$) |
| Faure and Nahas [26] | Total;<br>dry bottom | Rectangular channel<br>$L$ = 40.6 m, $W$ = 0.25 m<br>$Lr$ = 20.3 m, $S$ = 1.2·10$^{-4}$; rough | $h_u$ = 0.23 m | 0.25 m | Laboratoire National d'Hydraulique de Chatou, France | 1961 | Water depth time series;<br>front propagation | Video cameras | ✗ | 1D<br>SWE<br>MOC<br>($n$ = 0.016 s m$^{-1/3}$,<br>$n$ = 0.036 s m$^{-1/3}$) |
| Estrade [27] | Total;<br>dry bottom | Rectangular channel<br>$L$ = N.A., $W$ = 0.25, 0.5 m<br>$Lr$ = N.A., $S$ = 0; smooth | $h_u$ = 0.2–0.3 m | 0.25, 0.5 m | N.A. | 1967 | Wave profiles<br>at different times | N.A. | ✗ | |
| Nakagawa et al. [28] | Total;<br>dry and wet bottom | Rectangular channel<br>$L$ = 30 m, $W$ = 0.5 m<br>$Lr$ = 5 m, $S$ = 0; smooth | $h_u$ = 0.15–0.4 m<br>$h_d$ = 0–0.35 m | 0.5 m | Kyoto University, Japan | 1969 | Wave profiles;<br>flow depth hydrographs at three positions; flow velocity at two locations; wave celerity;<br>bore height | Video cameras<br>(8–64 fps);<br>pressure gauges | ✗ | |
| Chervet and Dallèves [29] | Total;<br>dry bottom | Rectangular channel<br>$L$ = 35 m, $W$ = 0.3 m<br>$Lr$ = 5, 7.5, 15 m, $S$ = −1, 4, 10%; rough | $h_u$ = 0.3 m | 0.3 m | Laboratory of Hydraulics, Hydrology and Glaciology,<br>Zurich, Switzerland | 1970 | Water depth and discharge hydrographs;<br>front position<br>and velocity | Video cameras | ✗ | 1D<br>SWE<br>MOC<br>($n$ = 0.0077–0.0167 s m$^{-1/3}$) |
| Cunge [30],<br>Cavaillé [31] | Total;<br>dry and wet bottom | Rectangular channel<br>$L$ = 40 m, $W$ = 0.25 m<br>$Lr$ = 20 m, $S$ = 0; rough | $h_u$ = 0.23 m<br>$h_d$ = 0, 0.005, 0.01, 0.04 m | 0.25 m | National Laboratory of Hydraulics,<br>Chatou, France | 1970 | Water depth hydrographs;<br>propagation path and discontinuity height | N.A. | ✗ | 1D<br>SWE<br>FD<br>($n$ = 0.01 s m$^{-1/3}$,<br>$n$ = 0.0125 s m$^{-1/3}$) |

**Table 1.** *Cont.*

| (1) Reference | (2) Dam-Break Type | (3) Setup Characteristics [1] | (4) Initial Conditions [2] | (5) Breach Width | (6) Laboratory | (7) Year | (8) Measured Data | (9) Measuring Technique [3] | (10) Data [4] | (11) Numerical Simulation [5] |
|---|---|---|---|---|---|---|---|---|---|---|
| Maxworthy [32] | Total; wet bottom; reflection against the closed end wall; interaction between solitary waves | Rectangular channel $L$ = 5 m, $W$ = 0.2 m, $Lr$ = N.A., $S$ = 0; smooth; | $h_d$ = 0.045–0.067 m solitary waves with height of 0.31–0.5 $h_d$ | 0.2 m | University of Southern California, Los Angeles, USA | 1976 | Wave motion; maximum wave amplitude; qualitative wave profiles at selected times | Video camera (64 fps) | ✗ | |
| Xanthopoulos and Koutitas [33] | Total; dry bottom | Rectangular channel $L$ = 6 m, $W$ = 0.25 m $Lr$ = 1.2 m, $S$ = 0; rough | $h_u$ = 0.02–0.15 m | 0.25 m | Aristoteles University, Thessaloniki, Greece | 1976 | Water depth and discharge hydrographs; front propagation | Video cameras | ✗ | 2D SWE FD ($n$ = 0.033 s m$^{-1/3}$) |
| Barr and Das [34] | Total; dry bottom; reflections against the end wall | Rectangular channel (a) $L$ = 33.5 m, $W$ = 1.5 m, $Lr$ = 7.62 m, $S$ = 0; (b) $L$ = 4.4 m, $W$ = 0.38 m $Lr$ = 1.0 m, $S$ = 0; smooth and rough | (a) $h_u$ = 0.3048 m (b) $h_u$ = 0.1676–0.3048 m | (a) 1.5 m (b) 0.38 m | University of Strathclyde, Glasgow, UK | 1980 | Water depth hydrographs; water surface profiles; front trajectories | Video cameras | ✗ | 1D SWE FD ($\varepsilon$ = 0.0134–0.0387 m) |
| Barr and Das [35] | Total; wet bottom; reflections against the end wall | Rectangular channel $L$ = 33.5 m, $W$ = 1.5 m $Lr$ = 7.62 m, $S$ = 0; rough | $h_u$ = 0.3048 m $h_d$ = 0.0762 m | 1.5 m | University of Strathclyde, Glasgow, UK | 1981 | Water depth hydrographs; water surface profiles; front trajectories | Video cameras | ✗ | 1D SWE FD ($\varepsilon$ = 0.0134 m, $\varepsilon$ = 0. 0387 m) |
| Memos et al. [36] | Total; dry bottom | Tank $L$ = 2.5 m, $W$ =1.5 m Plane $W$ = –, $S$ = 0; rough | $h_u$ = 0.03–0.105 m | 0.05 m | National Technical University of Athens, Greece | 1983 | Front propagation, velocity of the front along the $x$ axis, flow profile near the dam | Video camera (18 fps) | ✗ | ($n$ = 0.01 s m$^{-1/3}$) |
| Townson and Al-Salihi [37] | Total; dry and wet bottom | Rectangular channel $L$ = 4 m, $W$ = 0.1 m, $Lr \approx$ 1.9 m, $S$ = 0; smooth | $h_u$ = 0.10 m $h_d/h_u$ = 0.176 | 0.1 m | University of Strathclyde, Glasgow, UK | 1989 | Water depth hydrographs; water surface profiles at selected times | Video camera; resistance wave probes; pressure transducers | ✗ | 1D SWE (radial) MOC |
| Menendez and Navarro [38] | Total; dry bottom (different gate removal times) | Rectangular channel $L$ = 30 m, $W$ = 0.31 m, $Lr \approx$ 15 m, $S$ = 0; smooth | $h_u$ = 0.38 m (max) | 0.31 m | University of Buenos Aires, Argentina | 1990 | Flow images; discharge and flow depth hydrographs at the gate site | Wire gages; video cameras | ✗ | |
| Iverson et al. [39] Logan et al. [40] | Total; dry bottom (steep bottom slope) | Rectangular channel $L$ = 95 m, $W$ = 2 m, $Lr$ = 12 m, $S$ = 0.6; smooth and rough | Water volume: 6 m$^3$ | 2 m | H.J. Andrews Experimental Forest, Oregon, USA | 1992–2017 | Flow depth time series at three locations; bottom pressure, bottom normal and shear loads at selected locations; propagation of the front wave | Ultrasonic distance meters; pressure and force transducers; video cameras | ✓ (videos) | |
| Antunes Do Carmo et al. [41] | Total; wet bottom | Rectangular channel $L$ = 7.5 m, $W$ = 0.3 m, $Lr$ = 3.85 m, $S$ = 0; smooth | $h_u$ = 0.099 m $h_d/h_u$ = 0.587, 0.515 | 0.3 m | University of Coimbra, Portugal | 1993 | Water depth hydrographs at four positions | Water depth gauges | ✗ | 2D SGN FD |
| Tingsanchali and Rattanapitikon [42] | Partial; dry bottom | Downstream plane $L$ = 4 m, $W$ = 1.9 m, $Lr$ = 2.8 m (Reservoir, $W$ = 1.7 m; bottom step at the plane inlet: 0.4 m) $S$ = 0 and 1/200; smooth | $h_u$ = 0.1, 0.2, 0.25 m | 0.1 m | Asian Institute of Technology, Bangkok, Thailand | 1993 | Wave front propagation; water depth hydrographs at selected positions | Video camera; water depth gauges; mini-current meter | ✗ | 2D SWE FD ($n$ = 0.001–0.03 s m$^{-1/3}$) |
| Braschi et al. [43] | Partial; dry and wet bottom | Tank $L$ = 1.4 m, $W$ = 0.5 m, $Lr$ = 0.4 m, $S$ = 0; smooth | $h_u$ = 0.14 m $h_d$ = 0, 0.005 m | 0.05 m | University of Pavia, Italy | 1994 | Contour maps of water depth at different times | Video camera (25 fps) | ✗ | 2D SWE MOC-based ($n$ = 0.01 s m$^{-1/3}$) |
| Manciola et al. [44] | Total; wet and dry bottom; open and closed downstream end (three different gate opening velocities) | Rectangular channel $L$ = 9 m, $W$ = 0.49 m, $Lr$ = 3.366, 5.876 m, $S$ = 0; smooth | $h_u$ =0.2, 0.22, 0.3, 0.35 m $h_d$ = 0, 0.021 m | 0.49 m | University of Pavia, Italy | 1994 | Discharge hydrograph at the gate section; front celerity hydrographs; water depth time series at the gate section; wave front propagation | Video cameras (25 fps) | ✗ | 1D SWE FD ($n$ = 0.015 s m$^{-1/3}$) |
| Aguirre-Pe et al. [45] | Total; dry bottom; highly viscous fluid | Rectangular channel $L$ = 7 m, $W$ = 1 m, $Lr = h_u/\sin\vartheta$, $S$ = 0.03, 0.05, 0.07, 0.1, 0.15; smooth | $h_u$ =0.05, 0.08, 0.1 m | 1 m | University of Los Andes, Mérida, Venezuela | 1995 | Wave front propagation; wave profile at selected times; flow depth time series at selected locations | Video camera (30 fps) | ✗ | 1D SWE FD |
| Fraccarollo and Toro [46] | Partial; dry bottom | Plane $L$ = 3 m, $W$ = 2 m, $Lr$ = 1 m, $S$ = 0 and 7%; smooth | $h_u$ = 0.6 m (0.64 m) | 0.4 m | University of Trento, Italy | 1995 | Bottom pressure time series at 14 points; water depth time series at nine points; time series of flow velocity components at 14 locations | Pressure transducers; capacitance wave meters; electromagnetic velocity meters | ✗ | 2D SWE FV ($n$ = 0) |

**Table 1.** *Cont.*

| (1) Reference | (2) Dam-Break Type | (3) Setup Characteristics [1] | (4) Initial Conditions [2] | (5) Breach Width | (6) Laboratory | (7) Year | (8) Measured Data | (9) Measuring Technique [3] | (10) Data [4] | (11) Numerical Simulation [5] |
|---|---|---|---|---|---|---|---|---|---|---|
| Jovanović and Djordjević [47] | Total; dry bottom | Rectangular channel $L$ = 4.5 m, $W$ = 015 m, $Lr$ = 2.25 m, $S$ = 0.1%; smooth | $h_u$ = 0.3 m | 0.15 m | University of Belgrade, Yugoslavia | 1995 | Water depth hydrographs, water depth profiles | Water depth capacity probes and video camera | ✗ | 2D SWE FD ($n$ = 0.009 s m$^{-1/3}$) |
| Jovanović and Djordjević [47] | Partial; dry bottom | Downstream plane $L$ = 1 m, $W$ = 0.8 m, $Lr$ = 1 m (Reservoir, $W$ = 1 m), $S$ = 0; smooth | $h_u$ = 0.15 m | 0.1 m | University of Belgrade, Yugoslavia | 1995 | Water depth hydrographs, water depth profiles | Water depth capacity probes and video camera | ✗ | 2D SWE FD ($n$ = 0.01 s m$^{-1/3}$) |
| Koshizuka and Oka [48]; Koshizuka et al. [49] | Total, dry bottom; impact on a vertical wall | Rectangular channel $L$ = 0.584 m, $W$ = N.A., $Lr$ = 0.146 m, $S$ = 0; smooth | $h_u$ = 0.292 m | N.A. | University of Tokyo, Japan | 1996 | Water depth profiles, wave front evolution | Video camera (50 fps) | ✗ | 2D NSE MPS |
| Lauber and Hager [50] | Total; dry bottom | Rectangular channel $L$ = 14 m, $W$ = 0.5 m, $Lr$ = 3.5 m $S$ = 0; smooth | $h_u$ = 0.3 m | 0.5 m | ETH Zurich, Switzerland | 1998 | Free surface profiles, velocity and discharge profiles, wave front position | Video camera (50 fps) | ✗ | ($\varepsilon$ = 5 × 10$^{-6}$ m) |
| Lauber and Hager [51] | Total; dry bottom | Rectangular channel $L$ = 14 m, $W$ = 0.5 m, $Lr$ = 3.5 m $S$ = 0.1, 0.5; smooth | $h_u$ = 0.3 m | 0.5 m | ETH Zurich, Switzerland | 1998 | Surface profiles velocity distribution at fixed positions; discharge hydrographs | Video camera (50 fps) | ✗ | ($\varepsilon$ = 5 × 10$^{-6}$ m) |
| Stansby et al. [52] | Total; dry and wet bottom | Rectangular channel $L$ = 15.24 m, $W$ = 0.4 m, $Lr$ = 9.6 m, $S$ = 0; smooth | $h_u$ = 0.1, 0.36 m $h_d$ = 0, 0.01$h_u$, 0.45$h_u$ | 0.4 m | University of Manchester, UK | 1998 | Water elevation profiles | Laser, video camera (25 fps) | ✗ | |
| Blaser and Hager [53] | Total; dry bottom | Rectangular channel $L$ = 14 m, $W$ = 0.5 m, $Lr$ = N.A. $S$ = 0–0.5; rough | $h_u$ = 0.2–0.6 m | 0.5 m | ETH Zurich, Switzerland | 1999 | Wave front velocity and location | N.A. | ✗ | ($\varepsilon$ = 2.5 × 10$^{-3}$ m) |
| Nsom et al. [54] | Total; dry bottom; Newtonian solution (glucose syrup-water) | Rectangular channel $L$ = 5 m, $W$ = 0.3 m, $Lr$ = $h_u$ / $S$, $S$ = 3–12°; smooth | $h_u$ = 0.055 m | 0.3 m | Université de Savoie, Cedex, France | 2000 | Flow depth time series at a selected section; front wave propagation | Video camera (1000 fps); ultrasonic distance meters | ✗ | |
| Gallati and Braschi [55] | Total; dry and wet bottom | Tank $L$ = 1.2 m, $W$ = 0.05 m, $Lr$ = 0.3 m; rough | $h_u$ = 0.1 m $h_d$ = 0–0.02 m | 0.05 m | University of Pavia, Italy | 2000 | Water elevation profiles | Video camera (24 fps) | ✗ | 2D EUL SPH |
| Liem et al. [56] | Total; dry bottom | Rectangular channel $L$ = 14 m, $W$ = 0.5 m, $Lr$ = 5 m, $S$ = 0; smooth | $h_u$ = 0.3, 0.35, 0.4, 0.45 m | 0.5 m | Aachen University of Technology, Germany | 2001 | Front position and velocity | Video camera (4500 fps) | ✗ | 1D SWE FE, FV |
| Briechle and Köngeter [57] | Total; dry and wet bottom; inflow in the reservoir | Rectangular channel $L$ = 12.2 m, $W$ = 0.5 m, $Lr$ = 2.65 m, $S$ = 0.002; smooth | $h_u$ = 0.3, 0.35, 0.4, 0.45 m; steady inflow: 0, 40, 80, 120 l s$^{-1}$ | 0.5 m | Aachen University of Technology, Germany | 2002 | Water depth hydrographs in six sections; front position and velocity | Video camera (4500 fps) | ✗ | |
| Soares-Frazão and Zech [58] | Total; wet bottom (undular bore) | Tank: $L$ = 10 m, $W$ > 1 m Channel: $L$ = 26.15 m, $W$ = 1 m $S$ = 0; smooth | Different values of $h_u$–$h_d$ | 1.0 m | Université Catholique de Louvain, Belgium | 2002 | Water depth hydrographs at six positions | Water level gauges | ✗ | 1D BOU Hybrid FV–FD ($n$ = 0) |
| Shige-eda and Akiyama [59] | Partial (asymmetric); dry bottom | Tank $L$ = 4.8 m, $Wr$ = 2.98 m $Lr$ = 1.93 m, $S$ = 0; smooth | $h_u$ = 0.4 m | 0.5 m | Kyushu Institute of Technology, Kitakyushu, Japan | 2003 | Wave front position, flow depths and surface velocity hydrographs at six points | Digital video tape recorder; PTV | ✗ | 2D SWE FV ($n$ < 0.07 s m$^{-1/3}$) |
| Stelling and Duinmeijer [60]; Duinmeijer [61] | Partial; dry and wet bottom | Tank $L$ = 31 m, $W$ = 7.56 m, $Lr$ = 2.4 m, $S$ = 0; smooth | $h_u$ = 0.6 m $h_d$ = 0, 0.03–0.05 m | 0.4 m | Delft University of Technology, The Netherlands | 2003 | Water depth hydrographs; front position and velocity | Water depth resistance probes; video camera (30 fps) | ✗ | 2D SWE FD ($n$ = 0.012 s m$^{-1/3}$) |
| Chegini et al. [62] | Total; dry bottom | Rectangular channel $L$ = 15.24 m, $W$ = 0.4 m, $Lr$ = 9.76 m, $S$ = 0; smooth | $h_u$ = 0.1 m $h_d$ = 0.1–0.55 $h_u$ | 0.4 m | University of Manchester, UK | 2004 | Flow field and velocity | Particle tracking and streak velocimetry | ✗ | |
| Gallati and Sturla [63] | Partial; dry bottom | Tank $L$ = 1.4 m, $W$ = 0.5 m, $Lr$ = 0.4 m, $S$ = 0; smooth | $h_u$ = 0.08 m | 0.155 m | University of Pavia, Italy | 2004 | Images of the flow field in the flood plain at different time steps | Video camera (25 fps) | ✗ | 2D SWE SPH ($n$ = 0.01 s m$^{-1/3}$) |
| Jánosi et al. [64] | Total; dry and wet bottom | Tank $L$ = 9.93 m, $W$ = 0.15 m, $Lr$ = 0.38 m, $S$ = 0; smooth | $h_u$ = 0.11–0.25 m $h_d$ = 0, 0.018, 0.038 m | 0.15 m | Eötvös University, Budapest, Hungary | 2004 | Water surface profiles; front position and velocity | Video cameras | ✗ | |

**Table 1.** *Cont.*

| (1) Reference | (2) Dam-Break Type | (3) Setup Characteristics [1] | (4) Initial Conditions [2] | (5) Breach Width | (6) Laboratory | (7) Year | (8) Measured Data | (9) Measuring Technique [3] | (10) Data [4] | (11) Numerical Simulation [5] |
|---|---|---|---|---|---|---|---|---|---|---|
| Bukreev and Gusev [65] | Total; dry and wet bottom | Rectangular channel $L >> 1.3$ m, $W = 0.2$ m, $Lr >> 0.3$ m, $S = 0$; rough | $h_u = 0.205$ m $h_d = 0.0, 0.02$ m | 0.2 m | Russian Academy of Sciences, Novosibirsk, Russia | 2005 | Water level profiles | Wavemeters, video camera | ✗ | |
| Eaket et al. [66] | Partial; dry and wet bottom | Tank $L = 4.75$ m, $W = 2.31$ m, $Lr = 2.32$ m, $S = 0$; smooth | $h_u = 0.1, 0.2, 0.3$ m $h_d = 0.05, 0.1$ m | 0.89 m | University of Alberta, Edmonton AB, Canada | 2005 | Water surface profiles and velocities | Video stereoscopy, Video cameras (30 fps) | ✗ | |
| Piau and Debiane [67] | Total; dry bottom; highly viscous Newtonian solution (12, 85, 130 Pa s) | Rectangular channel $L = 5$ m, $W = 0.3$ m, $Lr = 2, 4, 6, 8h_u$, $S = 0$; smooth | $h_u = 0.054, 0.055$ m | 0.3 m | Université Joseph Fourier, Grenoble, France | 2005 | Wave front position with time; flow depth profiles at selected times | Video cameras (25, 1000 fps); ultrasonic distance meters | ✗ | |
| Barnes and Baldock [68] | Total; dry bottom | Rectangular channel $L = 4.0$ m, $W = 0.4$ m, $Lr = 2.25$ m, $S = 0$; rough | $h_u = 0.2$ m | 0.4 m | University of Queensland, Brisbane, Australia | 2006 | Shear stress; free surface elevation; velocity | Shear plate, ADV, acoustic displacement sensors | ✗ | ($\varepsilon = 0.1 \times 10^{-3}$ m) |
| Bateman et al. [69] | Total; dry bottom; end platform | Channel: $L = 9.0$ m, $W = 0.4$ m, $Lr = 2.0$ m, $S = 27°$; rough; Platform: 4 m × 2.4 m | $h_u = 0.5$ m | 0.4 m | Technical University of Catalonia, Barcelona, Spain | 2006 | Water surface profiles | Video cameras (30, 1000 fps) | ✗ | |
| Cruchaga et al. [70] | Total; dry bottom; impact on a vertical wall (two different fluids: shampoo and water) | Tank $L = 0.42$ m, $W = 0.228$ m, $Lr = 0.114$ m, $S = 0$; smooth | $h_u = 1Lr, 2Lr$ | 0.228 m | University of Santiago, Chile | 2007 | Water depth time series at selected sections; wave front position | Video cameras | ✗ | 2D NSE, ETILT FE |
| Maranzoni et al. [71] | Total; dry bottom; horizontal and sloping channel | Tank $L = 11$ m, $W = 0.18$ m, $Lr = 0.114$ m, $S = 0, 6\%$; smooth | $h_u = 0.1$ m | 0.18 m | University of Brescia, Italy | 2007 | Water surface profiles; Water depth hydrographs | Video camera (25 fps) | ✗ | 1D SWE FV; 2D EUL, VOF FV |
| Aureli et al. [14,72] | Partial; dry and wet bottom | Tank $L = 2.6$ m, $W = 1.2$ m, $Lr = 0.8$ m, $S = 0$; smooth | $h_u = 0.15$ m $h_d = 0.01$ m | 0.3 m | University of Parma, Italy | 2008 | Water surface at 10 times; water depth time series at a gauge point | Video camera (3 fps); ultrasonic distance meters | ✓ | 2D SWE FV ($n = 0.007$ s m$^{-1/3}$) |
| Mohamed [73] | Total; dry and wet bottom | Rectangular channel $L = 12.2$ m, $W = 1.22$ m, $Lr = 3.60$ m, $S = 0$; concrete bottom and glass side walls, smooth | $h_u = 0.3, 0.45, 0.6$ m $h_d = 0, 0.025, 0.05$ m | 1.22 m | University of Hawaii at Manoa | 2008 | Water surface profiles in time, bore height, shape and speed | Video camera (30 fps) | ✗ | |
| Ancey et al. [74] | Total; dry bottom; highly viscous Newtonian fluid (glucose solution) | Rectangular channel $L = 4$ m, $W = 0.3$ m $S = 0, 6, 12, 18, 24°$; smooth | Mass in the reservoir: 50.8–57.6 kg | 0.3 m | EPFL, Lausanne, Switzerland | 2009 | Free surface (imaging technique) and flow depth profiles at selected times; front position with time | Video camera | ✗ | |
| Yang et al. [75] | Partial; wet bottom | Rectangular channel $L = 28$ m, $W = 1.6$ m, $Lr = 10$ m, $S = 0$; concrete bottom and glass side walls; smooth | $h_u = 0.4$ m $h_d = 0.12$ m | 0.2 m | Tsinghua University, Beijing, China | 2010 | Water depth hydrographs; velocity fields at fixed times | Pressure probes, PIV, video cameras | ✗ | 3D RANS, VOF FV |
| Ozmen-Cagatay and Kocaman [76,77] | Total; dry and wet bottom | Rectangular channel $L = 9$ m, $W = 0.3$ m, $Lr = 4.65$ m, $S = 0$; smooth; | $h_u = 0.25$ m $h_d = 0, 0.025, 0.1$ m | 0.3 m | Cukurova University, Adana, Turkey | 2010 | Water depth profiles at different time steps | Video camera (50 fps) | ✗ | 2D RANS, VOF FV; 2D SWE FV |
| Duarte et al. [78]; Boillat et al. [79]; Ribeiro et al. [80] | Total; silted-up reservoir; dry bottom; multiphase flow | Rectangular channel $L = 5.5$ m, $W = 0.42$ m, $Lr = 1.5$ m, $S = 0$; smooth (2 mean grain size diameters) | $h_u = 0.4, 0.41, 0.42$ m (sediment depth: 0.22–0.39 m) | 0.42 m | EPFL, Lausanne, Switzerland | 2011 | Video images; water and sediment surface profiles at selected times; sediment deposition; water front propagation; maximum wave depth profile | Video camera (15 fps) | ✗ | |
| Marra et al. [81] | Total; dry bottom | Rectangular channel $L = 3$ m, $W = 0.1$ m, $S = 1.5–24°$; smooth and rough | Water volume in the reservoir = 3, 4, 5, 6, 7, 8 l | 0.1 m | EPFL, Lausanne, Switzerland | 2011 | Wave front position and velocity; water surface profiles at selected times; water depth hydrographs at two positions | Video camera (500–800 fps) | ✗ | (two rough bottoms: $n = 0.0133$ s m$^{-1/3}$, $n = 0.0153$ s m$^{-1/3}$) |

**Table 1.** *Cont.*

| (1) Reference | (2) Dam-Break Type | (3) Setup Characteristics [1] | (4) Initial Conditions [2] | (5) Breach Width | (6) Laboratory | (7) Year | (8) Measured Data | (9) Measuring Technique [3] | (10) Data [4] | (11) Numerical Simulation [5] |
|---|---|---|---|---|---|---|---|---|---|---|
| Aleixo et al. [82–85] | Total; dry bottom; first stages (upward and downward moving gate) | Rectangular channel $L$ = 6 m, $W$ = 0.25 m, $Lr$ = 3 m, $S$ = 0; smooth | $h_u$ = 0.325, 0.4 m | 0.25 | Université Catholique de Louvain, Belgium | 2011 | Flow images; velocity field and components at selected sections | Video camera (100 fps); PIV | ✗ | |
| Feizi Khankandi et al. [86] | Total; four different reservoir geometries; dry and wet bottom | 1: $Lr$ = 0.89 m, $W$ = 2 m, 2: $Lr$ = 1.79 m, $W$ = 1.5 m, 3: $Lr$ = 1.5-2.5 m, $W$ = 0.51 m, 4: $Lr$ = 3.5 m, $W$ = 0.51 m, Channel: $L$ = 9.3 m, $W$ = 0.51 m, $S$ = 0; smooth | $h_u$ = 0.35, 0.4, 0.45 m $h_d$ =0, 0.08 m | 0.51m | Amirkabir University of Technology, Tehran, Iran | 2012 | Water depth, velocity and discharge hydrographs at different positions; water surface profile at different times | Ultrasonic distance meters; ADV, video camera (110 fps) | ✗ | ($n$ = 0.011 s m$^{-1/3}$) |
| Oertel and Bung [87] | Total; dry bottom | Rectangular channel $L$ = 22 m, $W$ = 0.3 m, $Lr$ = 13 m, $S$ = 0; smooth | $h_u$ = 0.1, 0.2, 0.3, 0.4 m | 0.3 m | Bergische Universität Wuppertal, Germany | 2012 | Water depth in seven measuring points; water depth profiles at selected times; velocity field at selected times | Ultrasonic distance meters; video camera (1000 fps); PIV | ✗ | 2D RANS, VOF FV ($\varepsilon$ = 0.0015 × 10$^{-3}$ m) |
| LaRocque et al. [88] | Total; dry bottom | Rectangular channel $L$ = 7.31 m, $W$ = 0.18 m, $Lr$ = 3.37 m, $S$ = 0.93%; smooth | $h_u$ = 0.25, 0.3, 0.35 m | 0.18 m | University of South Carolina, USA | 2013 | Water surface profiles at selected times; velocity vertical profiles at eight locations | Ultrasonic distance meters; ultrasonic Doppler velocity profilers | ✗ | 2D RANS, VOF FV ($\varepsilon$ = 0.01 × 10$^{-3}$ m) |
| Miani et al. [89] | Total; wet bottom | Rectangular channel $L$ = 10 m, $W$ = 0.5 m, $Lr$ = 1 m, $S$ = 0; smooth | $h_u$ = 0.4 m $h_d$ = 0.2, 0.3 m; $h_u$ = 0.4 m $h_d$ = 0.1, 0.2, 0.4 m | 0.5 m | Joint Research Centre, Ispra, Italy | 2013 | Water depth hydrographs at 10 locations | Ultrasonic distance meters | ✗ | 1D SWE FV |
| Hooshyaripor and Tahershamsi [90] | Total; dry bottom | Rectangular channel $L$ = 9.3 m, $W$ = 0.51 m, $Lr$ = 4.5 m, $S$ = 0; smooth | $h_u$ = 0.35 m | 0.51 m | Amirkabir University of Technology, Iran | 2015 | Water depth hydrographs at 11 points; velocity and discharge hydrographs at six locations | Ultrasonic distance meters, ADV | ✗ | 3D RANS, VOF FV ($n$ = 0.011 s m$^{-1/3}$) |
| Jiang and Baldock [91] | Total; dry bottom | Rectangular channel $L$ = 3 m, $W$ = 0.4 m, $Lr$ = 1.7 m, $S$ = 0; smooth | $h_u$ = 0.1, 0.15, 0.2 m | 0.4 m | University of Queensland, St. Lucia, Australia | 2015 | Flow depth and bottom shear stress time series | Acoustic displacement sensors; shear plate; PIV | ✗ | 2D SWE FV ($n$ = 0.01, 0.011, 0.019 s m$^{-1/3}$) |
| Jiang and Baldock [91] | Total; dry bottom (fixed sand false bed, two grain sizes $d_{50}$ = 0.22, 2.85 mm) | Rectangular channel $L$ = 3 m, $W$ = 0.4 m, $Lr$ = 1 m, $S$ = 0, 1/10; rough (fine and coarse) | $h_u$ = 0.08–0.22 m | 0.4 m | University of Queensland, St. Lucia, Australia | 2015 | Flow depth and bottom shear stress time series | Acoustic displacement sensors; shear plate; PIV | ✗ | 2D SWE FV ($n$ = 0.01, 0.011, 0.019 s m$^{-1/3}$) |
| McMullin [92] | Total; dry and wet bottom (two gate removal mechanisms) | Rectangular channel $L$ = 0.5 m, $W$ = 0.175 m, $Lr$ = 0.2 m, $S$ = 0; smooth | $h_u$ = 0.06–0.14 m $h_d$ = 0.005–0.02 m | 0.175 m | University of Nottingham, UK | 2015 | Wave front position in time; wave profiles at selected times; horizontal and vertical velocity at selected times and positions | Video cameras, PIV | ✗ | 2D NSE, VOF FD |
| Mrokowska et al. [93] | Total; wet bottom; closed downstream end | Rectangular channel $L$ = 60 m, $W$ = 0.6 m $Lr$ = 5 m, $S$ = 0.002; smooth; | $h_u$ = 0.31, 0.36 m $h_d$ = 0.04, 0.06, 0.08 m | 0.6 m | Polish Academy of Science, Warsaw, Poland | 2015 | Water depth hydrographs at seven locations; velocity fields | Water level sensors; video camera (520 fps); PIV | ✗ | |
| Aleixo et al. [94] | Total; silted-up reservoir (tailings dam-break); dry bottom; sudden enlargement | Plane $L$ = 7.66 m, $W$ = 3.66 m, $S$ = 0; smooth Reservoir $Lr$ = 3.24 m, $Wr$ = 0.5 m | $h_u$ = 0.4 m (sediment depth 0.2 m) | 0.5 m | National Sedimentation Laboratory, Oxford, Mississippi, USA | 2016 | Velocity fields | Video cameras (400 fps); PIV-PTV | ✗ | |
| Elkholy et al. [95] | Partial; dry bottom | Tank $L$ = 11 m, $W$ = 4.3 m, $Lr$ = 3 m, $S$ = 0; smooth | $h_u$ = 0.25, 0.5, 0.75 m | 0.4 m | University of South Carolina, USA | 2016 | Pressure head at the bottom in nine points; water surface elevations and surface velocity; velocity profile at the center of the gate section | Pressure sensors; PTV (video cameras, 60 fps); ultrasonic velocity profiler | ✗ | |
| Javadian et al. [96] | Total; dry bottom closed downstream end | Rectangular channel $L$ = 2 m, $W$ = 0.2 m, $Lr$ = 1 m, $S$ = 0; smooth; | $h_u$ = 0.11, 0.12, 0.13 m | 0.2 m | Sharif University of Technology, Tehran, Iran | 2016 | Water surface profiles at selected times; wavefront position in time | Video camera (24 fps) | ✗ | |

**Table 1.** *Cont.*

| (1) Reference | (2) Dam-Break Type | (3) Setup Characteristics [1] | (4) Initial Conditions [2] | (5) Breach Width | (6) Laboratory | (7) Year | (8) Measured Data | (9) Measuring Technique [3] | (10) Data [4] | (11) Numerical Simulation [5] |
|---|---|---|---|---|---|---|---|---|---|---|
| Hooshyaripor et al. [97] | Total; dry bottom | Rectangular channel $L$ = 9.3 m, $W$ = 0.51 m, $S$ = 0; smooth Reservoir: $Lr$ = 4.5 m, $W$ = 2.25 m (different side slopes and lengths) | $h_u$ = 0.35 m | 0.51 m | Amirkabir University of Technology, Tehran, Iran | 2017 | Water depth and flow velocity time series at selected locations | Ultrasonic distance meters; ADV | ✗ | |
| Liu and Liu [98,99] | Total; dry and wet bottom | Rectangular channel $L$ = 6.5 m, $W$ = 0.4 m, $Lr$ = 1.5 m, $S$ = 0; smooth | $h_u$ = 0.16–0.36 m $h_d$ = 0, 0.02, 0.04 m | 0.4 m | Zhejiang University, Hangzhou, China | 2017 | Water surface profiles at selected times; water depth time series; flow velocity time series | Video camera (150 fps); capacitive wave gauges; ADV | ✗ | |
| Cordero et al. [100] | Patial; dry bottom | Reservoir $Lr$ = 1 m; $W$ = 1 m Floodable area $L$ = 4 m, W, 3 m $S$ = 0, 12°; smooth | $h_u$ = 0.1, 0.15, 0.2 m | $2h_u$ (triang. 1H:1V slope) | Polytechnic University of Turin, Italy | 2018 | Water surface at selected times; water depth time series; water depth profiles | Video camera (100 fps) | ✗ | |
| Liu et al. [101] | Total; dry and wet bottom | Rectangular channel $L$ = 18 m, $W$ = 1 m, $Lr$ = 8.37 m, $S$ = 0; smooth | $h_u$ = 0.6 m $h_d$ = 0.06, 0.12, 0.18, 0.24 m | 1 m | Sichuan University, Chengdu, China | 2018 | Water surface and average flow velocity profiles at selected times; wave front celerities | Video cameras (48 fps) | ✗ | 1D SWE |
| Hamid et al. [102,103] | Total; dry bottom open and closed downstream end | Rectangular channel $L$ = 6.7 m, $W$ = 0.3048 m, $Lr$ = 2.13 m, $S$ = 0.002; smooth | $h_u$ = 0.762 m | 0.3048 m | University of Engineering and Technology, Peshawar, Pakistan | 2018 | Water depth and flood wave velocity time series at selected sections | Point gauges and velocity sensor | ✗ | 2D SWE FV |
| Stolle et al. [104]; von Häfen et al. [105] | Total; wet bottom; swing gate (opening time influence) | Rectangular channel $L$ = 30 m, $W$ = 1.5 m, $Lr$ = 21.55 m, $S$ = 0; rough | $h_u$ = 0.2, 0.3, 0.4, 0.5 m | 1.4 m | University of Ottawa, Canada | 2018 | Water depth time series at four locations; flow velocity at a selected location; wave front arrival time | Capacitance wave gauges; propeller velocity flowmeter; video cameras (70, 120 fps) | ✗ | ($\varepsilon$ = 0.001·$10^{-3}$ m, $\lambda$ = 0.014, 0.0293) |
| Liu et al. [106] | Total; wet bottom | Rectangular channel $L$ = 18 m, $W$ = 1 m, $Lr$ = 8.37 m $S$ = 0; smooth | $h_u$ = 0.4 m $h_d$ = 0.02, 0.04, 0.08, 0.12, 0.16 m | 1 m | Sichuan University, Chengdu, China | 2019 | Video images; water surface profiles at selected times; water depth time series at selected locations | Video cameras (48 fps) | ✗ | 2D RANS, VOF FV |
| Melis et al. [107] | Total; dry bottom; effect of vegetation (polymeric cylinders) | Rectangular channel $L$ = 11.6 m, $W$ = 0.5 m, $Lr$ = N.A., $S$ = 0, 1, 2, 3%; smooth, rough | $h_u$ = 0.15, 0.2, 0.25, 0.3 m | 0.5 m | Polytechnic University of Turin, Italy | 2019 | Water surface profiles | Video cameras (30 fps) | ✓ | 1D SWE FD ($n$ = 0.05 s $m^{-1/3}$) |
| Turhan et al. [108]; Turhan et al. [109] | Total; dry and wet bottom; closed downstream end; salt water | Rectangular channel $L$ = 1.216 m, $W$ = 0.2 m, $Lr$ = 0.3 m, $S$ = 0; smooth; | $h_u$ = 0.15 m $h_d/h_u$ = 0, 0.1, 0.2, 0.4 | 0.2 m | Adana Science and Technology University, Turkey | 2019 | Water surface profiles at selected times; water depth time series at four locations | Video camera (60 fps) | ✗ | 3D RANS, VOF SPH |
| Wang et al. [110] | Total; wet bottom | Rectangular channel (rectangular and triangular section) $L$ = 18 m, $W$ = 1 m, $Lr$ = 8.37 m, $S$ = 0; smooth | $h_u$ = 0.4, 0.6 m $h_d/h_u$ = 0.1, 0.2, 0.3, 0.4 | 1 m | Sichuan University, Chengdu, China | 2019 | Water surface profiles at selected times; water depth time series at selected locations | Video cameras (48 fps) | ✗ | |
| Wu et al. [111] | Total; wet bottom; closed downstream end | Rectangular channel $L$ = 16.38 m, $W$ = 0.4 m, $Lr$ = 5.47 m, $S$ = 0; smooth; | $h_u$ = 0.16, 0.28 m $h_d$ = 0.12 m | 0.4 m | Dalian University of Technology, China | 2019 | Water depth hydrographs at 12 locations; flow velocity time series at four locations | Wave gauges; ADV | ✗ | 2D BOU Hybrid FD–FV ($n$ = 0.01 s $m^{-1/3}$) |
| Liu et al. [112] | Total; dry and wet bottom | Rectangular channel $L$ = 18 m, $W$ = 1 m, $Lr$ = 8.37 m $S$ = 0, 0.003, 0.02; smooth | $h_u$ = 0.2 m $h_d$ = 0–0.18 m; $h_u$ = 0.4 m $h_d$ = 0–0.36 m | 1 m | Sichuan University, Chengdu, China | 2020 | Video images; water surface and mean velocity profiles; wave front celerity | Video cameras (48 fps) | ✗ | |
| Oertel and Süfke [113] | Total; dry bottom | Rectangular channel $L$ = 12.5 m, $W$ = 0.3 m, $Lr$ = 6.5 m $S$ = 0; smooth | $h_u$ = 0.2, 0.3, 0.4 m | 0.3 m | Technical University of Applied Sciences, Luebeck, Germany | 2020 | Water depth at three selected locations; flow velocity vertical profiles | Ultrasonic distance meters; video camera (732 fps); PIV and optical flow methods | ✗ | |
| Shugan et al. [114] | Total; dry and wet bottom; first stages | Rectangular channel $L$ = 25 m, $W$ = 0.3 m, $Lr$ = ~11 m, $S$ = 0; smooth | $h_u$ = 0.3, 0.4 m $h_d$ = 0, 0.03, 0.06, 0.09 m | 0.3 m | National Cheng Kung University, Taiwan | 2020 | Water depth time series at 12 locations; water surface profile at selected times; front wave celerity; velocity profiles | Capacitance wave gauges; video camera (30 fps); PIV (video camera, 1000 fps) | ✗ | |

**Table 1.** *Cont.*

| (1) Reference | (2) Dam-Break Type | (3) Setup Characteristics [1] | (4) Initial Conditions [2] | (5) Breach Width | (6) Laboratory | (7) Year | (8) Measured Data | (9) Measuring Technique [3] | (10) Data [4] | (11) Numerical Simulation [5] |
|---|---|---|---|---|---|---|---|---|---|---|
| Vosoughi et al. [115–117] | Total; silted-up reservoir dry and wet bottom; multiphase flow | Rectangular channel $L$ = 6 m, $W$ = 0.3 m, $Lr$ = 1.52 m $S$ = 0; smooth | $h_u$ = 0.3 m $h_d$ = 0.02, 0.04, 0.05 m (sediment depth: 0–0.24 m) | 0.3 m | University of Shiraz, Iran | 2020 | Video images; water surface profiles; water and sediment depth time series at 16 points | Video cameras (50 fps) | ✓ | 3D NSE, VOF NSE, TFM FV |
| Wang et al. [118] | Total; dry and wet bottom | Rectangular channel (triangular section) $L$ = 18 m, $W$ = 1 m, $Lr$ = 8.37 m, $S$ = 0; smooth | $h_u$ = 0.2, 0.4, 0.6 m $h_d/h_u$ = 0–0.9 | 1 m | Sichuan University, Chengdu, China | 2020 | Water surface profiles at selected times; water depth time series at selected locations; wave front celerity | Video cameras (48 fps) | ✗ | |
| Wang et al. [119] | Total; wet bottom | Rectangular channel $L$ = 18 m, $W$ = 1 m, $Lr$ = 8.37 m, $S$ = 0; smooth | $h_u$ = 0.2, 0.4, 0.6 m $h_d/h_u$ = 0.05–0.9 | 1 m | Sichuan University, Chengdu, China | 2020 | Water surface profiles at selected times; water level hydrographs at selected locations | Video cameras (48 fps) | ✗ | 2D RANS, VOF FV |
| Ahmadi and Yamamoto [120] | Partial (trapezoidal and triangular breach); dry bottom | Rectangular channel $L$ = 12 m, $W$ = 0.5 m, $Lr$ = 2.5 m, $S$ = 0; smooth | $h_u$ = 0.25, 0.3 m | 0.2,0.3 m | Tokai University, Kanagawa, Japan | 2021 | Water depth hydrograph at a point located 50 cm upstream of the gate | Video camera | ✗ | |
| Ansari et al. [121] | Total; dry and wet bottom | Rectangular channel $L$ = 3.7 m, $W$ = 0.6 m, $Lr$ = 0.6 m, $S$ = 0; smooth | $h_u$ = 0.15 m $h_d$ = 0, 0.015, 0.03, 0.058, 0.07 m | 0.6 m | University of Zanjan, Iran | 2021 | Water surface profiles | Video camera (60fps) | ✗ | 2D (Molecular dynamics software) SPH |
| Ansari et al. [121] | Total; dry bottom; interaction of two opposite dam-break waves | Rectangular channel $L$ = 3.7 m, $W$ = 0.6 m, $Lr$ = 0.6 m (2 opposite reservoirs at the channel ends), $S$ = 0; smooth | $h_{u1}$ = 0.2 m $h_{u2}$ = 0.2, 0.3 m | 0.6 m | University of Zanjan, Iran | 2021 | Water surface profiles | Video camera (60fps) | ✗ | 2D (Molecular dynamics software) SPH |
| Birnbaum et al. [122] | Total; dry bottom; three-phase Newtonian suspensions | Rectangular channel $L$ = 1.2 m, $W$ = 0.15 m, $Lr$ = 0.2 m ($W$ = 1m), $S$ = 0; smooth | $h_u$ = 0.04–0.13 m | 0.15 m | Columbia University, New York, USA | 2021 | Wave front position with time | Video cameras (1 fps; 30 fps) | ✓ | |
| Espartel and Manica [123] | Total; dry and wet bottom; first stages | Rectangular channel $L$ = 6.71 m, $W$ = 0.24 m, $Lr$ = 0.71 m, $S$ = 0; smooth | $h_u$ = 0.1, 0.2, 0.4 m $h_d$ = 0, 0.02, 0.04, 0.08 m | 0.24 m | Universidade Federal do Rio Grande do Sul, Porto Alegre, Brazil | 2021 | Water surface profiles at selected times | Video cameras (240 fps) | ✗ | |
| Kocaman et al. [124] | Partial; dry and wet bottom | Tank $L$ = 1 m, $W$ = 0.5 m, $Lr$ = 0.25 m, $S$ = 0; smooth | $h_u$ = 0.15 m $h_d$ = 0.015, 0.030 m | 0.1 m | Iskenderun Technical University, Turkey | 2021 | Water surface at selected times; water depth time series at five points | Video camera (50 fps); ultrasonic distance meters | ✗ | 3D RANS, VOF FV; 2D SWE FV |
| Nguyen-Thi et al. [125] | Total; dry and wet bottom; water and three high-viscous Newtonian fluids | Rectangular channel $L$ = 2 m, $W$ = 0.055 m, $Lr$ = 0.28 m, $S$ = 0; smooth | $h_u$ = 0.11 m $h_d$ = 0–0.066 m | 0.055 m | Université de Picardie Jules Verne, Amiens, France | 2021 | Water surface profiles | Video camera (203 fps) | ✗ | 3D RANS, VOF FV |
| Takagi and Furukawa [126] | Total; dry bottom; different gate opening velocities (0.2–2.5 m/s) | Rectangular channel $L$ = 3 m, $W$ = 0.38 m, $Lr$ = 0.5 m, $S$ = 0; smooth | $h_u$ = 0.5 m | 0.38 m | Tokyo Institute of Technology, Japan | 2021 | Bottom pressure time series at four points along the channel centerline; water surface profiles | Pressure sensors; video camera (2400 fps) | ✗ | |
| Wang et al. [127] | Total; dry bottom | Triangular channel $L$ = 18 m, $W$ = 1 m, $Lr$ = 8.37 m, $S$ = 0; smooth | $h_u$ = 0.2, 0.4, 0.6 m $h_d/h_u$ = 0–0.9 | 1 m | Sichuan University, Chengdu, China | 2021 | Water surface profiles; water level hydrographs, wave front celerity | Video cameras (48 fps) | ✗ | |
| Xu et al. [128] | Total; dry and wet bottom | Rectangular channel $L$ = 13 m, $W$ = 0.25m, $Lr$ = N.A., $S$ = 0.0031; rough | $h_u$ = 0.4 m $h_d$ = 0–0.098 m | 0.25 m | University of Queensland, Brisbane, Australia | 2021 | Shear stress; water depth hydrographs | Shear plate; acoustic distance sensors | ✗ | ($\varepsilon$ = 0.084 m) |
| Ozmen-Cagatay et al. [129] | Total; dry bottom; closed downstream end; three Newtonian fluids | Rectangular channel $L$ = 1.216 m, $W$ = 0.2 m, $Lr$ = 0.3 m, $S$ = 0; smooth | $h_u$ = 0.15 m | 0.2 m | Adana Science and Technology University, Turkey | 2022 | Water surface profiles, water depth hydrographs | Video camera (60 fps) | ✗ | 2D RANS, VOF FV |
| Yang et al. [130,131] | Total; dry and wet bottom | Rectangular channel $L$ = 10.72 m, $W$ = 1.485 m, $Lr$ = 4.58 m, $S$ = 0; smooth | $h_u$ = 0.13–0.483 m $h_d$ = 0.02, 0.04, 0.06, 0.08, 0.1, 0.12, 0.14 m | 1.485 m | Southwest Jiaotong University, Chengdu, China | 2022 | Water depth hydrographs; wave front celerity; flow velocity | Wave gauges; ADV | ✗ | 2D RANS, VOF FV |

**Table 1.** *Cont.*

| (1) Reference | (2) Dam-Break Type | (3) Setup Characteristics [1] | (4) Initial Conditions [2] | (5) Breach Width | (6) Laboratory | (7) Year | (8) Measured Data | (9) Measuring Technique [3] | (10) Data [4] | (11) Numerical Simulation [5] |
|---|---|---|---|---|---|---|---|---|---|---|
| Nielsen et al. [132] | Total; dry and wet bottom | Rectangular channel $L$ = 13 m, $W$ = 0.5 m, $Lr$ = 0.625 m, $S$ = 0; smooth and rough (4 different values) | $h_u$ = 0.4 m $h_d$ = 0.018 m | 0.5 m | University of Queensland, Brisbane, Australia | 2022 | Water depth and bottom shear stresses hydrographs; dam-break front celerity | Acoustic transducers; shear plates | ✗ | |
| Zhang et al. [133] | Total; dry and wet bottom | Triangular channel (side slope: 45°) $L$ = 18 m, $W$ = 1 m, $Lr$ = 8.37 m, $S$ = 0, 0.003, 0.01, 0.02; smooth | $h_u$ = 0.6 m; 0.4 m $h_d/h_u$ = 0, 0.1, 0.2, 0.4 | 1 m | Sichuan University, Chengdu, China | 2022 | Water surface profiles; water depth hydrographs | Video cameras (50 fps) | ✗ | |

Note(s): [1] $L$ = facility length; $W$ = facility width; $Lr$ = reservoir length; $Wr$ = reservoir width (if different from $W$); $S$ = bottom slope; [2] $h_u$ = upstream water depth; $h_d$ = downstream water depth; [3] ADV = acoustic Doppler velocimeter; PIV = particle image velocimetry; PTV = particle tracking velocimetry; [4] ✗ = not freely available; ✓ = freely available; [5] Approach: 1D = one-dimensional; 2D = two-dimensional; 3D = three-dimensional–Mathematical model: BOU = Boussinesq equations; ETILT = edge-tracked interface locator technique; EUL = Euler equations; NSE = Navier–Stokes equations; RANS = Reynolds-averaged Navier–Stokes equations; SGN = Serre–Green–Naghdi equations; SWE = shallow water equations; VOF = volume of fluid–Numerical method: FD = finite difference; FE = finite element; FV = finite volume; MOC = method of characteristics; MPS = moving particle semi-implicit; SPH = smoothed-particle hydrodynamics; TFM = two-fluid method–$n$ = Manning roughness coefficient; $\varepsilon$ = surface roughness; $\lambda$ = friction factor; $\gamma$ = Bazin roughness coefficient; N.A. = not available.

**Table 2.** Experimental investigations of dam-break waves through geometric singularities.

| (1) Reference | (2) Dam-Break Type | (3) Setup Characteristics [1] | (4) Initial Conditions [2] | (5) Breach Width | (6) Laboratory | (7) Year | (8) Measured Data | (9) Measuring Technique [3] | (10) Data [4] | (11) Numerical Simulation [5] |
|---|---|---|---|---|---|---|---|---|---|---|
| Chervet and Dallèves [29] | Total; wet bottom; adverse slope; converging-diverging walls | Rectangular channel $L$ = 23 m, $W$ = 0.3 m $Lr$ = 5, 7.5, 15 m, $S$ = −1, 4, 10% rough channel | $h_u$ = 0.3 m $h_d$ = 0.02 m | 0.3 m | Laboratory of Hydraulics, Hydrology and Glaciology, Zurich, Switzerland | 1970 | Water depth and discharge hydrographs; front position and velocity | Video cameras | ✗ | 1D SWE MOC ($n$ = 0.0077–0.0167 s m$^{-1/3}$) |
| Matsutomi [134] | Total; dry bottom; adverse slope | Tank with $L$ = 3.9 m, $W$ = 0.3 m, $Lr$ = 1.5 m, $S$ = −0.075, −0.15; rough | $h_u$ = 0.13 m | 0.3 m | University of Akita, Japan | 1983 | Wave front trajectories | N.A. | ✗ | 2D SWE FD (specific resistance law) |
| Martin [135] | Total; dry and wet bottom | Radial reservoir with variable radius $r$ and diverging walls ($\theta$ = 5.71–90°) | $h_u$ = 0.36 m | $r \times \theta$ variable | Dresden Technical University, Germany | 1983 | Discharge hydrograph at the dam position; water surface profile; water level hydrographs | Photographic film sheeting; oscillograph; photogrammetric plotting | ✗ | 1D SWE MOC |
| Michouev and Sladkevich [136] | Total; wet bottom; sudden enlargement at the dam | Rectangular channel $L$ = 8.8 m, $W$ = 1.6 m, $Lr$ = 4 m, $Wr$ = 0.4 m, $S$ = 0 | $h_u$ = N.A. $h_d$ = 0.1 $h_u$ | 0.4 m | State University of Moscow, Russia | 1983 | Water depth hydrographs at four locations; water depth profiles at three times | N.A. | ✗ | 2D SWE FD |
| Miller and Chaudhry [137] | Total; dry bottom; 180° curved channel | Rectangular channel $L$ = 11.4 m, $W$ = 0.3 m; $S$ = 0; smooth Reservoir $Lr$ = 1.6 m, $Wr$ = 3.65 m | $h_u$ = 0.1, 0.152, 0.2, 0.254, 0.3 m | 0.3 m | State University of Washington, USA | 1988 | Water depth hydrographs at three points in the channel and five points in the reservoir | Capacitance probes; video camera (60 fps) | ✗ | 1D SWE FD ($n$ = 0.014–0.018 s m$^{-1/3}$) |
| Townson and Al-Salihi [37] | Total; dry and wet bottom; converging diverging walls ($\theta$ = 5°) | Rectangular channel $L$ = 4 m, $W$ = 0.1 m, $Lr$ ~1.9 m, $S$ = 0; smooth | $h_u$ = 0.1 m $h_d/h_u$ = 0.176 | 0.1 m | University of Strathclyde, Glasgow, UK | 1989 | Water depth hydrographs; wave front position; water surface profiles | High speed tape recorder; resistance wave probes; pressure transducers | ✗ | 1D SWE (radial) MOC |
| Bell et al. [138] | Total; dry and wet bottom; 180° curved rectangular channel | Reservoir $Lr$ = 2.29 m, $Wr$ = 3.66 m Rectangular channel $W$ = 0.3 m, $S$ = 0; smooth and rough | $h_u$ = 0.15, 0.2, 0.25, 0.3, 0.35 m $h_d$ = 0, 0.013, 0.025, 0.051, 0.0761 m | 0.305 m | State University of Washington, USA | 1992 | Water depth hydrographs; wave front position | Capacitance probes; video camera (60 fps) | ✗ | ($n$ = 0.0165, 0.04 s m$^{-1/3}$) |
| Bellos et al. [139] | Total; dry and wet bottom; gradually variable channel width | Rectangular channel $L$ = 21.2 m, $W$ = 1.4 m, $Lr$ = 8.5 m, $S$ = 0–0.01; smooth | $h_u$ = 0.15–0.3 m $h_d$ = 0, 0.053, 0.101 m | 0.6 m | University of Thrace, Xanthi, Greece | 1992 | Water depth hydrographs; water surface profiles at 10 positions | Wave meters, pressure transducers | ✗ | 2D SWE FD ($n$ = 0.012 s m$^{-1/3}$) |

**Table 2.** *Cont.*

| (1) Reference | (2) Dam-Break Type | (3) Setup Characteristics [1] | (4) Initial Conditions [2] | (5) Breach Width | (6) Laboratory | (7) Year | (8) Measured Data | (9) Measuring Technique [3] | (10) Data [4] | (11) Numerical Simulation [5] |
|---|---|---|---|---|---|---|---|---|---|---|
| Četina and Rajar [140] | Total; dry bottom; sudden enlargement (4 m downstream of the dam) | Rectangular channel $L$ = 20 m, $W$ = 0.4 and 2.8 m, $Lr$ = 8 m, $Wr$ = 1.2 m, $S$ = 0.2%; smooth | $h_u$ = 0.25, 0.35, 0.45 m | 0.4 m | University of Skopje, North Macedonia | 1994 | Water depth time series in 31 points; longitudinal and cross-sectional water surface profiles; flow velocity time series at selected points | Capacitance wave gauges; velocity probes | ✗ | 2D SWE FD ($n$ = 0.0137 s m$^{-1/3}$) |
| Manciola et al. [44] | Total; wet and dry bottom; adverse slope (−0.084, −0.096, −0.15) (three different gate opening velocities) | Rectangular channel $L$ = 9 m, $W$ = 0.49 m, $Lr$ = 3.366, 5.876 m, $S$ = 0, smooth | $h_u$ =0.2, 0.22, 0.3, 0.35 m $h_d$ = 0, 0.021 m | 0.49 m | University of Pavia, Italy | 1994 | Discharge and water depth hydrographs at the gate section; front celerity hydrographs; wave front propagation | Video cameras (25 fps) | ✗ | 1D SWE FD ($n$ = 0.015 s m$^{-1/3}$) |
| Aureli et al. [141] | Total; dry and wet bottom; bumps | Rectangular channel $L$ = 7 m, $W$ = 1 m, $Lr$ = 2.25 m, $S$ = 0–0.033; smooth | $h_u$ = 0.292, 0.342, 0.35 m above the bump | 1 m | University of Parma, Italy | 1999 | Water depth and velocity hydrographs | Video camera (25 fps); ADV | ✗ | 1D SWE FD ($n$ = 0.01 s m$^{-1/3}$) |
| Soares-Frazão and Zech [142]; Soares-Frazão et al. [143] | Total; dry and wet bottom; 90° bend (step at the channel entrance $\delta$ = 0.33 m) | Tank $L$ = 2.39 m, $W$ = 2.44 m Channel with 90° bend $L$ = 7.335 m, $W$ = 0.495m $S$ = 0; smooth | $h_u$ = 0.2 m $h_d$ = 0, 0.01 m | 0.495 m | Université Catholique de Louvain, Belgium | 1999 | Water depth time series at six locations; wave front velocity | Water level probes | ✓ | 2D SWE LB (bottom: $n$ = 0.0095 s m$^{-1/3}$; side walls: $n$ = 0.0195 s m$^{-1/3}$) |
| Soares-Frazão and Zech [142]; Soares-Frazão et al. [143] | Total; dry bottom; 45° bend (step at the channel entrance $\delta$ = 0.33 m) | Tank $L$ = 2.39 m, $W$ = 2.44 m Channel with 90° bend $L$ = 8.2 m, $W$ = 0.495m $S$ = 0; smooth | $h_u$ = 0.25 m $h_d$ = 0, 0.01 m | 0.495 m | Université Catholique de Louvain, Belgium | 1999 | Water depth time series at nine locations; wave front velocity | Water level probes | ✓ | 2D SWE LB (bottom: $n$ = 0.0095 s m$^{-1/3}$; side walls: $n$ = 0.0195 s m$^{-1/3}$) |
| Aureli et al. [144,145] | Total; dry and wet bottom; adverse slope (−8, −9, −10%) | Rectangular channel with adverse slope $L$ = 7 m, $W$ = 1 m, $Lr$ = 2.25 m, $S$ = 0, 1, 2%, smooth and rough | $h_u$ = 0.21, 0.25, 0.292 m $h_d$ = 0, 0.045, 0.05 m | 1 m | University of Parma, Italy | 2000 | Water depth and velocity hydrographs | Video camera (25 fps); ADV | ✗ | 1D SWE FD ($n$ = 0.01, 0.025 s m$^{-1/3}$) |
| Bento Franco and Betâmio de Almeida [146]; Viseu et al. [147] | Total; wet bottom; sudden enlargement (6.45 m downstream of the dam) | Rectangular channel $L$ = 19.3 m, $W$ = 0.5 m, 2.3 m, $Lr$ = 6.1 m, $S$ = 0; smooth | $h_u$ = 0.504 m $h_d$ = 0.003 m | 0.5 m | Istituto Superior Técnico, Lisbon, Portugal | 2000 | Water depth hydrographs at six points | N.A. | ✓ | ($n$ = 0.009 s m$^{-1/3}$) |
| Hiver [148] | Total; dry bottom upstream of the sill, dry and wet bottom downstream; triangular bottom sill | Rectangular channel $L$ = 38 m, $W$ = 1 m, $Lr$ = 15.5 m, $S$ = 0; smooth and rough | $h_u$ = 0.75 m $h_d$ = 0, 0.15 m | 1 m | Laboratoire de Recherches Hydrauliques, Châtelet, Belgium | 2000 | Water depth hydrographs | Gauge measurements | ✓ | ($n$ = 0.0125 s m$^{-1/3}$) |
| Soares-Frazão et al. [149]; Soares-Frazão [150] | Total; closed downstream end dry bottom upstream of the sill, wet bottom downstream; triangular bottom sill (±0.14 slopes, 0.065 m high) | Rectangular channel $L$ = 5.6 m, $W$ = 0.5 m, $Lr$ = 2.39 m, $S$ = 0; smooth | $h_u$ = 0.111 m $h_d$ = 0, 0.02, 0.025 m | 0.5 m | Université Catholique de Louvain, Belgium | 2002 | Water surface profiles | Video cameras (25 and 40 fps) | ✓ | 1D SWE FV ($n$ = 0.011 s m$^{-1/3}$) |
| Soares-Frazão and Zech [151] | Total; dry bottom; 90° bend (step at the channel entrance $\delta$ = 0.33 m) | Tank $L$ = 2.39 m, $W$ = 2.44 m Channel with 90° bend $L$ = 7.335 m, $W$ = 0.495m $S$ = 0; smooth | $h_u$ = 0.25 m | 0.495 m | Université Catholique de Louvain, Belgium | 2002 | Water depth profiles; velocity field at the bend | Video camera (200 fps and 40 fps); PIV | ✗ | Hybrid 1D–2D SWE FV ($n$ = 0.011 s m$^{-1/3}$) |
| Bukreev [152] | Total; dry and wet bottom; bottom drop ($\delta$ = 0.051, 0.072 m) | Channel $L$ = 4.2 m, $W$ = 0.202 Reservoir $L$ = 3.3 m, $W$ = 1 m, $S$ = 0; smooth | $h_u$ = 0.075, 0.102, 0.12, 0.152, 0.154, 0.212 m $h_d$ = N.A. | 0.202 m | Russian Academy of Sciences, Novosibirsk | 2003 | Dimensionless height of water impingement on a vertical wall | Powder coating on end wall | ✗ | |
| Bukreev and Gusev [153] | Total; dry and wet bottom; bottom drop ($\delta$ = 0.072 m) | Channel $L$ = 4.2 m, $W$ = 0.202 m Reservoir $Lr$ = 3.3 m, $W$ = 1 m, $S$ = 0; smooth | $h_u$ = 0.125 m $h_d$ = 0.022, 0.032, 0.05, 0.056, 0.072, 0.1 m | 0.202 m | Russian Academy of Sciences, Novosibirsk | 2003 | Dimensional and dimensionless hydrographs of water depth for different reservoir and channel depths, water profiles at selected times | Wavemeters; video camera | ✗ | |

**Table 2.** *Cont.*

| (1) Reference | (2) Dam-Break Type | (3) Setup Characteristics [1] | (4) Initial Conditions [2] | (5) Breach Width | (6) Laboratory | (7) Year | (8) Measured Data | (9) Measuring Technique [3] | (10) Data [4] | (11) Numerical Simulation [5] |
|---|---|---|---|---|---|---|---|---|---|---|
| Soares-Frazão et al. [154] | Total; dry bottom; sudden enlargement | Rectangular channel $L$ = 7.6 m, $W$ = 0.12–0.496 m, $Lr$ = 4 m, $S$ = 0; rough | $h_u$ = 0.2 m | 0.12 m | Université Catholique de Louvain, Belgium | 2003 | Water depth time series at five locations; surface-velocity fields at selected times | Water level gauges; water-level follower; digital imaging | ✗ | 2D SWE FV ($n$ = 0.015 s m$^{-1/3}$) |
| Bukreev et al. [155] | Total; dry and wet bottom bottom step ($\delta$ = 0.06 m) | Channel $L$ = 7.07 m, $W$ = 0.202 m Reservoir $Lr$ = 3.3 m, $W$ = 1–0.202 m, $S$ = 0; smooth | $h_u$ = 0.01–0.22 m $h_d$ = 0, 0.01, 0.09 m | 0.202 m | Russian Academy of Sciences, Novosibirsk | 2004 | Water-level profiles, water depth hydrographs | Wave recorders; video camera | ✗ | |
| Bellos [156] | Total; dry and wet bottom; gradually variable channel width | Rectangular channel $L$ = 21.2 m, $W$ = 1.4 m, $Lr$ = 8.5 m, $S$ = −0.005, 0, 0.01; smooth | $h_u$ = 0.1–0.4 m $h_d$ = 0, < 0.02 m; $h_d$ = 0.0635 m for $S$ = −0.005 | 0.6 m | University of Thrace, Xanthi, Greece | 2004 | Water depth time series at ten positions | Pressure transducers | ✗ | 2D SWE FD |
| Natale et al. [157] | Total; dry bottom; sluice gates (gate 1: $x$ = 8.4 m, $a$ = 0.04 m; gate 2: $x$ = 9.3 m, $a$ = 0.02 m) | Rectangular channel $L$ = 9.3 m, $W$ = 0.48 m, $Lr$ = 3.36 m, $S$ = 0; rough | $h_u$ = 0.2 m | 0.48 m | University of Pavia, Italy | 2004 | Water depth profiles | Video camera (25 fps); | ✗ | 1D SWE FV ($n$ = 0.12 s m$^{-1/3}$) |
| Bukreev [158] | Total; dry and wet bottom; bottom step ($\delta$ = 0.038, 0.056 m; $l$ = 0.036, 0.257 m) | Rectangular channel $L$ = 7.2 m, $W$ = 0.2 m, $S$ = 0; smooth | $h_u$ = 0.066, 0.13, 0.15 m $h_d$ = 0.055 m | 0.2 m | Russian Academy of Sciences, Novosibirsk | 2005 | Water-level profiles | Piezometers; wave recorders; video camera | ✗ | |
| Bukreev [159] | Partial; dry and wet bottom; bottom step ($\delta$ = 0.055 m; $l$ = 0.69 m) | Tank and channel (closed end) $L$ = 7.2 m, $W$ = 0.202 m, $Lr$ = 1.32 m, $Wr$ = 1 m; $S$ = 0; smooth | $h_u$ = 0.145, 0.16 m $h_d$ = N.A. | 0.1 m | Russian Academy of Sciences, Novosibirsk | 2006 | Water-level profiles; depth hydrographs and longitudinal and vertical velocities at three cross sections | Video camera; PIV | ✗ | |
| Aureli et al. [14,72] | Partial; dry and wet bottom; bottom sill | Tank $L$ = 2.6 m, $W$ = 1.2 m, $Lr$ = 0.8 m, $S$ = 0; smooth | $h_u$ = 0.15 m $h_d$ = 0.01 m | 0.3 m | University of Parma, Italy | 2008 | Water surface profiles; water depth hydrographs | Video camera (3 fps); ultrasonic distance meters | ✓ | 2D SWE FV ($n$ = 0.007 s m$^{-1/3}$) |
| Gusev et al. [160] | Total; wet bottom; bottom step ($\delta$ = 0.05 m) | Rectangular channel $L$ = 7.06 m, $W$ = 0.202 m $Lr$ = 4.76 m, $Wr$ = 1.0 m, $S$ = 0; smooth | $h_u$ = 0.205 m $h_d$ = 0.01–0.205 m | 0.202 m | Russian Academy of Sciences, Novosibirsk | 2008 | Free-surface hydrographs at two points; velocity of the front behind the step; velocity of the front reflected by the step | Wavemeters | ✗ | |
| Bukreev et al. [161] | Partial (vertically); wet bottom; lateral constriction and bottom step ($b$ = 0.06 m, $l$ = 0.38 m, $\delta$ = 0.072 m) | Rectangular channel $L$ = 8.3 m, $W$ = 0.20 m, $Lr$ = N.A., $S$ = 0; smooth | $0.08(h_u-\delta) < h_d < 1.1(h_u-\delta)$ | 0.06 m | Russian Academy of Sciences, Novosibirsk | 2008 | Dimensionless bore depth and propagation speed | Wavemeters | ✗ | |
| Evangelista et al. [162,163] | Total; dry bottom; bottom step ($\delta$ = 0.05 m) | Rectangular channel $L$ = 9 m, $W$ = 0.4 m, $Lr$ = N.A., $S$ = 0; smooth | $h_u$ = 0.4 m | 0.4 m | University of Cassino and Southern Lazio, Italy | 2011 | Water surface profiles at two selected times | Video camera (30 fps) | ✗ | 1D SWE FV ($n$ = 0.0125 s m$^{-1/3}$) |
| Ozmen-Cagatay and Kocaman [164] | Total; dry bottom; trapezoidal bottom sill ($\delta$ = 0.075 m, $l$ = 1 m) | Rectangular channel $L$ = 8.9 m, $W$ = 0.3 m, $Lr$ = 4.65 m, $S$ = 0; smooth | $h_u$ = 0.25 m | 0.3 m | Cukurova University, Adana, Turkey | 2011 | Water surface profiles at selected times | Video cameras (50 fps) | ✗ | 2D RANS, VOF FV; 1D SWE FV |
| Ozmen-Cagatay and Kocaman [165] | Total; dry bottom; trapezoidal contraction (0.95 m long, contraction ratio: 1/3) | Rectangular channel $L$ = 8.9 m, $W$ = 0.3 m, $Lr$ = 4.65 m, $S$ = 0; smooth | $h_u$ = 0.25 m | 0.3 m | Cukurova University, Adana, Turkey | 2012 | Water surface profiles at selected times; water depth hydrographs at seven points | Video cameras (50 fps) | ✗ | 3D RANS, VOF FV |

**Table 2.** *Cont.*

| (1) Reference | (2) Dam-Break Type | (3) Setup Characteristics [1] | (4) Initial Conditions [2] | (5) Breach Width | (6) Laboratory | (7) Year | (8) Measured Data | (9) Measuring Technique [3] | (10) Data [4] | (11) Numerical Simulation [5] |
|---|---|---|---|---|---|---|---|---|---|---|
| Kocaman and Ozmen-Cagatay [166] | Total; dry bottom; triangular obstruction (0.95 m long, contraction ratio: 1/3) | Rectangular channel $L$ = 8.9 m, $W$ = 0.3 m, $Lr$ = 4.65 m, $S$ = 0; smooth | $h_u$ = 0.25 m | 0.3 m | Cukurova University, Adana, Turkey | 2012 | Water surface profiles at selected times; water depth hydrographs at six points | Video cameras (50 fps) | ✗ | 3D RANS, VOF FV |
| Ozmen-Cagatay et al. [167] | Total; dry bottom; triangular bump ($\delta$ = 0.075 m, $l$ = 1 m) | Rectangular channel $L$ = 8.9 m, $W$ = 0.3 m, $Lr$ = 4.65 m, $S$ = 0; smooth | $h_u$ = 0.25 m | 0.3 m | Cukurova University, Adana, Turkey | 2014 | Water surface profiles at selected times; water depth hydrographs at six points | Video cameras (50 fps) | ✗ | 2D RANS, VOF FV; 1D SWE FV |
| Degtyarev et al. [168] | Total; wet bottom; contraction at the dam location | Rectangular channel $L$ = 10 m, $W$ = 0.254 m Reservoir $Lr$ = 5 m, $Wr$ = 0.38 m, $S$ = 0; smooth | $h_u$ = 0.4 m $h_d$ = 0.04, 0.06, 0.08, 0.1, 0.12, 0.14, 0.16, 0.18, 0.2 m | 0.254 m | State University of Novosibirsk, Russia | 2014 | Water depth hydrographs at three points | Conductive wave meters | ✗ | 1D SWE ($n$ = 0) |
| Wood and Wang [169] | Total; dry bottom; 90° bend | Rectangular channel with 90° bend $L$ = 6.72m, $W$ = 0.273 m Reservoir $Lr$ = 0.89 m, $Wr$ = 0.89 m, $S$ = 0; smooth | $h_u$ = 0.2794 m | 0.29 m | University of Huston, Texas, USA | 2015 | Water depth hydrographs at four points | Resistance-type water level measurements | ✗ | 2D SWE FD ($n$ = 0.009 s $m^{-1/3}$) |
| Hooshyaripor and Tahershamsi [90] | Total; dry bottom; reservoir with sloping sides (side angle = 30°, 45°, 60°) | Rectangular channel $L$ = 9.3 m, $W$ = 0.51 m, $S$ = 0; smooth Reservoir $Lr$ = 4.5 m, $Wr$ = 2.25 m | $h_u$ = 0.35 m | 0.51 m | Amirkabir University of Technology, Iran | 2015 | Water depth hydrographs at 11 points; velocity and discharge hydrographs at six locations | Ultrasonic distance meters, ADV | ✗ | 3D RANS, VOF FV ($n$ = 0.011 s $m^{-1/3}$) |
| Kikkert et al. [170] | Total; dry bottom; sudden contraction at the gate site | Rectangular channel $L$ = 6.6 m, $W$ = 0.3 m, $S$ = 1/20; smooth Reservoir $Lr$ = 7.5 m, $Wr$ = 2 m, $S$ = 0 | $h_u$ = 0.35 m | 0.3 m | Hong Kong University of Science and Technology | 2015 | Water depth time series; water depth profiles and wave propagation time | Video cameras (90 fps) | ✗ | 3D RANS, VOF FV ($\varepsilon$ = 5 × $10^{-5}$ m) |
| Chen et al. [171] | Total; wet bottom; Y-shaped junction | Rectangular channels with junction (Y-shaped; 30°, 45°, 60°, 90°) Side channel (with dam): $L$ = 2.5 m, $W$ = 0.3 m, $Lr$ = 1 m Main channel: $L$ = 5 m, $W$ = 0.3 m $S$ = 0; smooth | $h_u$ = 0.3, 0.4, 0.45 m $h_d$ = N.A. | 0.3 m | Sichuan University, Chengdu, China; | 2019 | Water depth and pressure hydrographs; velocity field | Video cameras; PIV; pressure gauges | ✗ | 3D RANS, VOF FV ($n$ = 0.008 s $m^{-1/3}$) |
| Kobayashi et al. [172] | Total; wet bottom; meanders | Meandering rectangular channel $L$ = 16.1 m, $W$ = 0.8 m, $Lr$ = 1.5 m, $S$ = 1/600; smooth | $h_u$ = 0.285 m $h_d$ = 0.107, 0.147 m | 0.8 m | University of Hiroshima, Japan | 2019 | Flow depth transversal profiles in eight cross-sections | Wave gauges | ✗ | 1D SWE MOC |
| Kavand et al. [173] | Total; dry bottom; three 90° bends | Rectangular channel $W$ = 0.2 m, $S$ = 0; smooth and rough | $h_u$ = 0.25, 0.35, 0.45, 0.55 m | 0.2 m | University of Ahvaz, Iran | 2020 | Wave front celerity; wave height al the bend sides | Video camera | ✗ | ($\varepsilon$ = 0, 10, 16, 20 × $10^{-3}$ m) |
| Kocaman et al. [174] | Total; dry bottom; triangular and trapezoidal channel contractions | Rectangular channel $L$ = 8.9 m, $W$ = 0.3 m, $Lr$ = 4.65 m, $S$ = 0; smooth | $h_u$ = 0.25 m | 0.3 m | Cukurova University, Adana, Turkey | 2020 | Free surface profiles; flow depth hydrographs | Video cameras (50 fps) | ✗ | 3D RANS, VOF FV; 2D SWE FV |
| Ansari et al. [121] | Total; dry and wet bottom; triangular bottom sill | Rectangular channel $L$ = 3.7 m, $W$ = 0.6 m, $Lr$ = 0.6 m, $S$ = 0; smooth | $h_u$ = 0.2 m $h_d$ = 0, 0.07 m | 0.6 m | University of Zanjan, Iran | 2021 | Water surface profiles | Video camera (60 fps) | ✗ | 3D RANS SPH |
| Ismail et al. [175] | Total; wet bottom; Y-shaped junction | Rectangular channels with a Y-shaped junction Side channel (with dam): $L$ = 1.83 m, $W$ = 0.304 m, $Lr$ = 0.91 m, $S$ = 0; smooth Main channel: $L$ = 3.35 m, $W$ = 0.304 m | $h_u$ = 0.25, 0.4, 0.5 m $h_d$ = 0.0425, 0.044, 0.052 m (flow rate and velocity in the main channel: $Q$ = 1.87–2.64 l/s; $v$ = 0.145–0.181 m/s) | 0.304 m | University of South Carolina, Columbia, USA | 2021 | Outflow hydrographs downstream of the junction; water surface elevation at the outlet | Ultrasonic distance meters | ✗ | |

**Table 2.** *Cont.*

| (1) Reference | (2) Dam-Break Type | (3) Setup Characteristics [1] | (4) Initial Conditions [2] | (5) Breach Width | (6) Laboratory | (7) Year | (8) Measured Data | (9) Measuring Technique [3] | (10) Data [4] | (11) Numerical Simulation [5] |
|---|---|---|---|---|---|---|---|---|---|---|
| Gamero et al. [176] | Total; dry and wet bottom; closed downstream end; Gaussian bottom sill in the reservoir | Rectangular channel $L$ = 15 m, $W$ = 0.405 m, $Lr$ = 9.275 m, $S$ = 0.0015; smooth | $h_u$ = 0.302, 0.3 m $h_d$ = 0, 0.12, 0.18, 0.24 m | 0.405 m | University of Córdoba, Spain | 2022 | Piezometric measures along the centerline of the obstacle; water surface profiles | Piezometers; video cameras (25 fps) | ✓ | 2D VAM Hybrid FV–FD ($n$ = 0.01 s m$^{-1/3}$) |
| Kobayashi et al. [177] | Total; wet bottom; meanders | Straight rectangular channel $L$ = 16.1 m, $W$ = 0.4 m, $Lr$ = 1.68 m, $S$ = 0; smooth Meandering rectangular channel $L$ = 16.1 m, $W$ = 0.39 m, $Lr$ = 1.66 m, $S$ = 0; smooth | Straight $h_u$ = 0.3 m $h_d$ = 0.02 m Meandering $h_u$ = 0.285 m $h_d$ = 0.107 m | Straight 0.4 m Meand. 0.39 m | University of Hiroshima, Japan | 2022 | Wave height time series in eight cross-sections; free surface profiles at selected times | Wave gauges | ✗ | 2D SWE; 3D RANS, VOF FV |
| Vosoughi et al. [178,179] | Total; silted-up reservoir (multiphase flow); dry and wet bottom; semi-circular bottom sill ($\delta$ = 0.045 m, $l$ = 0.09 m; $\delta$ = 0.075 m, $l$ = 0.15 m) | Rectangular channel $L$ = 6 m, $W$ = 0.3 m, $Lr$ = 1.52 m, $S$ = 0; smooth | $h_u$ = 0.3 m (7 sediment depths: 0.03–0.24 m) $h_d$ = 0, 0.02, 0.04, 0.05 m | 0.3 m | University of Shiraz, Iran | 2022 | Water surface profiles; profile of the saturated sediment layer | Video cameras (50 fps) | ✓ | 3D NSE, VOF FV |

Note(s): [1] $L$ = facility length; $W$ = facility width; $Lr$ = reservoir length; $Wr$ = reservoir width (if different from $W$); $S$ = bottom slope; θ = inclination angle; δ = bottom step/bump height; $l$ = singularity length; $b$ = constriction width; [2] $h_u$ = upstream water depth; $h_d$ = downstream water depth; [3] ADV = acoustic Doppler velocimeter; PIV = particle image velocimetry; [4] ✗ = not freely available; ✓ = freely available; [5] Approach: 1D = one-dimensional; 2D = two-dimensional; 3D = three-dimensional–Mathematical model: NSE = Navier–Stokes equations; RANS = Reynolds-averaged Navier–Stokes equations; SWE = shallow water equations; VOF = volume of fluid–Numerical method: FD = finite difference; FV = finite volume; MOC = method of characteristics; SPH = smoothed particle hydrodynamics–$n$ = Manning roughness coefficient; ε = surface roughness; N.A. = not available.

**Table 3.** Experimental investigations of the dam-break wave impact against obstacles.

| (1) Reference | (2) Dam-Break Type | (3) Setup Characteristics [1] | (4) Initial Conditions [2] | (5) Breach Width | (6) Laboratory | (7) Year | (8) Measured Data | (9) Measuring Technique [3] | (10) Data [4] | (11) Numerical Simulation [5] |
|---|---|---|---|---|---|---|---|---|---|---|
| Greenspan and Young [180] | Total; dry bottom; impact on containment dykes (θ = 90°, 60°, 30°; variable dyke distance from the gate) | Tank $L$ = 1.22 m, $W$ = 0.23 m, $Lr$ = 0.23 m; $S$ = 0; smooth | $h_u \leq 0.2032$ m | 0.23 m | Massachusetts Institute of Technology, USA | 1978 | Spillage fraction dependence on dyke inclination | Video recording | ✗ | 1D SWE MOC |
| Sicard and Nicollet [181] | Total; wet bottom; impact on a vertical wall | Rectangular channel $L$ = 18 m, $W$ = 0.6 m, $Lr$ = 3 m; $S$ = 0; smooth | $h_u$ = N.A. $h_d$ = N.A. | 0.6 m | Laboratoire National d'Hydraulique, Chatou, France | 1983 | Water depth and celerity of the incoming wave; pressure time series on the wall at seven elevations | Piezoresistive pressure transducers | ✗ | |
| Ramsden [182] | Total; dry and wet bottom; impact on a vertical wall | Rectangular channel $L$ = 36.6 m, $W$ = 0.396 m, $Lr$ = 8.97 m; $S$ = 0; smooth | $h_u$ = 0.502 m $h_d$ = 0 m; $h_u$ = 0.4801 m $h_d$ = 0.28 m | 0.396 m | California Institute of Technology, USA | 1996 | Impact force; pressure at the wall; position of the wave; 2D profiles near the wall | Force and pressure transducers; contact probes; Argon-ion laser; video camera (300 fps) | ✗ | |
| Liu et al. [183] | Total; wet bottom; impact on a vertical porous structure (0.29 m long, 0.37 m high, located 0.02 m downstream of the gate; 2 porous materials) | Tank $L$ = 0.892 m, $W$ = 0.44 m, $Lr$ = 0.28 m; $S$ = 0; smooth | $h_u$ = 0.35, 0.25, 0.15 m $h_d$ = 0.02 m | 0.44 m | Cornell University, Ithaca, USA | 1999 | Water surface profiles at 12 times; water level time series in the center of the porous structure | Camera (10 fps); wave gauge | ✗ | 2D RANS, VOF FD |
| Gallati and Braschi [55] | Total; dry bottom; impact on obstacle (0.03 × 0.06 m, 0.17 m downstream of the dam) | Tank $L$ = 1.2 m, $W$ = 0.03 m, $Lr$ = 0.3 m, rough | $h_u$ = 0.1 m $h_d$ = 0 m | 0.03 m | University of Pavia, Italy | 2000 | Water surface profiles | Video camera (25 fps) | ✗ | 2D EUL SPH |

**Table 3.** *Cont.*

| (1) Reference | (2) Dam-Break Type | (3) Setup Characteristics [1] | (4) Initial Conditions [2] | (5) Breach Width | (6) Laboratory | (7) Year | (8) Measured Data | (9) Measuring Technique [3] | (10) Data [4] | (11) Numerical Simulation [5] |
|---|---|---|---|---|---|---|---|---|---|---|
| Barakhnin et al. [184] | Total; wet bottom; impact on a reflective vertical wall | Tank $L = l_1 + l_2$, $Lr = l_1$ $50 < l_2/h_d < 90$ $l_1$ = N.A. | $0.5 \leq (h_u - h_d)/h_d \leq 1.4$ $h_d$ = 0.03, 0.04 m | 0.06 m | Russian Academy of Sciences, Novosibirsk | 2001 | Maximum water level at the wall, splash-up profile, free surface profiles | Video camera (25 fps), resistive wavemeter | ✗ | 1D BOU |
| Soares-Frazão and Zech [185,186] | Partial; wet bottom; impact on an isolated building (0.4 × 0.8 m) | Rectangular channel $L$ = 36 m; $W$ = 3.6 m, $Lr$ = 6.9 m, $S$ = 0; smooth | $h_u$ = 0.4 m $h_d$ = 0.02 m | 1 m | Université Catholique de Louvain, Belgium | 2002 | Water depth hydrographs at six locations; velocity fields at selected times; flow velocity time series at the gauge points | Resistive level gauges; ADV; video camera (40 fps) | ✓ | ($n$ = 0.01 s m$^{-1/3}$) |
| Brufau et al. [187]; Méndez et al. [188] | Partial (asymmetrical); wet bottom; pyramidal obstacle | Tank $L$ = 2.65 m, $W$ = 2.615 m, $Lr$ = 1.3, $S$ = 0; smooth | $h_u$ = 0.5 m $h_d$ = 0.1–0.3 m | 0.293 m | University of La Coruña, Spain | 2002 | Water depth time series at several points | N.A. | ✗ | 2D SWE FV |
| Ciobataru et al. [189] | Total; dry bottom; impact on pillars (square: 0.12 m × 0.12 m; circular: $D$ = 0.14 m) | Tank $L$ = 16.62 m, $W$ = 0.61 m, $Lr$ = 5.9 m; $S$ = 0; smooth and rough | $h_u$ = 0.1–0.3 m | 0.61 m | University of Washington, Seattle, USA | 2003 | Net force on the structure and velocity hydrographs, free surface profile at mid-channel | Load cell; LDV; PIV | ✗ | 3D NSE ELMMC |
| Trivellato [190]; Bertolazzi and Trivellato [191] | Total, dry bottom; impact on a vertical wall | Rectangular channel $L$ = 6 m, $W$ = 0.5 m, $0 \leq S \leq 25°$ | $h_f$ = 0.04 m $u_0$ = 2.77 ms$^{-1}$ | 0.5 m | University of Trento, Italy | 2003 | Maximum run-up, pressure at the wall, toe velocity and depth, wall force | Pressure transducers; video camera (25 fps) | ✗ | 2D EUL FV |
| Campisano et al. [192] | Total; dry bottom; downstream sediment deposit (0.03 m volcanic sand thickness) | Rectangular channel $L$ = 3.9 m, $W$ = 0.15 m, $Lr$ = 1.3 m; $S$ = 0.145%; rough | $h_u$ = 0.10–0.13 m | 0.15 m | University of Catania, Italy | 2004 | Water depth hydrographs, sediment bed profiles | Video camera (25 fps) | ✗ | 1D SWE FD ($n$ = 0.0105 s m$^{-1/3}$) |
| Gallati and Sturla [63] | Partial; dry bottom; impact on a square obstacle | Tank $L$ = 1.4 m, $W$ = 0.5 m, $Lr$ = 0.4 m, $S$ = 0; smooth | $h_u$ = 0.08 m | 0.155 m | University of Pavia, Italy | 2004 | Images of the flow field in the flood plain at different time steps | Video camera (25 fps) | ✗ | 2D SWE SPH ($n$ = 0.01 s m$^{-1/3}$) |
| Hu and Kashiwagi [193] | Total; dry bottom; impact on a vertical wall | Tank $L$ = 1.18 m, $W$ = 0.12 m, $Lr$ = 0.68 m; $S$ = 0 | $h_u$ = 0.12 | 0.12 m | Kyushu University, Japan | 2004 | Pressure hydrograph at the wall | Pressure transducers; video camera | ✗ | 2D NSE CIP, FD |
| Raad and Bidoe [194] | Total; wet bottom; impact on vertical columns (square: 0.12 m × 0.12 m, 0.75 m high) | Tank $L$ = 1.6 m, $W$ = 0.61 m, $Lr$ = 0.4 m; $S$ = 0; smooth | $h_u$ = 0.3 m $h_d$ = 0.01 m | 0.61 m | University of Washington, Seattle, USA | 2005 | Net force on the structure and velocity hydrographs | Load cell; LDV | ✗ | 3D NSE ELMMC |
| Arnason [195] | Total; dry bottom; impact on columns (square: 0.12 m × 0.12 m; circular: $D$ = 0.029, 0.0606, 0.14 m) | Tank $L$ = 16.62 m, $W$ = 0.61 m, $Lr$ = 5.9 m; $S$ = 0; smooth and rough | $h_u$ = 0.10–0.40 m | 0.61 m | University of Washington, Seattle, USA | 2005 | Net force on the structure and velocity hydrographs; free surface profiles | Load cell; LDV; video camera; PIV | ✗ | |
| Kleefsman et al. [196]; Issa and Violeau [197]; Larese et al. [198] | Total; dry bottom; impact on an obstacle | Tank $L$ = 3.22 m, $W$ = 1.0 m, $Lr$ = 1.228 m; $S$ = 0; smooth | $h_u$ = 0.55 m | 1.0 m | MARIN (Maritime Research Institute, The Netherlands) | 2005 | Water depth, pressure and force hydrographs | Height probes; pressure transducers | ✗ | 3D NSE, VOF FV; 3D NSE SPH, PFEM |
| Liang et al. [199] | Partial; wet bottom; impact on a column (circular: $D$ = 0.35 m) | Tank $L$ = 25 m, $W$ = 1.6 m, $Lr$ = 2.5 m $S$ = 0; smooth | $h_u$ = 0.235 m $h_d$ = 0.059 m | 0.15 m | Delft University of Technology, The Netherlands | 2007 | Water depth hydrographs; front position and velocity | Video camera (25 fps) | ✗ | 2D SWE FD ($n$ = 0.01 s m$^{-1/3}$) |
| Aureli et al. [14] | Partial; dry and wet bottom; insubmersible obstacle | Tank $L$ = 2.6 m, $W$ = 1.2 m, $Lr$ = 0.8 m, $S$ = 0; smooth | $h_u$ = 0.15 m $h_d$ = 0.01 m | 0.3 m | University of Parma, Italy | 2008 | Water surface profiles; water depth hydrographs | Video camera (3 fps); ultrasonic distance meters | ✓ | 2D SWE FV ($n$ = 0.007 s m$^{-1/3}$) |

**Table 3.** *Cont.*

| (1) Reference | (2) Dam-Break Type | (3) Setup Characteristics [1] | (4) Initial Conditions [2] | (5) Breach Width | (6) Laboratory | (7) Year | (8) Measured Data | (9) Measuring Technique [3] | (10) Data [4] | (11) Numerical Simulation [5] |
|---|---|---|---|---|---|---|---|---|---|---|
| Nouri [200]; Nistor et al. [201]; Nouri et al. [202] | Total; dry bottom; impact on columns (square: 0.2 m × 0.2 m; circular: $D$ = 0.32 m), constrictions | Rectangular channel $L$ = 10.6 m, $W$ = 2.7 m $Lr$ = 5.58 m, $S$ = 0; rough | $h_u$ = 0.5, 0.75, 0.85, 1.0 m | 2.7 m | Canadian Hydraulics Center, Ottawa, Canada | 2008 | Pressures, water level and impact force hydrographs; point velocities | Capacitance wave gauges; load cells; dynamometer; pressure transducers; ADV | ✗ | |
| Bukreev and Zykov [203] | Total; wet bottom; vertical plate | Rectangular channel $L$ = 8.2 m $W$ = 0.2 m $Lr$ > 1.4 m, $S$ = 0; rough | $h_u/h_d$ = 0.186, 0.419, 0.605 | 0.2 m | Russian Academy of Sciences, Novosibirsk | 2008 | Water depth and force hydrographs, velocity in the vertical plane | Wavemeters; force transducer; PIV | ✗ | |
| Arnason et al. [204] | Total; wet bottom; impact on vertical columns (square: 0.12 m × 0.12 m; circular: $D$ = 0.14 m; 5.2 m downstream of the gate) | Tank $L$ = 16.6 m, $W$ = 0.6 m, $Lr$ = 5.9 m, $S$ = 0; smooth | $h_u$ = 0.10–0.3 m ($\Delta h$ = 0.025m) $h_d$ = 0.02 m | 0.6 m | University of Washington, Seattle, USA | 2009 | Water depth and velocity hydrographs at different locations; time series of the horizontal force on the columns | Laser induced fluorescence technique; particle image and LDV; load cell | ✗ | |
| Cruchaga et al. [205] | Total; dry bottom; obstacles of different shapes | Tank $L$ = 0.456 m, $W$ = 0.228m $Lr$ = 0.114 m, $S$ = 0; smooth | $h_u$ = 0.228 m | 0.228 m | University of Santiago, Chile | 2009 | Water depth profiles at different times | Video camera | ✗ | 2D NSE, ETILT FE |
| Hu and Sueyoshi [206] | Total; dry bottom; impact on a vertical wall | Tank $L$ = 0.8 m, $W$ = 0.2 m, $Lr$ ~ 0.24 m, $S$ = 0; smooth; closed downstream end | $h_u$ = 0.42 m (estimated) | 0.2 m | Kyushu University, Japan | 2010 | Wave front position; water surface profiles at different times | Video camera | ✗ | 2D NSE CIP, MPS |
| Yang et al. [75] | Total; dry bottom; impact against a brick (0.22 m × 0.12 m, placed 0.6 m downstream of the gate) | Rectangular channel $L$ = 7 m, $W$ = 0.3 m, $Lr$ = 2 m, $S$ = 0; smooth | $h_u \leq 0.123$ m | 0.3 m | Tsinghua University, Beijing, China | 2010 | Critical reservoir depth $h_u$ causing brick movement | N.A. | ✗ | 3D RANS, VOF FV |
| Aureli et al. [207] | Partial; dry and wet bottom; insubmersible obstacle | Tank $L$ = 2.6 m, $W$= 1.2 m, $Lr$ = 0.8 m, $S$ = 0; smooth | $h_u$ = 0.030–0.064 m $h_d$ = 0.0068–0.0157m | 0.3 m | University of Parma, Italy | 2011 | Water depth hydrographs; free surface | Video camera (6.5 fps); ultrasonic distance meters | ✗ | |
| Al-Faesly et al. [208] | Total; dry and wet bottom; impact on structural models (square and circular: 0.305 m, placed 4.92 m downstream of the gate); effect of mitigation walls (flat or curved) | Rectangular channel $L$ = 14.56 m, $W$ = 2.7 m, $S$ = 0; smooth | $h_u$ = 0.55, 0.85, 1.15 m $h_d$ = N.A. | 2.7 m | University of Ottawa, Canada | 2012 | Base shear forces and moments on structural models; acceleration and displacement at the top edge; pressures at 10 points; water depth hydrographs on models and channel; wave front velocity | Load cell; accelerometer; displacement transducer; pressure transducers; capacitance wave gauges; free-standing wave gauges; video camera | ✗ | |
| Oertel and Bung [87] | Total; dry bottom; submersible obstacle | Rectangular channel $L$ = 22 m, $W$ = 0.3 m, $Lr$ = 13 m, $S$ = 0; smooth | $h_u$ = 0.1, 0.2, 0.3, 0.4 m | 0.3 m | Bergische University Wuppertal, Germany | 2012 | Drag force on the obstacle; water depth profiles and velocity field at selected times | Ultrasonic distance meters; video camera (1000 fps); PIV | ✗ | 2D RANS, VOF FV ($\varepsilon = 0.0015 \times 10^{-3}$ m) |
| Lara et al. [209] | Total; wet bottom; impact against a solid square prism (0.12 m × 0.12 m) | Tank $L$ = 1.6 m, $W$ = 0.6 m, $Lr$ = 0.4 m, $S$ = 0; smooth | $h_u$ = 0.3 m $h_d$ = 0.01 m | 0.6 m | University of Cantabria, Santander, Spain | 2012 | Flow velocity time series at a selected point; time history of the net force on the prism | LDV; load cell | ✗ | 3D RANS, VOF FV |
| Triatmadja and Nurhasanah [210] | Total; wet bottom; impact on a building; effects of a barrier | Rectangular channel $L$ = 24 m, $W$ = 1.45 m, $Lr$ = 8 m, $S$ = 0; smooth | $h_u$ = 0.6, 0.7, 0.8 m $h_d$ = 0.02 m | 1.45 m | Gadjah Mada University, Indonesia | 2012 | Water depth hydrographs; force on the structure | Wave gauges; load cell | ✗ | |
| Aguíñiga et al. [211] | Total; wet bottom; impact on a vertical wall placed 2.18 m downstream of the gate | Rectangular channel $L$ = 4.93 m, $W$ = 0.305 m, $Lr$ = 0.305 m, $S$ = 0; smooth | $h_u$ = N.A. $h_d$ = 0.051, 0.076, 0.102 m (bore height: 0.157, 0.203, 0.264 m) | 0.305 m | Texas A&M University, Kingsville, USA | 2013 | Maximum force on the wall | Spring system and video camera | ✗ | |

**Table 3.** *Cont.*

| (1) Reference | (2) Dam-Break Type | (3) Setup Characteristics [1] | (4) Initial Conditions [2] | (5) Breach Width | (6) Laboratory | (7) Year | (8) Measured Data | (9) Measuring Technique [3] | (10) Data [4] | (11) Numerical Simulation [5] |
|---|---|---|---|---|---|---|---|---|---|---|
| Nakao et al. [212] | Total; wet bottom; model T-girder bridges (placed 7.5 m downstream of the gate) | Rectangular channel $L$ = 30 m, $W$ = 1 m $Lr$ = 12 m, $S$ = 0; smooth | $h_u$ = 0.617 m $h_u$ = 0.1, 0.15, 0.2 m $h_d$ = N.A. | 1 m | Public Works Research Institute, Tsukuba, Japan | 2013 | Tsunami height and reaction force in time; dynamic pressure at the girder | Video cameras; load cells; wave gauges; pressure gauges | ✗ | |
| Lobovský et al. [213] | Tank; dry bottom; impact against the downstream end | Tank $L$ = 1.61 m, $W$ = 0.15 m, $Lr$ = 0.6 m, $S$ = 0; smooth | $h_u$ = 0.3, 0.6 m | 0.6 m | Technical University of Madrid, Spain | 2014 | Water surface profiles; wave front propagation; water level hydrographs at four locations; pressure hydrographs at five points | Video camera (300 fps); pressure transducers | ✓ | |
| Ratia et al. [214] | Total; wet bottom; closed downstream end; bridge models | Rectangular channel $L$ = 6 m, $W$ = 0.24 m, $Lr$ = 1.56 m, $Wr$ = 0.84 m, $S$ = 0; smooth | $h_u$ = 0.169–0.227 m $h_d$ = 0.009–0.011 m | 0.24 m | University of Zaragoza, Spain | 2014 | Water depth hydrographs in two positions | Water depth gauges | ✓ | 2D SWE FV |
| Aureli et al. [215] | Partial; dry bottom; impact on a insubmersible obstacle (0.3 m × 0.155 m) | Tank $L$ = 2.6 m, $W$ = 1.2 m, $Lr$ = 0.8 m, $S$ = 0; smooth | $h_u$ = 0.07–0.13 m | 0.3 m | University of Parma, Italy | 2015 | Impact force | Load cell | ✓ | 2D SWE FV ($n$ = 0.007 s m$^{-1/3}$) 3D RANS, VOF FV; 3D NSE SPH |
| Kocaman and Ozmen-Cagatay [216] | Total; wet bottom; impact on the downstream vertical end | Rectangular channel $L$ = 8.9 m, $W$ = 0.3 m, $Lr$ = 4.65 m, $S$ = 0; smooth | $h_u$ = 0.25 m $h_d$ = 0.025, 0.1 m | 0.3 m | Cukurova University, Adana, Turkey | 2015 | Water surface profiles; water depth hydrographs | Video cameras (50 fps) | ✗ | 2D RANS, VOF FV; 1D SWE FV |
| Liao et al. [217] | Total; dry bottom; impact on an elastic structure (0.1 m high, 0.4 m downstream of the gate) | Tank $L$ = 0.8 m, $W$ = 0.2 m, $Lr$ = 0.2 m, $S$ = 0; smooth | $h_u$ = 0.2, 0.3, 0.4 m | 0.2 m | Kyushu University, Japan | 2015 | Water surface profiles and deformation of the structure (three markers); longitudinal marker displacement hydrographs | Video camera (1000 fps) | ✗ | 2D NSE, VOF Coupled CIP, FD–FE (interaction fluid–structure) |
| Liang et al. [218] | Total; wet bottom; bridge | Rectangular channel $L$ = 35.5 m, $W$ = 1 m, $Lr$ = 5.5 m, $S$ = 0; smooth | $h_u$ = 0.4 m $h_d$ = 0.198 m; $h_u$ = 0.204 m $h_d$ = 0.105 m | 1 m | Hohai University, Nanjing, China | 2016 | Water depth and flow velocity time series in seven locations; pressure time series on the bridge piers | Wave gauges; ADV; pressure sensors | ✗ | 2D SWE FV ($n$ = 0.01 s m$^{-1/3}$) |
| Mohd et al. [219] | Total; dry bottom; impact on a vertical cylinder (square: 0.05 m × 0.05 m; circular $D$ = 0.05 m) | Tank $L$ = 0.8 m, $W$ = 0.2 m, $Lr$ = 0.2 m, $S$ = 0; smooth | $h_u$ = 0.4 m | 0.2 m | Kyushu University, Japan | 2017 | Flow images; wave front celerity; water depth hydrographs | Video cameras | ✗ | 3D LBM |
| Kamra et al. [220] | Total; dry bottom; impact on the closed downstream end | Tank $L$ = 0.8 m, $W$ = 0.2 m, $Lr$ = 0.2 m; $S$ = 0; smooth | $h_u$ = 0.2 m | 0.2 m | Kyushu University, Japan | 2018 | Water surface profiles; pressure hydrographs; wave front position | Pressure sensors | ✗ | 3D RANS, VOF FV |
| Liu et al. [221] | Partial; dry bottom; building (0.4 m × 0.2 m × 0.3 m, locked and unlocked door scenarios) | Rectangular channel $L$ = 40 m, $W$ = 2.2 m, $Wr$ = 3.5 m, $Lr$ = 11.5 m; $S$ = 0; smooth | $h_u$ = 0.15, 0.2 m | 0.8 m | Tsinghua University, Beijing, China | 2018 | Water level hydrographs | Pressure gauges; ultrasonic distance meters | ✗ | |
| Martínez-Aranda et al. [222] | Partial; dry bottom; obstacles, singularities, and a bridge model | Reservoir and rectangular channel $L$ = 6 m, $W$ = 0.24 m, $Lr$ = 1.57 m; $Wr$ = 0.81 m $S \approx 0$ (in the first 3.26 m downstream of the gate), 0.0404 downstream; smooth | $h_u$ = 0.055, 0.13 m | 0.24 m | University of Zaragoza, Spain | 2018 | Free surface; free surface profiles; flow depth time series | RGB-D sensor | ✓ | 2D SWE FV ($n$ = 0.008–0.012 s m$^{-1/3}$) |
| Stamataki et al. [223] | Total; dry bottom; building | Rectangular channel $L$ = 20 m, $W$ = 1.2 m, $Lr$ = 2.9 m, $S$ = 1/20; smooth and rough | $h_u$ = 0.1, 0.2 m | 1.2 m | University College London, UK | 2018 | Water depth and hydrodynamic force hydrographs; wave front celerity | Wave gauges; ultrasonic distance meters; load cell; pressure sensors; video camera (250 fps) | ✗ | 2D RANS, VOF FV |

**Table 3.** *Cont.*

| (1) Reference | (2) Dam-Break Type | (3) Setup Characteristics [1] | (4) Initial Conditions [2] | (5) Breach Width | (6) Laboratory | (7) Year | (8) Measured Data | (9) Measuring Technique [3] | (10) Data [4] | (11) Numerical Simulation [5] |
|---|---|---|---|---|---|---|---|---|---|---|
| Tinh et al. [224] | Total; dry and wet bottom; impact on a vertical structure | Rectangular channel $L$ = 17.6 m, $W$ = 0.3 m, $Lr$ = 3 m, $S$ = 1/20; smooth | $h_u$ = 0.15 m $h_d$ = 0; $h_u$ = 0.2 m $h_d$ = 0.05 m | 0.3 m | Tohoku University, Sendai, Japan | 2018 | Water depth hydrographs; water surface profiles; flow images | Ultrasonic distance meters; video camera | ✗ | |
| Demir et al. [225] | Total; dry bottom; impact on the downstream end; interaction with a deformable plate (3 different heights) | Tank $L$ = 0.6 m, $W$ = 0.2 m, $Lr$ = 0.15 m, $S$ = 0; smooth | $h_u$ = 0.3 m | 0.2 m | Technical University of Erzurum, Turkey | 2019 | Free surface profiles; tip displacement of the plate; pressure in time at the downstream end | Video camera (25 fps); pressure transducers | ✗ | 3D EUL Coupled SPH–FE (interaction fluid–structure) |
| Ghodoosipour et al. [226,227] | Total; dry and wet bottom; impact on a horizontal transversal pipe ($D$ = 0.1 m) | Rectangular channel $L$ = 30.1 m, $W$ = 1.5 m, $Lr$ = 21.55 m, $S$ = 0; smooth | $h_u$ = 0.3, 0.4, 0.5 m $h_d$ = 0, 0.03, 0.06, 0.08, 0.12, 0.17 m | 1.5 m | University of Ottawa, Canada | 2019 | Water depth time series at three locations; wave front celerity; flow velocity at a location; time series of the hydrodynamic force on the pipe | Capacitance wave gauges; ADV; dynamometer; video cameras (70 fps) | ✗ | |
| Kamra et al. [228] | Total; dry bottom; impact on a vertical cylinder (square and circular section, square: 0.05 m × 0.05 m, circular: $D$ = 0.05 m) | Tank $L$ = 0.8 m, $W$ = 0.2 m, $Lr$ = 0.2 m, $S$ = 0; smooth | $h_u$ = 0.2 m | 0.2 m | Kyushu University, Japan | 2019 | Flow images; pressure hydrographs | Video camera (1500 fps); piezoresistive pressure sensors | ✗ | |
| Mokhtar et al. [229] | Total; wet bottom; impact on a vertical seawall (solid or perforated, located 9 m downstream of the gate) | Rectangular channel $L$ = 100 m, $W$ = 1.5 m, $Lr$ = 44 m, $S$ = 0; smooth | $h_u$ = 0.55, 0.6, 0.65, 0.7, 0.75 m $h_d$ = 0.05 m | 1.5 m | National Hydraulic Research Institute, Selangor, Malaysia | 2019 | Wave depth and pressure hydrographs; flow velocity hydrographs; flow images | Resistance wave gauges; pressure sensors; ADV; video camera (240 fps) | ✗ | |
| Dutta et al. [230,231] | Total; dry bottom; impact on a vertical structure | Rectangular channel $L$ = 6 m, $W$ = 0.3 m, $Lr$ = 4 m, $S$ = 0; smooth | $h_u$ = 0.2, 0.25, 0.3, 0.35, 0.4 m | 0.3 m | Indian Institute of Technology, Kharagpur | 2020 | Flow velocity at two locations; water surface profiles | ADV; video camera | ✗ | 3D RANS, VOF FV |
| Farahmandpour et al. [232] | Total; dry bottom; impact on a vertical structure | Rectangular channel $L$ = 10 m, $W$ = 2.1 m $S$ = 0; smooth Reservoir (cylindrical, $D$ = 3 m) | $h_u$ = 0.5, 1, 1.25, 1.5, 1.75, 2 m | 3 m | Universiti Teknologi Malaysia | 2020 | Flow depth time series at two locations; pressure time series on the face of the structure; wave front celerity | Capacitance wave gauges; pressure cells; video cameras | ✗ | |
| Kocaman et al. [233] | Partial; dry bottom; insubmersible obstacle (0.15 m × 0.08 m) | Tank $L$ = 1 m, $W$ = 0.5 m, $Lr$ = 0.25 m, $S$ = 0; smooth | $h_u$ = 0.15 m | 0.1 m | Iskenderun Technical University, Turkey | 2020 | Wave front; water depth time series at five gauge points | Video camera (300 fps); ultrasonic distance meters | ✗ | 3D RANS, VOF FV |
| Pratiwi et al. [234] | Partial; dry bottom; insubmersible oblique obstacle | Rectangular channel $L$ = 10 m, $W$ = 1 m $S$ = 0; smooth Reservoir $Lr$ = 2 m, $Wr$ = 5.2 m | $h_u$ = 0.4 m | 1 m | Institut Teknologi Bandung, Indonesia | 2020 | Water depth and flow velocity at five locations | Ultrasonic distance meters; current meters | ✗ | |
| Shen et al. [235] | Total; dry bottom; impact on a vertical wall | Rectangular channel $L$ = 4 m, $W$ = 0.4 m, $Lr$ = 1 m $S$ = 0; smooth | $h_u$ = 0.3 m | 0.4 m | Zhejiang University, Hangzhou, China | 2020 | Pressure time series at five elevations on the vertical wall; water depth at the wall; flow images | Pressure transducers; capacitance wave gauge; video cameras (100 and 200 fps) | ✗ | |
| Ansari et al. [121] | Total; dry bottom; circular cylinder, square cylinder, and cubic obstacle | Rectangular channel $L$ = 3.7 m, $W$ = 0.6 m, $Lr$ = 0.6 m, $S$ = 0; smooth | $h_u$ = 0.2 m | 0.6 m | University of Zanjan, Iran | 2021 | Water surface profiles | Video camera (60fps) | ✗ | 3D (Molecular dynamics software) SPH |
| Memarzadeh et al. [236] | Total; dry and wet bottom; impact against an overtoppable vertical wall (0.33 m from the gate) | Rectangular channel $L$ = 1 m, $W$ = 0.5 m, $Lr$ = 0.32 m, $S$ = 0; smooth | $h_u$ = 0.25 m | 0.5 m | Shahid Bahonar University, Kerman, Iran | 2021 | Water surface profiles at selected times | Video camera | ✗ | 3D NSE SPH; 3D RANS, VOF FV ($\varepsilon$ = 0.3 × $10^{-5}$ m) |

**Table 3.** *Cont.*

| (1) Reference | (2) Dam-Break Type | (3) Setup Characteristics [1] | (4) Initial Conditions [2] | (5) Breach Width | (6) Laboratory | (7) Year | (8) Measured Data | (9) Measuring Technique [3] | (10) Data [4] | (11) Numerical Simulation [5] |
|---|---|---|---|---|---|---|---|---|---|---|
| Del Gaudio et al. [237] | Total; dry bottom; impact on the end vertical wall | Rectangular channel $L$ = 3 m, $W$ = 0.4 m, $Lr$ = 1.5 m, $S$ = 0; smooth | $h_u$ = 0.2 m | 0.4 m | University of Naples Federico II, Italy | 2022 | Water surface profiles at selected times; pressure time series at six locations on the end wall | Video cameras (164 fps); pressure transducers | ✗ | 1D SWE FV ($C/g^{1/2}$ = 22) |
| Fang et al. [238] | Total; dry and wet bottom; effect of front buildings on the wave impact on buildings | Rectangular channel $L$ = 17.3 m, $W$ = 0.8 m, $Lr$ = 0.625 m, $S$ = 0; smooth | $h_u$ = 0.35, 0.5, 0.65 m | 0.8 m | Tongji University, Shanghai, China | 2022 | Water depth time series at fourlocations; flow velocity at a gauge point; impact force on the building; pressure distribution on the impact front | Ultrasonic distance meters; ADV; multiaxial dynamometer; uniaxial force transducers | ✗ | |
| Garoosi et al. [239] | Total; dry and wet bottom; closed downstream end; impact on a vertical wall | Rectangular channel $L$ = 0.7 m, $W$ = 0.4 m, $Lr$ = 0.25 m, $S$ = 0; smooth (dry bottom case); $L$ = 1 m, $W$ = 0.4 m, $Lr$ = 0.25 m, $S$ = 0; smooth (wet bottom case) | $h_u$ = 0.15 m (dry bottom case); $h_u$ = 0.20 m (wet bottom case) $h_d$ = 0.02 m | 0.4 m | École Polytechnique de Montréal, Canada | 2022 | Water surface profiles; impact pressures on the downstream wall | Video camera (480 fps); pressure sensors | ✓ | 2D NSE, VOF FV; 2D NSE MPS |
| Lin et al. [240] | Total; wet bottom; movable boulder (placed 1.87 m from the gate) | Rectangular channel $L$ = 25 m, $W$ = 0.3 m $Lr$ = 0.25 m, $S$ = 0; smooth | $h_u$ = 0.23–0.35 m $h_d$ = 0.03–0.06 m | 0.3 m | Tainan Hydraulics Laboratory, Taiwan | 2022 | Images of the bore impact on the boulder; boulder transportation process and boulder final posture | Video camera (1000 fps); inertial measurement unit | ✗ | |
| Liu et al. [241] | Total; dry bottom; impact on a vertical wall (placed 0.85 m from the gate) | Tank $L$ = 1.2 m, $W$ = 0.44 m, $Lr$ = 0.25 m, $S$ = 0; smooth | $h_u$ = 0.2, 0.25, 0.3 m | 0.44 m | University of Ottawa, Canada | 2022 | Images of the wave propagation; water depth time series at the vertical wall; dynamic pressure time series at ten points on the wall | Video camera (60 fps); ultrasonic distance meters; pressure transducers | ✓ | |
| Wang et al. [242] | Total; dry bottom; impact on flood barriers (kinetic umbrellas, placed 1.11 m from the gate) | Tank $L$ = 3 m, $W$ = 0.56 m, $Lr$ = 0.616 m, $S$ = 0; smooth | $h_u$ = 0.1, 0.15, 0.2 m | 0.616 m | Princeton University, USA | 2022 | Hydrodynamic force time history; flow images | Resistive load cell; video cameras | ✗ | 3D NSE Coupled SPH–FE (interaction fluid–structure) |
| Xie and Shimozono [243] | Total; dry bottom; closed downstream end; impact on a vertical wall | Rectangular channel $L$ = 1.52 m, $W$ = 0.42 m, $Lr$ = 0.51 m, $S$ = 0; smooth | $h_u$ = 0.08–0.14 m | 0.42 m | University of Tokyo, Japan | 2022 | Dam-break wave front celerity; dam-break wave front slope; impact pressure on a vertical wall | Video camera (500 fps); pressure sensors | ✓ | |
| Yang et al. [131] | Total; dry and wet bottom; impact on a circular pier ($D$ = 0.08 m) located 4 m downstream of the gate | Rectangular channel $L$ = 10.72 m, $W$ = 1.485 m, $Lr$ = 4.58 m, $S$ = 0; smooth | $h_u$ = 0.13–0.483 m (dry bottom cases); $h_u$ = 0.13–0.487 m (wet bottom cases); $h_d$ = 0.02, 0.04, 0.06, 0.08, 0.1, 0.12, 0.14 m | 1.485 m | Southwest Jiaotong University, Chengdu, China | 2022 | Water depth hydrographs at five locations; forces and moments on the pier; pressure time series on 16 points on the front, back, and lateral sides of the pier | Wave gauges; load cell; pressure sensors | ✗ | |

Note(s): [1] $L$ = facility length; $W$ = facility width; $Lr$ = reservoir length; $Wr$ = reservoir width (if different from $W$); $S$ = bottom slope; $\theta$ = inclination angle; $D$ = diameter; [2] $h_u$ = upstream water depth; $h_d$ = downstream water depth; [3] ADV = acoustic Doppler velocimeter; LDV = laser Doppler velocimeter; PIV = particle image velocimetry; [4] ✗ = not freely available; ✓ = freely available; [5] Approach: 1D = one-dimensional; 2D = two-dimensional; 3D = three-dimensional–Mathematical model: BOU = Boussinesq equations; ETILT = edge-tracked interface locator technique; EUL = Euler equations; LBM = lattice Boltzmann method; NSE = Navier–Stokes equations; RANS = Reynolds-averaged Navier–Stokes equations; SWE = shallow water equations; VOF = volume of fluid–Numerical method: CIP = constrained interpolation profile; ELMMC = Eulerian–Lagrangian marker and micro cell method; FD = finite difference; FE = finite element; FV = finite volume; MOC = method of characteristics; MPS = moving particle semi-implicit; PFEM = particle finite element method; SPH = smoothed particle hydrodynamics–$n$ = Manning roughness coefficient; $\varepsilon$ = surface roughness; $C$ = Chézy's resistance factor; $g$ = gravity acceleration; N.A. = not available.

**Table 4.** Experimental investigations of the dam-break wave propagation in idealized urban areas.

| (1) Reference | (2) Dam-Break Type | (3) Setup Characteristics [1] | (4) Initial Conditions [2] | (5) Breach Width | (6) Laboratory | (7) Year | (8) Measured Data | (9) Measuring Technique [3] | (10) Data [4] | (11) Numerical Simulation [5] |
|---|---|---|---|---|---|---|---|---|---|---|
| Shige-eda and Akiyama [59] | Partial (asymmetric); dry bottom; impact on square pillars (0.06 m × 0.06 m) | Tank $L$ = 4.8 m, $Wr$ = 2.98 m $Lr$ = 1.93 m, $S$ = 0; smooth | $h_u$ = 0.2 m | 0.5 m | Kyushu Institute of Technology, Kitakyushu, Japan | 2003 | Wave front position, flow depths and surface velocity hydrographs at four positions, forces on selected pillars | Digital video tape recorder; particle tracking velocimetry; load cells | ✗ | 2D SWE FV ($n$ < 0.07 s m$^{-1/3}$) |
| Soares-Frazão et al. [244]; Soares-Frazão and Zech [245] | Partial; wet bottom; three urban district layouts (blocks: 0.3 m × 0.3 m; streets: 0.1 wide) | Trapezoidal channel $L$ = 35.8 m, $W$ = 3.6 m, $Lr$ = 6.75 m, $S$ = 0; smooth | $h_u$ = 0.40 m $h_d$ = 0.011 m | 1 m | Université Catholique de Louvain, Belgium | 2006 | Water levels time series at 64 points; water surface profiles; surface velocity measurements | Resistive water level gauges; digital imaging technique; Voronoï PTV technique | ✗ | 2D SWE FV ($n$ = 0.01 s m$^{-1/3}$) |
| Szydlowski and Twarog [246] | Partial; dry bottom; urban district layout with aligned buildings (0.1 m sides) | Tank $L$ = 6.75 m, $W$ = 3 m, $Lr$ = 3.0 m, $Wr$ = 3.5 m, $S$ = 0; smooth | $h_u$ = 0.21 m | 0.5 m | Gdansk University of Technology, Poland | 2006 | Water depth time series at 11 locations | Pressure transducers; depth-control gauge | ✗ | 2D SWE FV ($n$ = 0.018 s m$^{-1/3}$) |
| Yoon [247] Kim et al. [248] | Partial; dry bottom; 0.2 m × 0.2 m block arranged as two 3 × 3 groups | Plane $L$ =30 m, $W$ = 30 m, $Lr$ = 5 m, $S$ = 0; smooth | $h_u$ = 0.3, 0.45 m | 1 m | Urban Flood Disaster Management Research Center, Seoul, South Korea | 2007 | Water depth time series at 17 points | Capacitance wave gauges | ✗ | 2D SWE (with porosity) FV ($\varepsilon$ = 0.3–3 × 10$^{-3}$ m) |
| Albano et al. [249] | Total; dry bottom; two fixed buildings (0.3 m × 0.15 m × 0.3 m); three floating bodies (0.118 m × 0.045 m × 0.043 m, mass: 0.025 kg) | Rectangular channel $L$ = 2.5 m, $W$ = 0.5 m, $Lr$ = 0.5 m, $S$ = 0; smooth | $h_u$ = 0.1 m | 0.5 m | Basilicata University, Italy | 2016 | Water depth time series at two locations (in front of the fixed obstacles); displacement of movable bodies | Resistive water depth gauges; cameras | ✗ | 3D EUL (Euler-Newton equations for the rigid body dynamics) SPH |
| Norin et al. [250] | Total; dry bottom; staggered 0.1 m × 0.1 m parallelepipeds | Rectangular channel $L$ = 7 m, $W$ = 1.39 m, $Lr$ = N.A., $S$ = 0; smooth | $h_u$ = 0.225 m | 1.39 m | Scientific Research Institute of Power Structures, Russia | 2017 | Water level time series at two points; flow velocity profiles | Water level gauges; flow meters | ✗ | 2D SWE FV |
| Guinot et al. [251,252] | Total; dry bottom; blocks (0.5 m × 0.75 m); two configurations | Rectangular channel $L$ = 20 m, $W$ = 1 m, $Lr$ = N.A., $S$ = 0; smooth | $h_u$ = 0.35 m | 1 m | Université Catholique de Louvain, Belgium | 2018 | Water depth time series at selected locations | Ultrasonic distance meters | ✗ | 1D SWE (with porosity) FV |
| Kusuma et al. [253] | Partial; dry bottom; blocks (0.1 m × 0.1 m); four configurations (1, 3, 5, 8 blocks) | Rectangular channel $L$ = 10 m, $W$ = 1 m, $S$ = 0; smooth Reservoir $Lr$ = 2 m, $Wr$ = 4 m | $h_u$ = 0.2, 0.3, 0.4 m | 1 m | Institut Teknologi Bandung, Indonesia | 2019 | Water depth profiles at selected times; water depth and flow velocity hydrographs at selected locations | Wave probe and piezometers; current meter | ✗ | – |
| Chumchan and Rattanadecho [254] | Partial; dry bottom; blocks (0.085 m sides); two configurations | Tank $L$ = 0.984 m, $W$ = 0.484 m, $Lr$ = 0.24 m, $S$ = 0; smooth | $h_u$ = 0.15 m | 0.1 m | Thammasat University, Pathumthani, Thailand | 2020 | Flow images; wave front | Video camera (240 fps) | ✗ | 3D RANS, VOF FV, LB |
| Dong et al. [255] | Partial; dry bottom; idealized urban street; six configurations (with buildings, greenbelt sections, sidewalks, and an underground sewer system) | Rectangular channel $L$ = 20.5 m, $W$ = 3 m, $Lr$ = 4.5 m, $S$ = 0; smooth | $h_u$ = 0.09, 0.19, 0.29 m | 1 m | North China University of Water Resources and Electric Power, China | 2021 | Water hydrographs at seven points; flow velocity time series at three points; drainage discharge time series at inlets | Ultrasonic distance meters; electromagnetic velocity meter; electromagnetic flowmeters | ✗ | 2D SWE FV ($n$ = 0.009–0.011 s m$^{-1/3}$) |

Note(s): [1] $L$ = facility length; $W$ = facility width; $Lr$ = reservoir length; $Wr$ = reservoir width (if different from $W$); $S$ = bottom slope; [2] $h_u$ = upstream water depth; $h_d$ = downstream water depth; [3] PTV = particle tracking velocimetry; [4] ✗ = not freely available; [5] Approach: 1D = one-dimensional; 2D = two-dimensional; 3D = three-dimensional–Mathematical model: EUL = Euler equations; RANS = Reynolds-averaged Navier–Stokes equations; SWE = shallow water equations; VOF = volume of fluid–Numerical method: FV = finite volume; LB = lattice Boltzmann; SPH = smoothed particle hydrodynamics–$n$ = Manning roughness coefficient; $\varepsilon$ = surface roughness; N.A. = not available.

**Table 5.** Experimental investigations of the propagation of tsunami bores (generated by the removal of a gate) in the swash zone.

| (1) Reference | (2) Dam-Break Type | (3) Setup Characteristics [1] | (4) Initial Conditions [2] | (5) Breach Width | (6) Laboratory | (7) Year | (8) Measured Data | (9) Measuring Technique [3] | (10) Data [4] | (11) Numerical Simulation [5] |
|---|---|---|---|---|---|---|---|---|---|---|
| Yeh and Ghazali [256], Yeh et al. [257] | Total; wet bottom; sloping beach starting 0.4 m downstream of the gate | Tank $L$ = 9 m, $W$ = 1.2 m, $Lr$ = 2.97 m, $S_b$ = 7.5°; smooth | $h_u/h_d$ = 2.31 $h_d$ = 0.0975 m (fully developed bore); $h_u/h_d$ = 1.72 $h_d$ = 0.0975 m (undular bore) | 1.2 m | University of Washington, Seattle, USA | 1988 | Longitudinal profile of the bore; maximum run-up height; bore celerity | Video camcorder and photo camera (laser-induced fluorescence); water sensors | ✗ | |
| Petroff et al. [258] | Total; wet bottom; sloping beach; prismatic movable obstacles of different sizes and orientations | Rectangular channel $L$ = 20 m, $W$ = 0.6 m, $Lr$ = 7 m; $S_b$ = 0.1; smooth and rough | $h_u$ = 0.3 m $h_d$ = 0.02 m | 0.61 m | University of Washington, Seattle, USA | 2001 | Advection distance of obstacles | Video camera (18 fps) | ✗ | (beach roughened with sand: $d_{50}$ = 0.84 × $10^{-3}$ m) |
| Anh [259] | Total; dry bottom; adverse slope; Vetiver hedge 0.5 m thick (160–530 stems/$m^2$) | Tank $L$ > 12.5 m, $W$ = 0.4 m, $Lr$ = 6 m, $S_b$ = 1/30; smooth | $h_u$ = 0.35–0.5 m | 0.4 m | Delft University of Technology, The Netherlands | 2007 | Water depth hydrographs; overtopping discharge | Pressure transducers, water depth gauges | ✗ | |
| Barnes et al. [260] | Total; wet bottom; sloping beach starting 4 m downstream of the gate | Rectangular channel $L$ = 20 m, $W$ = 0.45 m, $Lr$ = 1 m, $S_b$ = 0.1; smooth and rough | $h_u$ = 0.65 m $h_d$ = 0.065 m | 0.45 m | University of Aberdeen, UK | 2009 | Flow depth, bottom shear stress, and flow velocity time series | Acoustic displacement sensors; shear plate; PIV | ✗ | |
| De Leffe et al. [261] | Total; dry bottom; sloping beach starting 1.15 m downstream of the gate | Rectangular channel $L$ = 8 m, $W$ = 1 m, $Lr$ = 2.25 m, $S_b$ = 0.1; smooth | $h_u$ = 0.25 m | 1 m | École Centrale Nantes, France | 2010 | Flow depth time series at 2 gauge points | N.A. | ✗ | 1D, 2D SWE SPH ($n$ = 0.001 s $m^{-1/3}$) |
| O'Donoghue et al. [262] | Total; wet bottom; sloping beach starting 3.8 m downstream of the gate | Rectangular channel $L$ = 20 m, $W$ = 0.45 m, $Lr$ = 1 m, $S_b$ = 0.1; smooth and rough | $h_u$ = 0.65 m $h_d$ = 0.06 m | 0.45 m | University of Aberdeen, UK | 2010 | Water depth time series at 25 locations; runup; flow velocity profiles at five cross-sections | Capacitance depth gauges; PIV | ✗ | 1D SWE FV (λ = 0.064, λ = 0.16) |
| Kikkert et al. [263] | Total; wet bottom; sloping beach starting 4.82 m downstream of the gate | Rectangular channel $L$ = 20 m, $W$ = 0.45 m; $Lr$ = 1 m, $S_b$ = 1/10; rough | $h_u$ = 0.6 m $h_d$ = 0.062 m | 0.45 m | University of Aberdeen, UK | 2012 | Flow depth time series and velocity profiles at six cross-sections | Laser induced fluorescence and video camera; PIV | ✗ | |
| Adegoke et al. [264] | Total; dry and wet bottom; sloping beach starting 2.7 m downstream of the gate | Rectangular channel $L$ = 4.7 m, $W$ = 0.4 m, $Lr$ = 1 m, $S_b$ = N.A.; smooth | $h_u$ = 0.15–0.55 m $h_d$ =0.05, 0.10, 0.15 m | 0.4 m | Liverpool John Moores University, UK | 2014 | Wave front velocity | Video Camera (40 fps); wave probes; pressure transducers | ✗ | |
| Rahman et al. [265] | Total; dry bottom; building model (cubic, $l$ = 0.08 m) placed 4 m from the gate; effect of solid and perforated sea walls (at various distances from the building model) | Rectangular channel $L$ = 17.5 m, $W$ = 0.6 m $Lr$ = 5 m, $S$ = 0; smooth | $h_u$ = 0.15, 0.2, 0.25, 0.3 m | 0.6 m | University of Malaya, Kuala Lumpur, Malaysia | 2014 | Wave height time series at four positions; force time series on the building model | Wave probes; load cell | ✗ | |
| Hartana and Murakami [266] | Total; wet bottom; adverse slope starting 5.5 m from the gate building models (0.2 × 0.2 × 0.26 m): solid and with 40% opening ratio | Rectangular channel $L$ = 12 m, $W$ = 0.4 m $Lr$ = 5 m, $S$ = 0, $S_b$ = 1/40; smooth | $h_u$ = 0.15, 0.2, 0.25, 0.3 m $h_d$ = 0.05 m | 0.4 m | University of Mataram, Indonesia | 2015 | Water depth hydrographs at three locations; flow velocity hydrographs at two locations; pressure time series at 15 points on the building faces | Video cameras; wave gauges; propeller current meters; pressure gauges | ✗ | 3D NSE, VOF FV, FE |

**Table 5.** *Cont.*

| (1) Reference | (2) Dam-Break Type | (3) Setup Characteristics [1] | (4) Initial Conditions [2] | (5) Breach Width | (6) Laboratory | (7) Year | (8) Measured Data | (9) Measuring Technique [3] | (10) Data [4] | (11) Numerical Simulation [5] |
|---|---|---|---|---|---|---|---|---|---|---|
| Chen et al. [267] | Total; two-dam-break systems (1 m apart) wet bottom; adverse slope of starting 3.006 m downstream of the first gate; swash-swash interaction | Rectangular channel $L$ = 12.5 m, $W$ = 0.3 m, $Lr$ = 2.443 m, $S$ = 0, $S_b$ =1/10; smooth, rough adverse slope | $h_{u1}$ = 0.35 m, $h_{u2}$ = 0.5 m, $h_d$ =0.035 m; $h_{u1}$ = 0.4 m, $h_{u2}$ = 0.4 m, $h_d$ =0.04 m (time delay between the opening of the two gates: 1.5–6.5 s) | 0.3 m | Hong Kong University of the Science and Technology | 2016 | Water depth hydrographs at five locations; velocity profiles and water surface elevation | Acoustic distance sensors; PIV | ✗ | |
| Chen et al. [268] | Total; dry bottom (wet bottom in the foreshore area); impact on a wharf model (three deck heights and eight wharf slopes) | Reservoir area 77 $m^2$, capacity 50 $m^3$ Rectangular channel $L$ = 14 m, $W$ = 1.2 m, $S$ = 0, $S_b$ = 30°; smooth | $h_u$ = 0.3, 0.4, 0.5, 0.6 m ($h_d$ = 0.05 m); (different gate openings) | 1.2 m | University of Auckland, New Zealand | 2016 | Water level hydrographs at two locations; bore velocities; time series of uplift pressures at eight points on the wharf | Wave gauges; video camera (210 fps); pressure sensors | ✗ | |
| Chen et al. [269] | Total; dry bottom (wet bottom in the foreshore area); impact on a wharf model and a protective vertical wall (four positions and three wall heights) | Reservoir $Lr$ = 11 m, $Wr$ = 7.3 m Rectangular channel $L$ = 14 m, $W$ = 1.2 m, $S$ = 0, $S_b$ = 30°; smooth | $h_u$ = 0.3, 0.4, 0.6 m ($h_d$ = 0.05 m); (different gate openings) | 1.2 m | University of Auckland, New Zealand | 2017 | Water level hydrographs at three locations; bore velocities; pressure time series on the wharf and the wall | Wave gauges; pressure sensors | ✗ | |
| Esteban et al. [270] | Total; dry bottom (wet bottom in the foreshore area); sloping beach; impact on different overtoppable structures (high vertical wall, low block, dyke) | Rectangular channel $L$ = 14 m, $W$ = 0.41 m, $Lr$ = 4.5 m; $S$ = 0, $S_b$ = 1/10; smooth | $h_u$ = 0.3, 0.4, 0.6 m ($h_d$ = 0, 0.1, 0.2 m) | 0.41 m | Waseda University, Tokyo, Japan | 2017 | Wave depth hydrographs at six locations; overtopping flow velocity; bore impact images | Wave gauges; electromagnetic current meters; video camera | ✗ | |
| Dai et al. [271] | Total; wet bottom; sloping beach starting 3.006 m downstream of the first gate | Rectangular channel $L$ = 12.5 m, $W$ = 0.3 m, $Lr$ = 1.006 m, $Wr$ = 0.279 m; $S$ = 0, $S_b$ = 1/10; smooth, rough adverse slope | $h_u$ = 0.5 m $h_d$ =0.05 m | 0.3 m | Hong Kong University of the Science and Technology | 2017 | Flow depth and velocity hydrographs at five locations; entrained air | Combined laser-induced fluorescence and PIV; phase detection optical probe system; bubble image velocimetry | ✗ | |
| Tar et al. [272] | Total; wet bottom; sloping beach; impact on a oil storage tank model and protective multiple flexible pipes | Rectangular channel $L$ = 44 m, $W$ = 0.7 m, $Lr$ = 7.9 m; $S$ = 0, $S_b$ = 1/40 and 1/100; smooth | $h_u$ = 0.65 m $h_d$ = 0.4 m | 0.7 m | University of Osaka, Japan | 2017 | Flow velocity upstream and downstream of the flexible pipes; hydrodynamic force on the tank model; flow images | Electromagnetic velocity meters; load cell; video camera | ✗ | 3D RANS, VOF FV |
| Chen et al. [273] | Total; dry bottom (wet bottom in the foreshore area); impact on the piles of a wharf model; protective effect of a vertical wall (four positions and three wall heights) | Reservoir $Lr$ = 11 m, $Wr$ = 7.3 m Rectangular channel $L$ = 14 m, $W$ = 1.2 m, $S$ = 0, $S_b$ = 30°; smooth | $h_u$ = 0.3, 0.4, 0.6 m ($h_d$ = 0.05 m); (different gate openings) | 1.2 m | University of Auckland, New Zealand | 2018 | Water level time series at three locations; bore velocities; pressure time series on the piles and deck | Wave gauges; pressure sensors | ✗ | |
| Chen et al. [274] | Total; dry bottom; impact on a bridge model (four different contraction ratios) | Reservoir: 50 $m^3$ Rectangular channel $L$ = 14 m, $W$ = 1.2 m, $S$ = 0, $S_b$ = 30°; smooth | $h_u$ = 0.3, 0.4, 0.6 m (different gate openings) | 1.2 m | University of Auckland, New Zealand | 2018 | Force and momentum acting on the bridge; pressure time series on the bridge deck; wave height time series | Load cell; pressure transducers; capacitance wave gauges; video camera (30 fps) | ✗ | |

**Table 5.** *Cont.*

| (1) Reference | (2) Dam-Break Type | (3) Setup Characteristics [1] | (4) Initial Conditions [2] | (5) Breach Width | (6) Laboratory | (7) Year | (8) Measured Data | (9) Measuring Technique [3] | (10) Data [4] | (11) Numerical Simulation [5] |
|---|---|---|---|---|---|---|---|---|---|---|
| Ishii et al. [275] | Total; dry bottom (wet bottom in the foreshore area); sloping beach starting 4.45 m downstream of the upstream end; impact on a vertical structure | Tank $L$ = 9 m, $W$ = 4 m, $Lr$ = N.A., $S$ = 0, $S_b \approx 8.5^{\circ}$; smooth | $h_u$ = N.A. ($h_d$ = 0.2 m) | 4 m | Waseda University, Tokyo, Japan | 2018 | Flow vortices behind the structure | Load cell; wave gauges, PIV | ✗ | 3D RANS, VOF FV |
| Lu et al. [276] | Total; dry and wet (in the foreshore area) bottom; sloping beach starting 1.8 m downstream of the gate | Rectangular channel $L$ = 6.5 m, $W$ = 0.4 m, $Lr$ = 1.5 m, $S$ = 0, $S_b$ = 1/7.5; smooth | $h_u$ = 0.08–0.24 m ($h_d$ = 0, 0.02, 0.04, 0.06, 0.08 m) | 0.4 m | Zhejiang University, Hangzhou, China | 2018 | Wave front position; maximum run-up; flow images | Video camera (150 fps) | ✗ | |
| Chen et al. [277] | Total; dry bottom; sloping beach starting 0.76 m downstream of the dam; run-up height of balls with different diameters and densities | Rectangular channel $L$ = 4.4 m, $W$ = 0.3 m, $Lr$ = 1.29 m, $S$ = 0; $S_b$ = 15–90°; smooth | $h_u$ = 0.06, 0.1, 0.14, 0.18, 0.22 m | 0.3 m | University of Fuzhou, China | 2020 | Water surface profiles; ball climbing height | Video camera | ✗ | |
| Chen et al. [278] | Total; dry bottom; impact on a container model | Rectangular channel $L$ = 4.4 m, $W$ = 0.3 m, $Lr$ = 1.27 m, $S$ = 0, −1°; smooth | $h_u$ = 0.13, 0.14, 0.15, 0.16, 0.17 m | 0.3 m | University of Fuzhou, China | 2020 | Tsunami wave height; shift of the container model; flow images | Water level gauge; video camera | ✗ | |
| Elsheikh et al. [279,280] | Total; dry bottom; interaction with a transverse canal located 3 m downstream of the gate (three different depths and widths) | Rectangular channel $L$ = 15.56 m, $W$ = 0.38 m, $Lr$ = 7.76 m, $S$ = 0; smooth | $h_u$ = 0.2, 0.3, 0.4 m | 0.38 m | University of Ottawa, Canada | 2020 | Wave front motion and wave height over the canal; wave profiles; water level hydrographs at four locations; flow velocity time series at three points | Video cameras; capacitance wave gauge and ultrasonic distance meters; ADV | ✗ | 3D RANS, VOF FV |
| Barranco and Liu [281] | Total; wet bottom; sloping beach starting 11.1 m downstream of the gate | Rectangular channel $L$ = 36 m, $W$ = 0.9 m, $Lr$ = 2, 4, 8, 17.6 m; $S$ = 0; $S_b$ = 1/10; smooth | $h_u$ = 0.128, 0.157, 0.188, 0.221, 0.256, 0.292, 0.329, 0.368, 0.408 m $h_d$ =0.1 m | 0.9 m | National University of Singapore | 2021 | Water depth time series at seven locations; run-up on the adverse slope | Capacitance gauges; ultrasonic distance meters; video camera (100fps) | ✓ | 2D SWE (non-hydrostatic) FD |
| Chen and Wang [282] | Total; dry bottom; sloping beach starting 0.76 m downstream of the gate energy dissipation effect of grasses; run-up height of steel balls | Rectangular channel $L$ = 4.4 m, $W$ = 0.3 m, $Lr$ = 1.29 m, $S$ = 0, $S_b$ = 30°; smooth, rough reach (artificial grasses) | $h_u$ = 0.06, 0.1, 0.14, 0.18, 0.22 m | 0.3 m | University of Fuzhou, China | 2022 | Wave maximum height at a location; wave celerity; ball climbing height | Water level gauges | ✗ | |
| Liu et al. [283] | Total; dry bottom; sloping channel starting 0.45 m downstream of the gate; impact on a vertical wall placed 0.85 m from the gate | Tank $L$ = 1.2 m, $W$ = 0.44 m, $Lr$ = 0.25 m, $S$ = 0; $S_b$ =5°, 10°, 15°; smooth | $h_u$ = 0.25 m | 0.44 m | University of Ottawa, Canada | 2022 | Wave runup on the vertical wall; images of the wave propagation; free surface profiles at selected times; time history of the wave front | Ultrasonic distance meters; video camera (60 fps) | ✗ | |
| Liu et al. [284] | Total; dry bottom; sloping channel starting 0.45 m downstream of the gate; impact on a vertical wall placed 0.85 m from the gate | Tank $L$ = 1.2 m, $W$ = 0.44 m, $Lr$ = 0.25 m, $S$ = 0, $S_b$ = 5°, 10°, 15°; smooth | $h_u$ = 0.3 m | 0.44 m | University of Ottawa, Canada | 2022 | Dynamic pressure time series at five points on the wall | Pressure transducers | ✗ | 3D RANS, VOF FV; 3D NSE SPH |

**Table 5.** *Cont.*

| (1) Reference | (2) Dam-Break Type | (3) Setup Characteristics [1] | (4) Initial Conditions [2] | (5) Breach Width | (6) Laboratory | (7) Year | (8) Measured Data | (9) Measuring Technique [3] | (10) Data [4] | (11) Numerical Simulation [5] |
|---|---|---|---|---|---|---|---|---|---|---|
| Rajaie et al. [285] | Total; wet bottom; sloping channel starting 4.3 m downstream of the gate insub-mersible structure | Rectangular channel $L$ = 30 m, $W$ = 1.5 m, $Lr$ = 21.55 m, $S$ = 0, $S_b$ = 5%; smooth, rough reach (sand bed) | $h_u$ = 0.25, 0.3, 0.35, 0.4 m $h_d$ = 0.03, 0.1 m | 1.5 m | University of Ottawa, Canada | 2022 | Water depth time series at two locations and in front of the structure; flow velocity time series at a gauge point | Capacitance wave gauges and ultrasonic distance meters; ADV | ✗ | |
| von Häfen et al. [286] | Total; dry bottom; sloping beach starting 10 m downstream of the (swing) gate composite bathymetry (horizontal inland) | Rectangular channel $L$ = 100 m, $W$ = 2 m, $Lr$ = 80 m, $S$ = 0, $S_b$ =5%, followed by a horizontal bottom; smooth | $h_u$ = 0.4, 0.5, 0.6 m | 2 m | Technische Universität Braunschweig, Germany | 2022 | Water depth time series at four locations | Capacitance wave gauges | ✗ | 3D RANS, LSM FD; 2D SWE (non-hydrostatic) FD ($\varepsilon$ = 0.001 m) |

Note(s): [1] $L$ = facility length; $W$ = facility width; $Lr$ = reservoir length; $Wr$ = reservoir width (if different from $W$); $S$ = bottom slope; $S_b$ = beach (adverse) slope; $l$ = obstacle characteristic length; [2] $h_u$ = upstream water depth; $h_d$ = downstream water depth; [3] ADV = acoustic Doppler velocimeter; PIV = particle image velocimetry; [4] ✗ = not freely available; ✓ = freely available; [5] Approach: 1D = one-dimensional; 2D = two-dimensional; 3D = three-dimensional–Mathematical model: LSM = level set method; NSE = Navier–Stokes equations; RANS = Reynolds-averaged Navier–Stokes equations; SWE = shallow water equations; VOF = volume of fluid–Numerical method: FD = finite difference; FE = finite element; FV = finite volume; SPH = smoothed-particle hydrodynamics–$n$ = Manning roughness coefficient; ε = surface roughness; λ = friction factor; N.A. = not available.

**Table 6.** Experimental investigations on green water events using dam-break waves.

| (1) Reference | (2) Dam-Break Type | (3) Setup Characteristics [1] | (4) Initial Conditions [2] | (5) Breach Width | (6) Laboratory | (7) Year | (8) Measured Data | (9) Measuring Technique [3] | (10) Data [4] | (11) Numerical Simulation [5] |
|---|---|---|---|---|---|---|---|---|---|---|
| Buchner [287] | Total; dry bottom; impact on a rigid panel | Tank $L$ = 3.22 m, $W$ = 1 m, $Lr$ = 1.2 m, $S$ = 0; smooth | $h_u$ = 0.6 m | 1 m | Delft University of Technology, The Netherlands | 2002 | Water depth hydrographs at four locations; time series of impact loads on the panel in different areas | Force and pressure transducers | ✗ | |
| Hernández-Fontes et al. [288,289] | Total; wet bottom; vessel structure located 0.505 m downstream of the gate | Tank $L$ = 1 m, $W$ = 0.355 m, $Lr$ = 0.3 m, $S$ = 0; smooth; $f$ = 0.006, 0.024, 0.042 m | $h_u$ = 0.18, 0.2, 0.21, 0.22, 0.24 m $h_d/h_u$ = 0.6 | 0.355 m | Federal University of Rio de Janeiro, Brazil | 2017 | Water elevation hydrographs at two locations; video-images of green water flow | Conductive wave probes; video cameras (500 fps) | ✗ | |
| Hernández-Fontes et al. [290] | Total; wet bottom; vessel structure located 1.258 m downstream of the gate | Tank $L$ = 1.95 m, $W$ = 0.5 m, $Lr$ = 0.3 m, $S$ = 0; smooth; $f$ = 0.006–0.042 m | $h_u$ = 0.18, 0.21, 0.24 m $h_d/h_u$ = 0.6 | 0.5 m | Federal University of Rio de Janeiro, Brazil | 2019 | Freeboard exceedance time series; vertical load on the structure deck | Load cells; video cameras (500 fps); | ✓ | 1D SWE |
| Hernández-Fontes et al. [291] | Total; wet bottom; vessel structure located 0.505 m downstream of the gate | Tank $L$ = 1 m, $W$ = 0.355 m, $Lr$ = 0.3 m, $S$ = 0; smooth; $f$ = 0.03–0.042 m | $h_d$ = 0.108, 0.12 m $h_d/h_u$ = 0.8, 0.7, 0.6, 0.5, 0.4 | 0.355 m | Federal University of Rio de Janeiro, Brazil | 2020 | Water elevation hydrographs at four locations; freeboard exceedance time series; vertical load on the structure deck; video-images of green water flow | Conductive wave probes); load cells; video cameras (500 fps) | ✗ | |
| Hernández-Fontes et al. [292] | Total; wet bottom; vessel structure located 1.455 m downstream of the gate | Tank $L$ = 1.95 m, $W$ = 0.5 m, $Lr$ = 0.3 m, $S$ = 0; smooth; $f$ = 0.006–0.042 m | $h_u$ = 0.18, 0.2, 0.21, 0.22, 0.24, 0.27, 0.3 m $h_d/h_u$ = 0.6, 0.5, 0.4 | 0.5 m | Federal University of Rio de Janeiro, Brazil | 2020 | Water elevation hydrographs at five locations; freeboard exceedance time series; vertical load on the structure deck; video-images of green water flow | Conductive wave probes); load cells; video cameras (500 fps) | ✗ | |
| Hernández-Fontes et al. [293] | Total; wet bottom; vessel structure located 0.505 m downstream of the gate | Tank $L$ = 1 m, $W$ = 0.355 m, $Lr$ = 0.3 m, $S$ = 0; smooth; $f$ = 0.03 m | $h_u$ = 0.3 m $h_d$ = 0.12 m | 0.355 m | Federal University of Rio de Janeiro, Brazil | 2020 | Water elevation hydrographs at five locations; water surface profiles; video-images of green water flow | Conductive wave probes; video cameras (250 fps) | ✗ | |

**Table 6.** *Cont.*

| (1) Reference | (2) Dam-Break Type | (3) Setup Characteristics [1] | (4) Initial Conditions [2] | (5) Breach Width | (6) Laboratory | (7) Year | (8) Measured Data | (9) Measuring Technique [3] | (10) Data [4] | (11) Numerical Simulation [5] |
|---|---|---|---|---|---|---|---|---|---|---|
| Wang and Dong [294] | Total; wet bottom; interaction with a floating box (0.3 m × 0.595 m × 0.1 m, placed 0.75 m or 1.2 m from the gate) | Tank $L$ = 2 m, $W$ = 0.6 m, $Lr$ = 0.5 m, $S$ = 0; smooth; $f$ = 0.07 m | $h_u$ = 0.25, 0.3, 0.35 m $h_d$ = 0.15 m | 0.6 m | Ocean University, Qingdao, China | 2022 | Pressure hydrographs at two points on the box upstream face; water surface hydrographs at two locations; motion of the floating structure | Pressure probes; wave gauges; motion capture system | ✗ | |

Note(s): [1] $L$ = facility length; $W$ = facility width; $Lr$ = reservoir length; $Wr$ = reservoir width (if different from $W$); $S$ = bottom slope; $f$ = freeboard; [2] $h_u$ = upstream water depth; $h_d$ = downstream water depth; [3] –; [4] ✗ = not freely available; ✓ = freely available; [5] Approach: 1D = one-dimensional–Mathematical model: SWE = shallow water equations; N.A. = not available.

**Table 7.** Experimental investigations of dam-break waves of non-Newtonian fluids.

| (1) Reference | (2) Dam-Break Type | (3) Setup Characteristics [1] | (4) Initial Conditions [2] | (5) Breach Width | (6) Laboratory | (7) Year | (8) Measured Data | (9) Measuring Technique [3] | (10) Data [4] | (11) Numerical Simulation [5] |
|---|---|---|---|---|---|---|---|---|---|---|
| Chanson et al. [295]; Chanson et al. [296] | Total; dry bottom; thixotropic fluid (bentonite suspension) | Rectangular channel $L$ = 2 m, $W$ = 0.34 m, $Lr = h_u/\sin(15^\circ)$, $S = 15^\circ$; rough | $h_u$ = 0.0472–0.0784 m | 0.34 m | Laboratory of Materials and Structures in Civil Engineering, Champs sur Marne, France | 2004 | Free surface; wave front propagation; wave front profiles | Video cameras (25 fps) | ✗ | |
| Jánosi et al. [64] | Total; dry and wet bottom; polyethylene-oxide; different concentrations | Tank $L$ = 9.93 m, $W$ = 0.15 m, $Lr$ = 0.38 m, $S$ = 0; smooth | $h_u$ = 0.11–0.25 m $h_d$ = 0–0.005 m | 0.15 m | Eötvös University, Budapest, Hungary | 2004 | Water profiles; front position and velocity | Video cameras | ✗ | |
| Komatina and Đorđević [297] | Total; dry bottom; mixture of water and copper tailings; different volumetric concentrations of the solid phase | Rectangular channel $L$ = 4.5 m, $W$ = 0.15 m, $Lr$ = 2 m, $Wr$ = 0.155 m, $S$ = 0–0.01; smooth | $h_u$ = 0.1–0.3 m | 0.155 m | University of Belgrade, Serbia & Montenegro | 2004 | Flow depth profiles at different times | Video camera (5 fps) | ✗ | 1D SWE FD |
| Cochard and Ancey [298]; Cochard [299]; Cochard and Ancey [300] | Total; dry bottom; viscoplastic fluid (Carbopol Ultrez 10) | Plane $L$ = 6 m, $W$ = 1.8 m, $S = 0$–$18^\circ$; smooth Reservoir $Wr$ = 1.8 m, Mass = 120 kg | N.A. | 1.6 m | EPFL, Lausanne, Switzerland | 2006 | Free surface and flow depth profiles at different times | Video camera | ✗ | |
| Balmforth et al. [301] | Total; dry bottom; Newtonian and non-Newtonian fluids (corn syrup and aqueous suspensions of xanthan gum, kaolin, Carbopol, and cornstarch) | Rectangular channel $L$ > 1 m, $W$ = 0.1 m, $Lr$ = 0.4 m, $S$ = 0; smooth | $h_u$ = 0.02–0.0435 m | 0.1 m | N.A. | 2007 | Wave front position | Video camera | ✗ | |
| Ancey and Cochard [302] | Total; dry bottom; viscoplastic (Herschel–Bulkley) fluid (Carbopol Ultrez 10) | Rectangular channel $L$ = 4 m, $W$ = 0.3 m, $Lr$ = 0.51 m, $S = 6, 12, 18, 24^\circ$; smooth | Mass in the reservoir: 23–43 kg | 0.3 m | EPFL, Lausanne, Switzerland | 2009 | Free surface and flow depth profiles at selected times; front position with time | Video camera | ✗ | |
| Cochard and Ancey [303] | Partial; dry bottom; viscoplastic (Herschel–Bulkley) fluid (Carbopol Ultrez 10) | Plane $L$ = 5.5 m, $W$ = 1.8 m, $S = 0$–$18^\circ$; smooth Reservoir $Lr$ = 0.51 m, $Wr$ = 0.3 m | $h_u$ = 0.3–0.36 m | 0.3 m | EPFL, Lausanne, Switzerland | 2009 | Free surface at selected times | Video camera (45 fps) | ✗ | |

**Table 7.** *Cont.*

| (1) Reference | (2) Dam-Break Type | (3) Setup Characteristics [1] | (4) Initial Conditions [2] | (5) Breach Width | (6) Laboratory | (7) Year | (8) Measured Data | (9) Measuring Technique [3] | (10) Data [4] | (11) Numerical Simulation [5] |
|---|---|---|---|---|---|---|---|---|---|---|
| Brondani Minussi and de Freitas Maciel [304] | Total; dry bottom; viscoplastic (Herschel–Bulkley) fluid (Carbopol 940, different concentrations) | Rectangular channel $L$ = 1.91 m, $W$ = 0.32 m, $Lr$ = 0.5 m, $S$ = 0; smooth | $h_u$ = 0.07, 0.1, 0.13 m | 0.32 m | Paulista State University, Ilha Solteira, Brazil | 2012 | Free surface at selected times; wave front position | Video camera | ✗ | 2D NSE, VOF FV |
| Bates and Ancey [305] | Total; dry bottom; viscoplastic (Herschel–Bulkley) fluid; contact with a stationary layer of the same fluid | Rectangular channel $L$ = 3.5 m, $W$ = 0.1 m, $Lr$ = 0.3 m; $S$ = 12°, 16°, 20°, 24°; smooth | Fluid mass: 3 kg | 0.1 m | EPFL, Lausanne, Switzerland | 2017 | Wave front position; water surface profiles; velocity field | PIV; video cameras | ✓ | 1D (lubrification theory) GM |
| Jing et al. [306] | Total; dry bottom; mudflow (three different grain sizes) | Rectangular channel $L$ = 6 m, $W$ = 0.3 m; $S$ = 0.02; smooth Reservoir $Lr$ = 2 m, $Wr$ = 0.6 m | $h_u$ = 0.30 m | 0.3 m | University of Mining and Technology, Beijing, China | 2019 | Flow depth, velocity and pressure hydrographs at four locations | Video cameras (300 fps); pressure sensors | ✗ | |
| Modolo et al. [307] | Total; dry bottom; Bingham fluid (different solutions) | Tank $L$ = 1.52 m, $W$ = 0.05 m, $Lr$ = 0.4 m, S = 0; smooth and rough | $h_u$ = 0.24 m | 0.05 m | Federal University of Rio de Janeiro, Brazil | 2019 | Flow images; flow depth profiles at selected times | Video camera; PIV | ✗ | |
| Tang et al. [308] | Total; dry bottom; mud flow (Herschel–Bulkley fluid) | Rectangular channel $L$ = 3 m, $W$ = 0.23 m, $Lr$ = 0.48 m, $S$ = 0, 5°, 10°; smooth | Mud volume: 38.6, 36.3, 34 l | 0.23 m | Sichuan University, Chengdu, China | 2022 | Flow depth and bottom pressure hydrographs at two locations | Pressure sensors; laser sensors | ✗ | 2D NSE, VOF FD |

Note(s): [1] $L$ = facility length; $W$ = facility width; $Lr$ = reservoir length; $Wr$ = reservoir width (if different from $W$); $S$ = bottom slope; [2] $h_u$ = upstream water depth; $h_d$ = downstream water depth; [3] PIV = particle image velocimetry; [4] ✗ = not freely available; ✓ = freely available; [5] Approach: 1D = one-dimensional; 2D = two-dimensional–Mathematical model: NSE = Navier–Stokes equations; SWE = shallow water equations; VOF = volume of fluid–Numerical method: FD = finite difference; FV = finite volume; GM = Galerkin method; N.A. = not available.

**Table 8.** Experimental investigations of dam-breaks in cascade reservoirs.

| (1) Reference | (2) Dam-Break Type | (3) Setup Characteristics [1] | (4) Initial Conditions [2] | (5) Breach Width | (6) Laboratory | (7) Year | (8) Measured Data | (9) Measuring Technique [3] | (10) Data [4] | (11) Numerical Simulation [5] |
|---|---|---|---|---|---|---|---|---|---|---|
| Yang et al. [309] | Two total dam-breaks; three different distances between the two dams (7.8, 9.8, 11.8 m); dry bottom | Rectangular channel $L$ = 20 m, $W$ = 0.5 m, $S$ = 12°; smooth | $h_u$ = 0.184–0.531 m | 0.5 m | Sichuan University, Chengdu, China | 2011 | Water depth hydrographs in 10 positions | Water probes; high resolution camera | ✗ | |
| Chen et al. [310] | Total dam-break; pressure load on a downstream dam; dry bottom | Upstream reservoir $Lr$ = 2 m, $Wr$ = 0.4 m, $S$ = 0 Rectangular channel $L$ = 10 m, $W$ = 0.4 m $S$ = 4, 8, 12°; smooth | $h_u$ = 0.1–0.3 m (upstream reservoir); $h_d$ = 0–0.3 m (downstream reservoir) | 0.4 m | Sichuan University, Chengdu, China | 2014 | Pressure hydrographs 20 positions at five different elevations on the downstream dam | Pressure sensors | ✗ | |
| Liu et al. [311] | Two total dam-breaks; dry bottom (dam height: 0.4 m) | Reservoirs $Lr$ = 2 m, $W$ = 0.8 m Rectangular channel $L$ = 12 m, $W$ = 0.4 m, $S$ = 1/12.5, smooth; | $h_{u1} = h_{u2}$ = 0.3 m (downstream dam breaks 0, 2, 4 s after the upstream one); $h_{u1} = h_{u2}$ = 0.2 m (downstream dam breaks due to overtopping) | 0.4 m | Changjiang River Scientific Research Institute, Wuhan, China | 2017 | Water depth hydrographs at six locations | Ultrasonic distance meters | ✗ | |

**Table 8.** *Cont.*

| (1) Reference | (2) Dam-Break Type | (3) Setup Characteristics [1] | (4) Initial Conditions [2] | (5) Breach Width | (6) Laboratory | (7) Year | (8) Measured Data | (9) Measuring Technique [3] | (10) Data [4] | (11) Numerical Simulation [5] |
|---|---|---|---|---|---|---|---|---|---|---|
| Zhang and Xu [312] | Three dams; total break of the upstream dam; dry bottom; retarding effects of an intermediate intact dam (dam height: 0–0.6 m) | Upstream reservoir $Lr$ = 2.97 m, $Wr$ = 1.93 m Rectangular channel $L$ = 20 m, $W$ = 0.5 m, $S = 12^{\circ}$, smooth; | $h_u$ = 0.1–0.3 m (upstream dam); $h_u$ = 0.1–0.5 m (downstream dam); $h_u$ = 0–0.6 m (intermediate dam) | 0.5 m | Sichuan University, Chengdu, China | 2017 | Pressure time series on the face of the intermediate dam; flow images | Pressure sensors; video cameras | ✓ | |
| Luo et al. [313] | Two dams; total break of the upstream dam; dry bottom; flow in the downstream reservoir | Rectangular channel $L$ = 10 m, $W$ = 0.4 m, $S = 4^{\circ}$; smooth | $h_u$ = 0.2 m (upstream dam); $h_u$ = 0.15, 0.3 m (downstream dam) | 0.4 m | Sichuan University, Chengdu, China | 2019 | Flow images; water depth and pressure hydrographs at three points | N.A | ✗ | 3D NSE SPH |
| Luo et al. [313] | Three dam-breaks; dry bottom | Rectangular channel $L$ = 15.6 m, $W$ = 0.5 m, $S = 4^{\circ}$; smooth | $h_u$ = 0.5 m (upstream dam); $h_u$ = 0.5 m (downstream dams) | 0.5 m | Sichuan University, Chengdu, China | 2019 | Flow images; water depth hydrograph at six points | N.A | ✗ | 3D NSE SPH |
| Kocaman and Dal [314] | Two dams; total break of the upstream dam on the reservoir of the downstream one; overtopping of the downstream dam | Rectangular channel $L$ = 2.5 m, $W$ = 0.25 m, $Lr$ = 0.75 m (both dams) $S$ = 1/5, smooth | $h_u$ = 0.15 m (both dams) | 0.25 | Iskenderun Technical University, Turkey | 2020 | Water depth hydrographs; images of the free surface profiles | Video cameras (120 and 50 fps) | ✗ | 3D NSE SPH |

Note(s): [1] $L$ = facility length; $W$ = facility width; $Lr$ = reservoir length; $Wr$ = reservoir width (if different from $W$); $S$ = bottom slope; [2] $h_u$ = upstream water depth; $h_d$ = downstream water depth; [3] –; [4] ✗ = not freely available; ✓ = freely available; [5] Approach: 3D = three-dimensional–Mathematical model: NSE = Navier–Stokes equations–Numerical method: SPH = smoothed particle hydrodynamics; N.A. = not available.

**Table 9.** Experimental investigations of dike-break induced flows on a lateral floodplain.

| (1) Reference | (2) Dike-Break type | (3) Setup Characteristics [1] | (4) Initial Conditions [2] | (5) Breach Width | (6) Laboratory | (7) Year | (8) Measured Data | (9) Measuring Technique [3] | (10) Data [4] | (11) Numerical Simulation [5] |
|---|---|---|---|---|---|---|---|---|---|---|
| Bechteler et al. [315] | Sudden trapezoidal opening (1V:1.11H slope) | Rectangular channel $L$ = 30 m, $W$ = 2 m, $S$ = 0 Floodplain $L$ = 5 m, $W$ = 10 m, $S$ = 0; smooth | $h_u$ = 0.2 m | 0.5 m | University of German Federal Armed Forces, Munich Germany | 1992 | Pressure hydrographs at 29 locations; flooded area perimeter | Pressure transducers; video camera | ✗ | 2D SWE FV ($n = 0.001$ s m$^{-1/3}$) |
| Liem and Köngeter [316] | N.A. | Rectangular channel $L$ = N.A., $W$ = N.A., $S$ = N.A. Floodplain $L$ = 8.5 m, $W$ = 3.5 m, $S$ = 0.05; smooth | N.A. | 0.6 m | Aachen University of Technology, Germany | 1999 | Water levels hydrographs in 72 points; front wave propagation | Electrode system; capacity sensors | ✗ | ($n = 0.01$ s m$^{-1/3}$) |
| Aureli and Mignosa [317,318] | Sudden opening | Rectangular channel $L$ = 10 m, $W$ = 0.3 m, $S$ = 0.001 Floodplain $L$ = 1.5 m, $W$ = 2.6 m; smooth | Steady flow 5–15 l/s | 0.28 m | University of Parma, Italy | 2002 | Water depth hydrographs at nine locations; transverse velocity profiles; discharge flowing through the breach | Ultrasonic distance meters; ADV; triangular weir | ✗ | 2D SWE FD ($n = 0.01$ s m$^{-1/3}$) |
| Sarma and Das [319] | Sudden opening | Compound channel $L$ = 9.2 m, $W$ = N.A., $S$ = N.A. Floodplain $L$ = 2 m, $W$ = 2.5 m, $S$ = 0; smooth | N.A. | N.A. | Indian Institute of Technology, Guwahati, India | 2003 | Wave front in the flooding plane at three times | N.A. | ✗ | ($n = 0.013$ s m$^{-1/3}$) |
| Briechle et al. [320]; Briechle [321]; Harms et al. [322] | Sudden opening | Rectangular channel $L$ = N.A., $W$ = 1 m, $S$ = N.A. Floodplain $L$ = 3.5 m, W = 4 m, $S$ = N.A.; smooth | Steady flow: 300 l/s $h_u$ = 0.3–0.5 m | 0.5 m | Aachen University of Technology, Germany | 2004 | Water depth hydrographs; wave front position and velocity | Ultrasonic distance meters; Video cameras (>50 fps) | ✗ | 2D SWE DG ($n = 0.0083$ s m$^{-1/3}$) |

**Table 9.** *Cont.*

| (1) Reference | (2) Dike-Break type | (3) Setup Characteristics [1] | (4) Initial Conditions [2] | (5) Breach Width | (6) Laboratory | (7) Year | (8) Measured Data | (9) Measuring Technique [3] | (10) Data [4] | (11) Numerical Simulation [5] |
|---|---|---|---|---|---|---|---|---|---|---|
| Oertel and Schlenkhoff [323]; Oertel [324] | N.A. | Rectangular channel $W \approx 0.6$ m Floodplain $L = 4$ m, $W = 5.6$ m, $S = 0$; smooth | N.A. | 0.5 m | Bergische University Wuppertal, Germany | 2008 | Water depth contour maps | Ultrasonic distance meters | ✗ | |
| Roger et al. [325] | Sudden opening | Rectangular channel $L$ = N.A., $W = 1$ m, $S$ = N.A. Floodplain $L = 4$ m, $W = 3.5$ m, $S = 0$; smooth | Steady flow: 100–300 l/s $h_u = 0.3$–$0.5$ m | 0.3–0.7 m | Aachen University of Technology, Germany | 2009 | Surface profiles at different times; breach discharge | Ultrasonic distance meters; LDA | ✗ | 2D SWE DG, FV ($n = 0.005$–$0.02$ s m$^{-1/3}$) |
| Sun et al. [326] | Sudden breaching | Rectangular channel $L = 40$ m, $W = 1$ m, $Lr = 15.5$ m Floodplain $L = 25$ m, $W = 2.5$ m, $S = 0$; smooth | Steady flow: 80 l/s | 1 m | University of Tsinghua, Beijing, China | 2017 | Water depth and flow velocity hydrographs at several locations; | Pressure gauges; ADV | ✗ | 2D SWE FD ($n = 0.012$ s m$^{-1/3}$) |
| Al-Hafidh et al. [327] | Sudden breaching | Rectangular channel $L = 11$ m, $W = 0.4$ m, $S = 0$ Floodplain $L = 1.83$ m, $W = 4.87$ m; smooth | Different inflow hydrographs | 0.2, 0.4, 0.8 m | University of South Carolina, USA | 2022 | Water depth hydrographs at eight locations | Ultrasonic distance meters | ✗ | |
| Yoon et al. [328] | Gradual trapezoidal breaching (sliding opening) 1V:0.3H | Rectangular channel $L = 30$ m, $W = 5$ m, $S = 0$; Floodplain $L = 25$ m, $W = 30$ m; smooth | $h_u = 0.3, 0.35, 0.4, 0.45, 0.5, 0.55$ m | 0.5, 1, 1.5, 2, 2.5, 3 m | Institute of Civil Engineering and Building Technology, Korea | 2022 | Water depth hydrographs; propagation of the wave front | Wave height meters | ✗ | |

Note(s): [1] $L$ = facility length; $W$ = facility width; $Lr$ = reservoir length; $Wr$ = reservoir width (if different from $W$); $S$ = bottom slope; [2] $h_u$ = water depth in the channel; [3] ADV = acoustic Doppler velocimeter; LDA = laser Doppler anemometer; [4] ✗ = not freely available; [5] Approach: 2D = two-dimensional–Mathematical model: SWE = shallow water equations–Numerical method: DG = discontinuous Galerkin; FD = finite difference; FV = finite volume–$n$ = Manning roughness coefficient; N.A. = not available.

**Table 10.** Experimental investigations of collapses of storage tanks and bunds or dike overtopping.

| (1) Reference | (2) Dam-Break Type | (3) Setup Characteristics [1] | (4) Initial Conditions [2] | (5) Bund Characteristics | (6) Laboratory | (7) Year | (8) Measured Data | (9) Measuring Technique [3] | (10) Data [4] | (11) Numerical Simulation [5] |
|---|---|---|---|---|---|---|---|---|---|---|
| Greenspan and Johansson [329] | Total and partial (orifice over a 30° arc: 0.0254 m wide, $h = 0.076$ m high); dry bottom | Cylindrical tank $D = 0.19$ m, $S = 0$; smooth | $0.05 \text{ m} < h_u < 0.22$ m | Circular: bund radius = 0.127, 0.178, 0.229, 0.279 m; bund inclination = 30°, 60°, 90°; bund height = 0.033, 0.038, 0.051, 0.064 m | Massachusetts Institute of Technology, USA | 1981 | Overtopping fraction (as a function of the dike characteristics) | Needle depth gauge; video camera | ✗ | |
| Sharifi [330] | Total; dry bottom; three configurations: unconfined flow, barrier flow, and confined flow (wall height = $0.25h_u$) | Cylindrical tank $D = 0.087$ m, $S = 0$; smooth | $h_u = 0.5D$, $0.75D$, $D$ | Circular: bund radius = 0.175, 0.24, 0.258, 0.3, 0.34 m; bund inclination = 40°, 90° bund height = 0.022, 0.032, 0.044 0.065 m | Imperial College of Science and Technology, London, UK | 1987 | Water depth hydrographs at eight positions; wave front propagation | Light-sensitive photodiodes; video camera (128 fps) | ✗ | |
| Maschek et al. [331] | Total; dry and wet bottom; symmetric and asymmetric water column (off-centeredness = 0.055, 0.0825, 0.11 m); effect of obstacles in the flow: rings, rods, and particles | Cylindrical tanks Inner $D = 0.11, 0.19$ m; Outer $D = 0.44$ m; $S = 0$; smooth | $h_u = 0.05, 0.1, 0.2, 0.22, 0.23$ m $h_d = 0, 0.01, 0.03, 0.05, 0.1$ m | Circular: bund height = 0.02, 0.03 m | Karlsruhe Nuclear Research Centre, Germany | 1992 | Arrival time at the wall; time of maximum height; maximum height at the container wall; time of maximum height; maximum height at pool center | Video camera | ✗ | |

**Table 10.** *Cont.*

| (1) Reference | (2) Dam-Break Type | (3) Setup Characteristics [1] | (4) Initial Conditions [2] | (5) Bund Characteristics | (6) Laboratory | (7) Year | (8) Measured Data | (9) Measuring Technique [3] | (10) Data [4] | (11) Numerical Simulation [5] |
|---|---|---|---|---|---|---|---|---|---|---|
| Cleaver et al. [332]; Cronin and Evans [333] | Total; dry bottom; different bunding arrangements; impact on an additional cylindrical tank ($D$ = 3.5 m) | Quarter of cylinder tank $D$ = 3.5 m; $S$ = 0; smooth | $h_u$ = 1.45, 1.6, 1.75 m | Circular: bund radius = 5, 7.1, 10 m; bund inclination = 30°; 45°, 90°; bund height = 0.05, 0.1, 0.2 m; Square: bund distance = 6.27, 4.43, 8.89 m; bund inclination = 90°; bund height = 0.05, 0.2 m | Advantica Technologies Ltd. (for Health and Safety Executive), Loughborough, UK | 2001 | Time of water arrival at 60 positions; water head in the tank; overtopping volume | Video camera (125 fps); pressure transducer; depth resistance probes; calibrated container | ✗ | |
| Atherton [334] | Total; dry bottom; different bunding arrangements | Quarter of cylinder tank, $D$ = 0.6 m; $S$ = 0; smooth | $h_u$ = 0.12, 0.3, 0.6 m | Circular: bund radius = 0.315–1.9 m; bund inclination = 90°; bund height = 0.006–0.72 m; Triangular and Rectangular: bund distance = 0.441, 1.247 m; bund inclination = 90°; bund height = 0.012, 0.12 m | Liverpool John Moores University, UK | 2005 | Dynamic pressure vertical profiles on the bund; wave heights; fluid mass overtopping the bund | Piezotronic pressure transducers; resistive wave gauges; water balance; video camera | ✗ | |
| Atherton [335] | Partial; (orifice: 0.019–0.084 m diameter; slot: 0.157 m wide, 0.007–0.18 m high) | Quarter of cylinder tank, $D$ = 0.6 m; $S$ = 0; smooth | $h_u$ = 0.12, 0.3, 0.6 m | Circular: bund radius = 0.497–1.407 m; bund inclination = 90°; bund height = 0.006–0.24 m | Liverpool John Moores University, UK | 2008 | Dynamic pressure vertical profiles on the bund; wave heights; fluid mass overtopping the bund | Piezotronic pressure transducers; resistive wave gauges; water balance; video camera | ✗ | |
| Zhang et al. [336] | Total; dry bottom; straight and curved dikes | Cylindrical tank $D$ = 0.1, 0.2 m; $S$ = 0; smooth | $h_u$ > 0.3 m (for $D$ = 0.1 m); $h_u$ > 0.2 m (for $D$ = 0.2 m) | Circular: bund radius = 0.1–0.15 m; bund inclination = 90°; bund height = 0.022-0.051 m; Square: bund distance (equivalent radius) = 0.11–0.23 m; bund inclination = 90°; bund height = 0.022–0.045 m | Mary Kay O'Connor Process Safety Center, Texas A&M University, USA | 2017 | Fluid mass overtopping the bund | Balance; video camera | ✗ | |
| Zhang et al. [336] | Total; dry bottom; straight and curved dikes | Cylindrical tank $D$ = 0.229 m; $S$ = 0; smooth | $h_u$ = 0.5 m | Square: bund distance (equivalent radius) = 0.516 m; bund inclination = 90°; bund height = 0.08–0.098 m | Mary Kay O'Connor Process Safety Center, Texas A&M University, USA | 2017 | Fluid mass overtopping the bund | Balance; video camera | ✗ | |
| Megdiche [337] | Total and partial (slot: 0.157 m wide, 0.018–0.09 m high); dry bottom; different bunding arrangements; viscous fluid (olive oil) | Quarter of cylinder tank, $D$ = 0.6 m; $S$ = 0; smooth | $h_u$ = 0.12, 0.3, 0.6 m | Circular: bund radius = 0.497–1.9 m; bund inclination = 90°; bund height = 0.03–0.72 m; Triangular, square, and rectangular: bund distance = 0.324–1.095 m; bund inclination = 90°; bund height = 0.012, 0.12 m | Liverpool John Moores University, UK | 2018 | Dynamic pressure vertical profiles on the bunds; wave heights; fluid mass overtopping the bund | Piezotronic pressure transducers; resistive wave gauges; water balance, video camera | ✗ | 3D RANS, VOF FV |
| Zhao et al. [338] | Total; dry bottom; bunds with different shapes, inclinations and breakwaters | Cylindrical tank $D$ = 0.27 m; $S$ = 0; smooth | Various tank filling ratios | Circular: bund radius = 0.272 m; bund inclination = 45°, 60°, 90°, 120°; bund height = 0.1 m; Square: (0.483 m × 0.483 m) and rectangular (0.341 m × 0.683 m): bund inclination = 45°, 60°, 90°, 120°; bund height = 0.1 m | Nanjing Tech University, China | 2022 | Dynamic pressure time series at selected points on the bunds overtopping fraction | Pressure sensors; balance; video camera | ✗ | 3D RANS, VOF FV |

Note(s): [1] $D$ = diameter of the cylindrical tank; $S$ = bottom slope; [2] $h_u$ = upstream water depth; $h_d$ = downstream water depth; [3] –; [4] ✗ = not freely available; [5] Approach: 3D = three-dimensional–Mathematical model: RANS = Reynolds-averaged Navier–Stokes equations; VOF = volume of fluid–Numerical method: FV = finite volume; N.A. = not available.

## 3. Discussion and Advances

Tables 1–10 show the considerable amount of experimental investigations performed, covering a broad spectrum of dam-break flow conditions. The first laboratory tests dated back even more than 100 years ago [19,20], but more than 70% of the dam-break experiments reviewed here were carried out in the last 20 years, suggesting an increasing interest worldwide in experimental research on dam-break flows.

Basic features of dam-break flows (wave profile, wavefront motion, etc.) have been the most investigated, especially in the past, as indicated by Table 1. To this end, capacitive or resistive probes and pressure gauges were used in most investigations before 2000. The former probes are very easy to implement in laboratory facilities, but they are intrusive devices locally disturbing the flow [150]. Accordingly, non-intrusive pressure gauges or ultrasonic distance meters have sometimes been preferred (e.g., [46,95,207]), even if they may show spurious dynamic oscillations in fast transient flows, especially when the slope of the free surface is high [207]. The limitation of such gauges is that they provide a local flow depth measure. Therefore, since earlier times, there has been an interest in measurements over extended areas of the flow. Martin and Moyce [23] and Dressler [13] were pioneers in using video cameras to record images of a dam-break flow from which quantitative information about the wave motion, especially wave profiles at fixed times, can be extracted. In particular, Dressler [13] used five electrically synchronized cameras with an impressive acquisition speed for the time (1800 frames per second). Experimental wave profiles are of utmost relevance to understanding the characteristics of the flow and verifying the capability of the classic analytical solutions of the dam-break problem (i.e., Ritter's [339] and Stoker's [340] solutions) or numerical solutions of dam-break models to predict the dam-break wave profile (e.g., [52,76]). Recent optical and image-processing techniques overcome the limitations of the punctual gauges and the cumbersome post-treatment of analogic video records, allowing for the accurate non-intrusive measurement of the free surface on an area of selected extension with a suitable time rate [4].

In addition to the wave profile, the velocity field is a flow characteristic of interest in dam-break experiments. Earlier investigations focused only on the wavefront velocity, tracking its position on flow images (e.g., [26,29]). Local flow velocity has often been measured using acoustic Doppler velocimetry (ADV) [186], despite the disturbances induced by the measuring device on the flow. Moreover, the fast variation in time of the free-surface elevation implies that the probe's position below the free surface does not remain constant, making it difficult to interpret the measures [186]. Velocity fields are efficiently measured on selected regions of the flow using non-intrusive imaging techniques (e.g., particle imaging velocimetry-PIV or particle tracking velocimetry-PTV) based on the tracking of particles floating on the flow surface [245] or buoyant within the flow [82]. The measurement of the surface velocity field provides insight into the flow features because it allows the reconstruction of flow trajectories on the flow surface. Moreover, surface velocities are a good approximation of depth-averaged flow velocities in fast transient shallow flows, where the turbulent velocity profile is not yet established. The measurement of the vertical velocity field (e.g., [82]) further enhances the understanding of the flow dynamics allowing the validity of the basic assumptions of the numerical simulation tools to be checked.

Experimental investigations on the effect of geometrical singularities and the impact of dam-break flows against obstacles have gradually taken hold alongside research on basic features of the dam-break flow. Experiments listed in Table 2 concern flows in more complex geometries than a simple straight channel due to the presence of contractions, bottom sills, bends, etc. The variety of cases reported in Table 2 demonstrates the need for an in-depth understanding of complex flow features generated by geometric singularities, each isolated in well-defined experimental situations. Accordingly, such test cases should not be considered scale physical models of real situations but prototype cases highlighting specific flow features. The availability of experimental data allows for modelers to check the treatment of each type of singularity in numerical models. The key challenge for new numerical approaches is indeed to reproduce the effects of the geometric singularities in the best possible way, especially in the context of shallow water models, because most of the considered singularities induce local deviations from the hydrostatic pressure assumption.

Table 3 reports test cases and laboratory investigations of the effects of isolated obstacles or structures on a dam-break flow. The experimental analysis of such situations is of practical interest. Indeed, natural and artificial obstacles are commonly present in real-field applications, and flooding propagation in flood-prone areas can be strongly influenced by such singularities, which may act as barriers to the flow. Obstacles of different sizes, shapes, and orientations were considered in the dam-break experiments. Prismatic blocks, vertical columns (of a square, rectangular, circular, but also pyramidal shape [187]), and solid walls (simulating protective barriers) were mainly used as obstacles, but occasionally also bridge models [214,218,222]. Furthermore, the obstacle's position and distance from the gate are crucial to defining the test conditions. A few tests involved obstacles overtopped by the flow [87,236] or deformable structures [217,225], which induce complex flow features and wave-structure interactions, respectively. Moreover, the impact of the dam-break wave against a structure was investigated in detail by some studies (e.g., [215]). Other applications concern the effect of mitigation walls placed in front of model structures for protection purposes [208,210] or the performance of new flood protection structures [242]; others concern permeable structures (i.e., buildings with openings [221,266] or perforated walls [229], and even the presence of movable obstacles carried away by the flow [240,258]. Despite this variety of cases investigated in the literature, the experimental analysis of flood scenarios in which a structure is destroyed by the flow is lacking. Flow depth and velocity were typically measured at selected locations to describe the features of the flow, especially near the obstacles (e.g., [186]). In recent years, the use of imaging techniques to capture wave propagation and measure the free surface over an extended area (e.g., [63,207]) has become widespread. The hydrodynamic load acting on the whole structure (e.g., [215,223]) or impact pressures at selected gauge points on the structure faces (e.g., [218,228]) were also measured. These data are valuable for the validation of numerical models used for evaluating hydrodynamic forces and other hydraulic variables useful for the structural design and verification of structural reliability.

Flood inundation of urban areas (possibly induced by a dam-break or a tsunami invading a city) is a research topic that arouses considerable interest nowadays due to the high exposure of residential or industrial settlements close to waterways, dams, or coastal areas [341,342]. Table 4 lists the studies on urban flooding conducted through experimental modelling. In these models, dam-break experiments were performed using idealized urban districts constituted by arrays of solid blocks with different configurations and orientations, which simulate the idealized layouts of buildings and cannot be considered scale models of existing urban areas [245]. Complex flow processes occur in these experiments, with multiple flow paths (dictated by the arrangement of buildings and streets) and high flow velocities. Hydraulic variables describing flow dynamics and directly involved in flood impact assessment were typically measured. Accordingly, flow depth and velocity time series were usually provided at selected locations both inside and around the city layout (e.g., [245,252,253]). Moreover, the measurement of hydrodynamic loads on buildings has received less attention [59]. More insight into urban flooding could come from considering quasi-realistic urban district models [255], taking into account additional events associated with urban floods [342], such as the penetration of water into buildings through openings [221], the flow exchange between the streets and the sewer system, the transport of cars or urban debris [249], and the diffusion of pollutants. Experimental data from such experiments would better support the validation of urban flood simulation models, which have become increasingly sophisticated in recent years [341]. Among these numerical models, the coarse-grid ones (for example based on the porosity approach [248,252]) can provide accurate results preserving computational efficiency. Models of that type require such experiments in an idealized urban environment for their validation.

Wave runup prediction on sloping beaches is one of the main concerns in the swash zone studies. Wave runup and overtopping on coastal structures have historically been investigated through physical models, since storm waves occur infrequently, and field measurements are expensive and difficult during storms. Laboratory investigations of waves normally incident on structures and beaches were usually conducted in wave flumes. More in-depth investigations of the wave dynamics require large basins equipped with more complex and expensive facilities due to the nearshore non-uniformity. In laboratory investigations, a single bore was often generated by lifting a gate separating the initially quiescent water on the beach from the deeper water behind the gate, exploiting the strict similarity between tsunami and dam-break waves. Table 5 includes only experiments in which single bores were generated through a dam-break. In addition to basic investigations of the characteristics of waves propagating on simple sloping beaches, advanced ones considered the presence of vegetation, moving objects, wharves, overtoppable or insubmersible structures, floating tanks, bridges, crossing canals, vertical walls, or composite bathymetries. Flow depth hydrographs and velocity profiles at selected positions were often measured, as well as the wavefront position in time and the maximum run-up height, thanks to the analysis of images acquired through video cameras. Wave profiles at selected times were measured less frequently (e.g., [283]). Time series of pressure and force against structures hit by the bore were measured in several studies (e.g., [269,274]), whereas data related to overtopping phenomena are seldom recorded [270]. Only a few works focused on bottom shear stress data, flow vortices behind structures, and phenomena related to moving objects transported by the flow (e.g., [277,278]).

Vessels and offshore structures can be affected by extreme waves causing green water run-up and wave impingement, with consequent extensive damage and failure to superstructures, deck plating, hatches, and topside equipment. Moreover, green water represents a serious concern for the safety of personnel. In past years, a significant resemblance was recognized between the green water event and dam-break flow [343]. Therefore, as shown by Table 6, many studies applied the dam-break theory to green water predictions [344], and the use of dam-break solutions has become the standard design analysis approach to estimate the front velocity in green water phenomena. For at least two decades, researchers have tried to obtain experimental data useful for the validation of theories and numerical codes through laboratory investigations of green water phenomena caused by dam-breaks (e.g., [287,343,345]), taking advantage of the relative simplicity of dam-break setups. Conditions characterized by different freeboards were usually considered. The interaction between a dam-break flow and a floating box was also investigated [294]. Loads and pressures exerted on structures are of primary interest in such applications and were acquired through force and pressure transducers, respectively. Moreover, measures of free surface elevation at selected positions were often performed using conventional wave probes. In recent years, the availability of high-speed video cameras has allowed a more in-depth investigation of the initial phases of the phenomenon (e.g., [291,292]).

The dam-break flow of non-Newtonian fluids has recently received considerable attention due to environmental and industrial applications, such as the flood hazard assessments associated with tailings dam failures. Experimental data are even more valuable given the complex rheological behavior of such fluids and the scarcity of analytical solutions available. As shown in Table 7, experiments were conducted in simple laboratory facilities (planforms or rectangular channels), sometimes with steep bottom slopes [302]. Typically, the liquids used were aqueous suspensions or mudflows with viscoplastic behavior, but also Bingham fluids are used [307]. Moreover, the test conditions usually considered are characterized by a total dam-break and dry downstream bottom, with few exceptions [64,303]. Non-intrusive imaging techniques were preferably used to record data.

Table 8 lists experimental investigations of dam-break flows in cascade reservoirs. This line of research has recently been developed, motivated by the significant number of cascade dams built in recent years along several rivers. In this case, the channel bottom downstream of the dam is always assumed to be dry in the experiments. The influence of the initial reservoir levels and the distances between the dams are analyzed to highlight the attenuation effect on the dam-break flood in case the downstream dam does not fail. Flow depths time series were typically measured at selected positions. Sometimes, pressure time series were recorded on the upstream face of the dam hit by the flood wave [310]. Numerical simulations accompanying the experimental investigations were usually performed through 3D models.

In experimental investigations of a dike-break induced flow presented in Table 9, the laboratory facilities consisted of an initially dry, smooth lateral floodplain linked to a straight main channel. A gate on the side wall of the channel was lifted to simulate the dike failure and induce the flooding of the lateral floodplain. In most cases, the gate opening was sudden, and the breach was rectangular or trapezoidal. Seldom was the gate removed gradually to represent the typical progressive failure of earth-fill embankments [328]. The flow in the main channel was typically assumed to be steady, even if a river embankment realistically fails during a flood event [327]. The wavefront propagation and flood depth time series at different positions in the floodplain were usually measured with non-intrusive devices. The experimental data acquired are particularly useful for validating 2D depth-averaged numerical models.

Dangerous liquids for industrial applications are often stored in large tanks built above ground. The failure of such storage tanks can lead to disastrous consequences for people, assets, and the surrounding environment, due to the sudden and uncontrolled release of large volumes of impounded materials, sometimes potentially flammable. Many major incidents occurred in recent years due to natural disasters, atmospheric phenomena, maintenance or operational errors, equipment failures, or corrosion [337]. A containment system formed by dikes or bunds is crucial (and required by technical regulations) to mitigate the risk associated with these catastrophic events. The bund system must be designed to prevent massive liquid overflow and withstand the dynamic pressures generated by the wave impact. Table 10 shows that in the past 40 years, several experimental studies have dealt with the problem of predicting the bund overtopping fraction as a function of the level of the impounded liquid, as well as the bund shape and characteristic parameters (distance from the tank, height, inclination, presence of breakwaters, etc.). To this end, small-scale experimental investigations have typically been conducted in dam-break setups by suddenly releasing fixed volumes of water or oil stored in cylindrical or quarter-cylinder-shaped tanks. Few medium-scale experimental investigations have so far been conducted [332,333]. Sometimes, the liquid release resulting from the opening of fractures or holes in the tank walls is considered [335]. In recent years, computational fluid dynamics (CFD) has increasingly been used in this context, since it gives the possibility to study in detail the phenomenon. The accuracy of the CFD models is assessed through validation against experimental data [337,338].

In over half of the total entries of Tables 1–10, a numerical analysis was coupled with the laboratory investigation, and the experimental data were immediately used to validate the numerical models. The information about those numerical simulations provided in Column 11 of the tables indicates that the most adopted solution approach is the two-dimensional one (approximately 50% of cases); the one- and three-dimensional approaches are equally adopted in about 25% of cases. One- and two-dimensional numerical models are usually based on the depth-averaged shallow water equations (SWE), while three-dimensional models on the Reynolds averaged Navier–Stokes equations (RANS), coupled with the volume of fluid (VOF) technique for the tracking of the free surface. In the examined studies, the most used numerical method for the solution of the governing equations is the finite volume method (over 50% of cases), followed by the finite difference method (over 20% of cases, especially before 2000). The mesh-free particle methods, such as the smoothed-particle hydrodynamics (SPH) and the moving particle semi-implicit (MPS) ones, have spread rapidly more recently and were used in about 15% of the cases considered.

The impact of scale effects in open channel flow physical models deserves special attention [346,347]. Some analyses in the literature have confirmed that the Froude number is dominant in dam-break flows over a fixed bed (e.g., [150]). However, the validation of numerical simulation tools designed for real applications against small-scale laboratory tests must take into account the distortions introduced by the scale effects.

In all experiments listed in the previous tables, the waves were generated by the sudden removal of a gate. In most cases, a lift gate moving upward is used, but there are also examples of downward-moving lift gates [82] or flap gates (e.g., [104]). Experimental and numerical studies have compared gate-opening modalities, investigating the gate motion effect on the dam-break flow [105,348]. However, none of these systems mimics exactly the instantaneous disappearance of the gate assumed in the classic theoretical approach to the dam-break problem, nor a real dam collapse. Technical regulations on dam-break flood risk assessment adopted worldwide prescribe that the structural failure of concrete gravity and arch dams is assumed to occur practically instantaneously (e.g., [349,350]). If this assumption is made, the gate opening time in dam-break experiments should be short enough to represent a 'nearly-instantaneous' dam collapse. To this end, suitable criteria for the gate opening timing have been presented in the literature [50,351] and are usually checked at the beginning of the experimental investigations. However, in the hydraulics laboratory, the question of the 'instantaneous' removal of the gate (or of the actual non-presence of the gate itself) remains a subject of debate, and often suggestive and imaginative hypotheses are formulated in the breaks between the experimental tests to remove the gate as quickly as possible.

The large number of articles reviewed here demonstrates that an impressive amount of experimental work has been carried out on dam-break flows, considering a variety of test conditions covering a wide range of flow situations. Many aspects of the physical process having practical implications have been investigated, including the effects of obstacles and structures that interfere with the flow. Nevertheless, the dam-break flow remains a topic of current research that continues to attract considerable interest, also from an experimental point of view [352]. Non-intrusive techniques appear preferable in dam-break flow measurements as they do not disturb the flow. In particular, digital imagery enables the acquisition of flow data (such as free surface profiles or flow depth and velocity fields at selected times) over an extended area, but requires optical access and often free surface seeding or the use of a coloring agent, as well as laborious calibration procedures [4].

The literature review shows that no systematic experimental investigations have been conducted on floods caused by a partial dam collapse in the vertical direction, producing a breach in the upper portion of the dam. To the authors' knowledge, this dam-break scenario was only hypothesized in a historical study based on a physical model [5,353]. Therefore, it could be considered for future research to collect experimental data to support the development of hybrid 3D-2D numerical models simulating the breach outflow with a 3D model and the downstream flooding with a depth-averaged 2D model (e.g., [354]). Furthermore, the movement of the pieces of a breached dam within the flow has never been experimentally studied since the release of the impounded water is usually simulated by removing (and not breaking) a retaining plate. This aspect related to the collapse of a concrete or masonry dam could also be the subject of future experimental research; after all, the modeling capabilities of current CFD software include the possibility of handling moving objects which dynamically interact with the flow and rigid body interactions (e.g., [355]).

## 4. Conclusions

This paper provides a comprehensive review of the state-of-the-art experimental investigations on unsteady, rapidly varying flows generated by the sudden removal of a retaining structure. Only experiments performed in schematic laboratory setups with a fixed, non-erodible bottom were considered. This review, based on journal papers, reports, theses, and documents published until the end of 2022, was carried out with passion and dedication by four researchers who share the experience of conducting physical experimentation of dam-break phenomena for over twenty years. Although the authors tried to conduct an extensive and meticulous review, it may not be exhaustive. Some studies on the subject, especially the older ones, may be missing since they were published in journals of local diffusion or not written in a vehicular language, or those in which the experimental data are marginal and do not represent the focus of the research.

A large number of references was reviewed and divided into tables according to the investigation's purposes. These tables report extensive information on test conditions, datasets, measuring techniques, relevant bibliographic references, and data availability.

This review may guide researchers to compare existing datasets and identify remaining knowledge gaps deserving additional experimental investigation. Moreover, it may help modelers select suitable test cases for validating their numerical models and testing new numerical approaches. Indeed, most experiments aimed at collecting benchmark data were expressly designed to highlight specific computational difficulties for numerical schemes. This review may also support practitioners looking for new technical solutions for mitigating the destructive effects of dam-break flood waves.

Unfortunately, most datasets are not directly accessible in digital format as supplemental material linked to the original works. Therefore, we hope a public repository will soon be made available, where experimental data can be freely uploaded to form a comprehensive open-access database for all researchers interested in dam-break flows.

An impressive amount of laboratory investigations was carried out on dam-break flows, and a variety of test conditions were considered in the literature. However, experimental studies on flows caused by dam breaches with height and width lower than those of the dam and on the movement of the blocks resulting from the dam collapse are still lacking and may be the subject of future research.

**Author Contributions:** F.A., A.M., G.P. and S.S.-F. contributed equally to the conceptualization and implementation of the research, to the revision of the existing literature, and to the writing of the manuscript. All authors have read and agreed to the published version of the manuscript.

**Funding:** This work was supported by the Italian Ministry of University and Research through the PRIN 2017 Project RELAID (REnaissance of LArge Italian Dams), project number 2017T4JC5K. The support from Italian Ministry of University and Research and University of Pavia (Italy) within the program "Dipartimenti di Eccellenza 2023–2027" is acknowledged.

**Data Availability Statement:** No new data were created or analyzed in this study. Data sharing is not applicable to this article.

**Conflicts of Interest:** The authors declare no conflict of interest.

## References

1. Friedrich, H.; Ravazzolo, D.; Ruiz-Villanueva, V.; Schalko, I.; Spreitzer, G.; Tunnicliffe, J.; Weitbrecht, V. Physical Modelling of Large Wood (LW) Processes Relevant for River Management: Perspectives from New Zealand and Switzerland. *Earth Surf. Process. Landforms* **2022**, *47*, 32–57. [CrossRef]
2. Nezu, I.; Sanjou, M. PIV and PTV Measurements in Hydro-Sciences with Focus on Turbulent Open-Channel Flows. *J. Hydro-environ. Res.* **2011**, *5*, 215–230. [CrossRef]
3. Soares-Frazão, S. Review of Imaging-Based Measurement Techniques for Free Surface Flows Involving Sediment Transport and Morphological Changes. *J. Hydroinform.* **2020**, *22*, 958–971. [CrossRef]
4. Gomit, G.; Chatellier, L.; David, L. Free-Surface Flow Measurements by Non-Intrusive Methods: A Survey. *Exp. Fluids* **2022**, *63*, 94. [CrossRef]
5. Aureli, F.; Maranzoni, A.; Petaccia, G. Review of Historical Dam-Break Events and Laboratory Tests on Real Topography for the Validation of Numerical Models. *Water* **2021**, *13*, 1968. [CrossRef]
6. Testa, G.; Zuccalà, D.; Alcrudo, F.; Mulet, J.; Soares-Frazão, S. Flash Flood Flow Experiment in a Simplified Urban District. *J. Hydraul. Res.* **2007**, *45* (Suppl. 1), 37–44. [CrossRef]
7. Levin, L. Mouvement Non Permanent sur les Cours d'Eau à la Suite de Rupture de Barrage [Unsteady River Flow Caused by a Dam-Break]. *Rev. Gén. Hydr.* **1952**, *18*, 297–315. (In French)
8. Escande, L.; Nougaro, J.; Castex, L.; Barthet, H. Influence de Quelques Paramètres sur une Onde de Crue Subite à l'Aval d'un Barrage [The Influence of Certain parameters on a Sudden Flood Wave Downstream from a Dam]. *Houille Blanche* **1961**, *5*, 565–575. Available online: https://www.shf-lhb.org/articles/lhb/pdf/1961/07/lhb1961043.pdf (accessed on 25 January 2023). (In French) [CrossRef]

9. Özgenç Aksoy, A.; Doğan, M.; Oğuzhan Güven, S.; Tanır, G.; Güney, M.Ş. Experimental and Numerical Investigation of the Flood Waves due to Partial Dam Break. *Iran. J. Sci. Technol. Trans. Civ. Eng.* **2022**, *46*, 4689–4704. [CrossRef]
10. Chanson, H. Application of the Method of Characteristics to the Dam Break Wave Problem. *J. Hydraul. Res.* **2009**, *47*, 41–49. [CrossRef]
11. Hager, W.H.; Lauber, G. Hydraulische Experimente zum Talsperrenbruchproblem [Hydraulic Experiments on the Dam-Break Problem]. *Schweiz. Ing. Archit.* **1996**, *114*, 515–524. (In German) [CrossRef]
12. Hager, W.H.; Chervet, A. Geschichte der Dammbruchwelle [Hystory of dam-break wave]. *Wasser Energ. Luft* **1996**, *88*, 49–54. Available online: https://www.e-periodica.ch/digbib/view?pid=wel-004%3A1996%3A88%3A%3A61#67 (accessed on 25 January 2023). (In German)
13. Dressler, R. Comparison of Theories and Experiments for the Hydraulic Dam-Break Wave. In Proceedings of the International Association of Scientific Hydrology, Assemblée Générale, Rome, Italy, 14–25 September 1954; Volume 3, pp. 319–328.
14. Aureli, F.; Maranzoni, A.; Mignosa, P.; Ziveri, C. Dam-Break Flows: Acquisition of Experimental Data through an Imaging Technique and 2D Numerical Modeling. *J. Hydraul. Eng.* **2008**, *134*, 1089–1101. [CrossRef]
15. Toro, E.F.; Garcia-Navarro, P. Godunov-Type Methods for Free-Surface Shallow Flows: A Review. *J. Hydraul. Res.* **2007**, *45*, 736–751. [CrossRef]
16. Hui Pu, J.; Shao, S.; Huang, Y.; Hussain, K. Evaluations of SWEs and SPH Numerical Modelling Techniques for Dam Break Flows. *Eng. Appl. Comput. Fluid Mech.* **2013**, *7*, 544–563. [CrossRef]
17. Teng, J.; Jakeman, A.J.; Vaze, J.; Croke, B.F.W.; Dutta, D.; Kim, S. Flood Inundation Modelling: A Review of Methods, Recent Advances and Uncertainty Analysis. *Environ. Model. Softw.* **2017**, *90*, 201–216. [CrossRef]
18. Bates, P.D. Flood Inundation Prediction. *Annu. Rev. Fluid Mech.* **2022**, *54*, 287–315. [CrossRef]
19. Schoklitsch, A. Über Dambruchwellen [On Waves Produced by Broken Dams]. In *Sitzungsberichte, Mathematisch-Naturwissenschaftliche Klasse*; Akademie der Wissenschaften in Wien: Vienna, Austria, 1917; Volume 126 (IIa), pp. 1489–1514. (In German)
20. Trifonov, E.K. Experimental Investigation of Positive Wave's Propagation along Dry Bottom. *Sci. Research Inst. Hydrotechnics Trans.* **1933**, *10*, 169–188. (In Russian)
21. Trifonov, E.K. Étude Expérimental de la Propagation d'une Onde Positive le Long d'un Fond Sec [Experimental Investigation of the Propagation of a Positive Wave over a Dry Bottom]. *Bull. Congr. Navig.* **1935**, *10*, 66–77. (In French)
22. Eguiazaroff, J.B. Réglage du Niveau de l'Eau dans les Biefs des Rivières Canaliséés et Réglage du Débit en Aval du Dernier Barrage Selon que la Puissance Hydraulique Est, ou Non, Utilisée [Regulation of the Water Level in the Reaches of Canalized Rivers and Regulation of the Flow Below the Last Lock Dam According to Whether the Water Power Is or Is Not Used]. In Proceedings of the 16th International Congress of Navigation, Brussels, Belgium, 3–10 September 1935. (In French)
23. Martin, J.C.; Moyce, W.J. An Experimental Study of the Collapse of Liquid Columns on a Rigid Horizontal Plane. *Philos. Trans. R. Soc. Lond. Ser. A* **1952**, *244*, 312–324. [CrossRef]
24. U.S. Army Engineer Waterways Experiment Station (WES). *Floods Resulting from Suddenly Breached Dams. Conditions of Minimum Resistance. Hydraulic Model Investigation*; Miscellaneous Paper No. 2-374, Report I; U.S. Corps of Engineers: Vicksburg, MS, USA, 1960.
25. U.S. Army Engineer Waterways Experiment Station (WES). *Floods Resulting from Suddenly Breached Dams. Conditions of High Resistance. Hydraulic Model Investigation*; Miscellaneous Paper No. 2-374, Report II; U.S. Corps of Engineers: Vicksburg, MS, USA, 1961.
26. Faure, J.; Nahas, N. Étude Numérique et Expérimentale d'Intumescences à Forte Courbure du Front [A Numerical and Experimental Study of Steep-Fronted Solitary Waves]. *La Houille Blanche* **1961**, *47*, 576–587. (In French) [CrossRef]
27. Estrade, J. Contribution à l'Étude de la Suppression d'un Barrage—Phase Initial de l'Écoulement (Contribution to the Study of Dam-Break—Initial Flow Phase). *Dir. Etudes Rech. Bullet* **1967**, *1*, 5–90. (In French)
28. Nakagawa, H.; Nakamura, S.; Ichihashi, K. Generation and Development of a Hydraulic Bore Due to the Breaking of a Dam (1). *Bull. Disas. Prev. Res. Inst. Kyoto Univ.* **1969**, *19*, 1–17. Available online: https://core.ac.uk/download/pdf/39254633.pdf (accessed on 25 January 2023).
29. Chervet, A.; Dallèves, P. Calcul de l'Onde de Submersion Consécutive à la Rupture d'un Barrage. Deuxième Partie: Comparaisons Entre Observations et Calculs [Calculation of a Dam-Break Wave. Second Part: Comparison Between Observations and Numerical Results]. *Schweiz. Bauztg.* **1970**, *88*, 425–432. (In French) [CrossRef]
30. Cunge, J.-A. Calcul de Propagation des Ondes de Rupture de Barrage [Dam-Break Wave Propagation Modelling]. *Houille Blanche* **1970**, *56*, 25–33. [CrossRef]
31. Cavaillé, Y. Contribution à l'Étude de l'Écoulement Variable Accompagnant la Vidange Brusque d'une Retenue [Contribution to the Analysis of Dam-Break Flow]. In *Aeronautical Documentation and Technical Information Service (No. 410)*; Service de Documentation et D'information Technique de L'aéronautique: Paris, France, 1965. (In French)
32. Maxworthy, T. Experiments on Collisions Between Solitary Waves. *J. Fluid Mech.* **1976**, *76*, 177–186. [CrossRef]
33. Xanthopoulos, T.; Koutitas, C. Numerical simulation of a two dimensional flood wave propagation due to dam failure. *J. Hydraul. Res.* **1976**, *14*, 321–331. [CrossRef]
34. Barr, D.I.H.; Das, M.M. Numerical Simulation of Dam-Burst and Reflections, with Verification against Laboratory Data. *Proc. Inst. Civ. Eng.* **1980**, *69*, 359–373. [CrossRef]

35. Barr, D.I.H.; Das, M.M. Simulation of Surges After Removal of a Separating Barrier Between Shallower and Deeper Bodies of Water. *Proc. Inst. Civ. Eng.* **1981**, *71*, 911–919. [CrossRef]
36. Memos, C.D.; Georgakakos, A.; Vomvoris, S. Some Experimental Results of the Two-Dimensional Dam-Break Problem. In Proceedings of the 20th Congress of International Association for Hydraulic Research, Moscow, Russia, 5–9 September 1983; Volume 2, pp. 555–563.
37. Townson, J.M.; Al-Salihi, A.H. Models of Dam-Break Flow in R-T Space. *J. Hydraul. Eng.* **1989**, *115*, 561–575. [CrossRef]
38. Menendez, A.N.; Navarro, F. An Experimental Study on the Continuous Breaking of a Dam. *J. Hydraul. Res.* **1990**, *28*, 753–772. [CrossRef]
39. Iverson, R.M.; Costa, J.E.; LaHusen, R.G. *Debris-Flow Flume at H.J. Andrews Experimental Forest, Oregon*; Open-File Report 92-483; U.S. Geological Survey, Department of the Interior: Reston, VA, USA, 1992. [CrossRef]
40. Logan, M.; Iverson, R.M.; Obryk, M.K. *Video Documentation of Experiments at the USGS Debris-Flow Flume 1992–2017 (Ver. 1.4, January 2018)*; Open-File Report 2007-1315; U.S. Geological Survey, Department of the Interior: Reston, VA, USA, 2018. [CrossRef]
41. Antunes Do Carmo, J.S.; Seabra Santos, F.J.; Almeida, A.B. Numerical Solution of the Generalized Serre Equations with the MacCormack Finite-Difference Scheme. *Int. J. Numer. Methods Fluids* **1993**, *16*, 725–738. [CrossRef]
42. Tingsanchali, T.; Rattanapitikon, W. 2-D Mathematical Modelling for Dam Break Wave Propagation in Supercritical and Subcritical Flows. In Proceedings of the 25th IAHR World Congress, Tokyo, Japan, 30 August–9 September 1993; pp. 25–32.
43. Braschi, G.; Dadone, F.; Gallati, M. Plain Flooding: Near Field and Far Fields Simulations. In *Modelling of Flood Propagation over Initially Dry Areas, Proceedings of the Specialty Conference, Milan, Italy, 29 June–1 July 1994*; Molinaro, P., Natale, L., Eds.; American Society of Civil Engineers: New York, NY, USA, 1994; pp. 45–59.
44. Manciola, P.; Mazzoni, A.; Savi, F. Formation and Propagation of Steep Wave: An Investigative Experimental Interpretation. In *Modelling of Flood Propagation over Initially Dry Areas, Proceedings of the specialty Conference, Milan, Italy, 29 June–1 July 1994*; Molinaro, P., Natale, L., Eds.; American Society of Civil Engineers: New York, NY, USA, 1994; pp. 283–297.
45. Aguirre-Pe, J.; Plachco, F.P.; Quisca, S. Tests and Numerical One-Dimensional Modelling of a High-Viscosity Fluid Dam-Break Wave. *J. Hydraul. Res.* **1995**, *33*, 17–26. [CrossRef]
46. Fraccarollo, L.; Toro, E.F. Experimental and Numerical Assessment of the Shallow Water Model for Two-Dimensional Dam-Break Type Problems. *J. Hydraul. Res.* **1995**, *33*, 843–864. [CrossRef]
47. Jovanović, M.; Djordjević, D. Experimental Verification of the MacCormack Numerical Scheme. *Adv. Eng. Softw.* **1995**, *23*, 61–67. [CrossRef]
48. Koshizuka, S.; Oka, Y. Moving-Particle Semi-Implicit Method for Fragmentation of Incompressible Fluid. *Nucl. Sci. Eng.* **1996**, *123*, 421–434. [CrossRef]
49. Koshizuka, S.; Tamako, H.; Oka, Y. A Particle Method for Incompressible Viscous Flow with Fluid Fragmentation. *Comput. Fluid Dyn. J.* **1995**, *4*, 29–46.
50. Lauber, G.; Hager, W.H. Experiments to Dambreak Wave: Horizontal Channel. *J. Hydraul. Res.* **1998**, *36*, 291–307. [CrossRef]
51. Lauber, G.; Hager, W.H. Experiments to Dambreak Wave: Sloping Channel. *J. Hydraul. Res.* **1998**, *36*, 761–773. [CrossRef]
52. Stansby, P.K.; Chegini, A.; Barnes, T.C.D. The initial stages of dam-break flow. *J. Fluid Mech.* **1998**, *374*, 407–424. [CrossRef]
53. Blaser, F.; Hager, W.H. Positive Front of Dambreak Wave on Rough Bottom. In Proceedings of the 28th IAHR World Congress, Graz, Austria, 22–27 August 1999; Technical University Graz: Graz, Austria, 1999. Available online: https://www.iahr.org/library/infor?pid=13612 (accessed on 14 July 2022).
54. Nsom, B.; Debiane, K.; Piau, J.-M. Bed Slope Effect on the Dam Break Problem. *J. Hydraul. Res.* **2000**, *38*, 459–464. [CrossRef]
55. Gallati, M.; Braschi, G. Simulazione Lagrangiana di Flussi con Superficie Libera in Problemi di Idraulica [Lagrangian Simulation of Free Surface Flows in Hydraulic Problems]. *L'Acqua* **2000**, *5*, 7–18. Available online: https://www.idrotecnicaitaliana.it/wp-content/uploads/2020/04/Gallati-et-al-LAcqua-n.-5-2000.pdf (accessed on 19 October 2022). (In Italian)
56. Liem, R.; Schramm, J.; Köngeter, J. Evaluating the Implementation of Shallow Water Equations within Numerical Models Focusing the Propagation of Dambreak Waves. *WIT Trans. Modelling Simul.* **2001**, *30*, 231–240. [CrossRef]
57. Briechle, S.; Köngeter, J. Experimental Data for Dike-Break Waves. In *River Flow 2002, Proceedings of the International Conference on Fluvial Hydraulics, Louvain-la-Neuve, Belgium, 4–6 September 2002*; Bousmar, D., Zech, Y., Eds.; Balkema: Lisse, The Netherlands, 2002; Volume 1, pp. 467–473.
58. Soares-Frazão, S.; Zech, Y. Undular Bores and Secondary Waves–Experiments and Hybrid Finite-Volume Modelling. *J. Hydraul. Res.* **2002**, *40*, 33–43. [CrossRef]
59. Shige-eda, M.; Akiyama, J. Numerical and Experimental Study on Two-Dimensional Flood Flows with and without Structures. *J. Hydraul. Eng.* **2003**, *129*, 817–821. [CrossRef]
60. Stelling, G.S.; Duinmeijer, S.P.A. A Staggered Conservative Scheme for Every Froude Number in Rapidly Varied Shallow Water Flows. *Int. J. Numer. Methods Fluids* **2003**, *43*, 1329–1354. [CrossRef]
61. Duinmeijer, A. *Verification of Delft FLS*; Delft University of Technology: Delft, The Netherlands, 2002.
62. Chegini, A.H.N.; Pender, G.; Slaouti, A.; Tait, S.J. Velocity Measurements in Dam-Break Flow Using Imaging System. In *River Flow 2004, Proceedings of the International Conference on Fluvial Hydraulics, Naples, Italy, 23–25 June 2004*; Greco, M., Carravetta, A., Della Morte, R., Eds.; Balkema: Lisse, The Netherlands, 2004; Volume 2, pp. 859–866.

63. Gallati, M.; Sturla, D. SPH Simulation of Dam-Break Flow in Shallow Water Approximation. In *River Flow 2004, Proceedings of the International Conference on Fluvial Hydraulics, Naples, Italy, 23–25 June 2004*; Greco, M., Carravetta, A., Della Morte, R., Eds.; Balkema: Lisse, The Netherlands, 2004; Volume 2, pp. 919–928.
64. Jánosi, M.I.; Jan, D.; Szabó, K.G.; Tél, T. Turbulent Drag Reduction in Dam-Break Flows. *Exp. Fluids* **2004**, *37*, 219–229. [CrossRef]
65. Bukreev, V.I.; Gusev, A.V. Initial Stage of the Generation of Dam-Break Waves. *Dokl. Phys.* **2005**, *50*, 200–203. [CrossRef]
66. Eaket, J.; Hicks, F.E.; Peterson, A.E. Use of Stereoscopy for Dam Break Flow Measurement. *J. Hydraul. Eng.* **2005**, *131*, 24–29. [CrossRef]
67. Piau, J.-M.; Debiane, K. Consistometers Rheometry of Power-Law Viscous Fluids. *J. Non-Newton. Fluid Mech.* **2005**, *127*, 213–224. [CrossRef]
68. Barnes, M.P.; Baldock, T.E. Bed Shear Stress Measurements in Dam Break and Swash Flows. In Proceedings of the International Conference on Civil and Environmental Engineering, Hiroshima, Japan, 28–29 September 2006. Available online: https://www.researchgate.net/publication/37620092_Bed_shear_stress_measurements_in_dam_break_and_swash_flows (accessed on 14 June 2022).
69. Bateman, A.; Granados, A.; Medina, V.; Velasco, D.; Nalesso, M. Experimental Procedure to Obtain 2D Time-Space High-Speed Water Surfaces. In *River Flow 2006, International Conference on Fluvial Hydraulics, Lisbon, Portugal, 6–8 September 2006*; Ferreira, R., Alves, E., Leal, J., Cardoso, A., Eds.; Taylor & Francis: London, UK, 2006; Volume 2, pp. 1879–1888.
70. Cruchaga, M.A.; Celentano, D.J.; Tezduyar, T.E. Collapse of a Liquid Column: Numerical Simulation and Experimental Validation. *Comput. Mech.* **2007**, *39*, 453–476. [CrossRef]
71. Maranzoni, A.; Pilotti, M.; Tomirotti, M.; Valerio, G. Modellazione Numerica e Sperimentale dei Primi Istanti di Moto Conseguenti alla Rapida Rimozione di uno Sbarramento [Numerical and Experimental Modelling of the Early Stages of a Dam-Break Flow]. In *AIMETA 2007, Proceedings of 18th Congress of Italian Association of Theoretical and Applied Mechanics, Brescia, 11–14 September 2007*; Carini, A., Mimmi, G., Piva, R., Eds.; Starrylink: Brescia, Italy, 2007.
72. Aureli, F.; Maranzoni, A.; Mignosa, P. Experimental Modeling of Rapidly Varying Flows on Wet Bed and in Presence of Submersible Obstacles. In *River Flow 2004, Proceedings of the International Conference on Fluvial Hydraulics, Naples, Italy, 23–25 June 2004*; Greco, M., Carravetta, A., Della Morte, R., Eds.; Balkema: Lisse, The Netherlands, 2004; Volume 2, pp. 849–858.
73. Mohamed, A. Characterization of Tsunami-Like Bores in Support of Loading Structures. Master's Thesis, University of Hawaii, Manoa, HI, USA, 2008. Available online: https://scholarspace.manoa.hawaii.edu/items/a7b0cee7-82fe-47ad-abbd-03a5a07705ee (accessed on 19 October 2022).
74. Ancey, C.; Cochard, S.; Andreini, N. The Dam-Break Problem for Viscous Fluids in the High-Capillary-Number Limit. *J. Fluid Mech.* **2009**, *624*, 1–22. [CrossRef]
75. Yang, C.; Lin, B.; Jiang, C.; Liu, Y. Predicting Near-Field Dam-Break Flow and Impact Force using a 3D Model. *J. Hydraul. Res.* **2010**, *48*, 784–792. [CrossRef]
76. Ozmen-Cagatay, H.; Kocaman, S. Dam-Break Flows During Initial Stage Using SWE and RANS Approaches. *J. Hydraul. Res.* **2010**, *48*, 603–611. [CrossRef]
77. Çağatay, H.; Kocaman, S. Experimental Study of Tailwater Level Effects on Dam-Break Flood Wave Propagation. In *River Flow 2008, Proceedings of the International Conference on Fluvial Hydraulics, Çeşme, Izmir, Turkey, 3–5 September 2008*; Altinakar, M.S., Kokpinar, M.A., Aydin, I., Cokgor, S., Kirkgoz, S., Eds.; Kubaba Congress Department and Travel Services: Ankara, Turkey, 2008; Volume 1, pp. 635–644.
78. Duarte, R.; Ribeiro, J.; Boillat, J.-L.; Schleiss, A. Experimental Study on Dam-Break Waves for Silted-Up Reservoirs. *J. Hydraul. Eng.* **2011**, *137*, 1385–1393. [CrossRef]
79. Boillat, J.-L.; Ribeiro, J.; Duarte, R.; Darbre, G. Dam Break in Case of Silted-Up Reservoirs. In *River Flow 2008, Proceedings of the International Conference on Fluvial Hydraulics, Çeşme, Izmir, Turkey, 3–5 September 2008*; Altinakar, M.S., Kokpinar, M.A., Aydin, I., Cokgor, S., Kirkgoz, S., Eds.; Kubaba Congress Department and Travel Services: Ankara, Turkey, 2008; Volume 1, pp. 689–695.
80. Ribeiro, J.; Boillat, J.-L.; Duarte, R.; Darbre, G. Front Wave Propagation in Case of Dam Break. Comparison of Water Filled and Silted-Up Reservoirs. In Proceedings of the 33th IAHR World Congress, Vancouver, BC, Canada, 9–14 August 2009; pp. 6010–6017.
81. Marra, D.; Earl, T.; Ancey, C. Experimental Investigations of Dam Break Flows down an Inclined Channel. In Proceedings of the 34th IAHR World Congress, Brisbane, Australia, 26 June–1 July 2011; pp. 623–630.
82. Aleixo, R.; Soares-Frazão, S.; Zech, Y. Velocity-Field Measurements in a Dam-Break Flow Using a PTV Voronoï Imaging Technique. *Exp. Fluids* **2011**, *50*, 1633–1649. [CrossRef]
83. Aleixo, R.; Zech, Y.; Soares-Frazão, S. Turbulence Measurements in Dam-Break Flows. In *River Flow 2012, Proceedings of the International Conference on Fluvial Hydraulics, San José, Costa Rica, 5–7 September 2012*; Murillo Muñoz, R.E., Ed.; CRC Press: London, UK, 2012; pp. 311–318.
84. Aleixo, R.; Soares-Frazão, S.; Zech, Y. Before the Dam Breaks: Analysis of the Flow Behind a Downward Moving Gate. In *River Flow 2016, Proceedings of the International Conference on Fluvial Hydraulics, Iowa City, IA, USA, 11–14 July 2016*; Constantinescu, G., Garcia, M., Hanes, D., Eds.; CRC Press: London, UK, 2016; pp. 436–442.
85. Aleixo, R.; Soares-Frazão, S.; Zech, Y. Statistical Analysis Methods for Transient Flows–The Dam-Break Case. *J. Hydraul. Res.* **2018**, *57*, 688–701. [CrossRef]
86. Feizi Khankandi, A.; Tahershamsi, A.; Soares-Frazão, S. Experimental Investigation of Reservoir Geometry Effect on Dam-Break Flow. *J. Hydraul. Res.* **2012**, *50*, 376–387. [CrossRef]

87. Oertel, M.; Bung, D.B. Initial Stage of Two-Dimensional Dam-Break Waves: Laboratory versus VOF. *J. Hydraul. Res.* **2012**, *50*, 89–97. [CrossRef]
88. LaRocque, L.A.; Imran, J.; Chaudhry, M.H. Experimental and Numerical Investigations of Two-Dimensional Dam-Break Flows. *J. Hydraul. Eng.* **2013**, *139*, 569–579. [CrossRef]
89. Miani, M.; Consoli, S.; Rossi, E.; Galliano, D.; Annunziato, A. *Physical and Numerical Simulation of a Scaled Tsunami Wave*; Technical Report EUR 26079 EN; Joint Research Centre–Institute for the Protection and Security of the Citizen; Publications Office of the European Union: Luxembourg, 2013. [CrossRef]
90. Hooshyaripor, F.; Tahershamsi, A. Effect of Reservoir Side Slopes on Dam-Break Flood Waves. *Eng. Appl. Comput. Fluid Mech.* **2015**, *9*, 458–468. [CrossRef]
91. Jiang, Z.; Baldock, T.E. Direct Bed Shear Measurements under Loose Bed Swash Flows. *Coast. Eng.* **2015**, *100*, 67–76. [CrossRef]
92. McMullin, N. Numerical and Experimental Modelling of Dam Break Interaction with a Sediment Bed. Ph.D. Thesis, University of Nottingham, Nottingham, UK, 2015. Available online: https://core.ac.uk/download/pdf/33573992.pdf (accessed on 24 January 2023).
93. Mrokowska, M.M.; Rowiński, P.M.; Kalinowska, M.B. Evaluation of Friction Velocity in Unsteady Flow Experiments. *J. Hydraul. Res.* **2015**, *53*, 659–669. [CrossRef]
94. Aleixo, R.; Ozeren, Y.; Altinakar, M. PIV-PTV Measurements of a Tailings Dam-Break Flow. In *Hydrodynamic and Mass Transport at Freshwater Aquatic Interfaces*; Rowiński, P.M., Marion, A., Eds.; Springer: Cham, Switzerland, 2016; pp. 255–268. [CrossRef]
95. Elkholy, M.; LaRocque, L.A.; Chaudhry, M.H.; Imran, J. Experimental Investigations of Partial-Breach Dam-Break Flows. *J. Hydraul. Eng.* **2016**, *142*, 04016042. [CrossRef]
96. Javadian, M.; Kaveh, R.; Mahmoodinasab, F. A Study on Experimental Model of Dam Break Problem and Comparison Experimental Results with Analytical Solution of Saint-Venant Equations. *Int. J. Adv. Biotechnol. Res.* **2016**, *7*, 1239–1245.
97. Hooshyaripor, F.; Tahershamsi, A.; Razi, S. Dam Break Flood Wave under Different Reservoir's Capacities and Lengths. *Sādhanā* **2017**, *42*, 1557–1569. [CrossRef]
98. Liu, H.; Liu, H.; Guo, L.; Lu, S. Experimental Study on Dam-Break Hydrodynamic Characteristics under Different Conditions. *J. Disaster Res.* **2017**, *12*, 198–207. [CrossRef]
99. Liu, H.; Liu, H. Experimental Study on the Dam-Break Hydrographs at the Gate Location. *J. Ocean Univ. China* **2017**, *16*, 697–702. [CrossRef]
100. Cordero, S.; Cagninei, A.; Poggi, D. Dam-Break on an Idealised Hill Side: Preliminary Results of a Physical Model. *E3S Web Conf.* **2018**, *40*, 05002. [CrossRef]
101. Liu, W.; Wang, B.; Chen, Y.; Wu, C.; Liu, X. Assessing the Analytical Solution of One-Dimensional Gravity Wave Model Equations Using Dam-Break Experimental Measurements. *Water* **2018**, *10*, 1261. [CrossRef]
102. Hamid, H.; Khan, M.; Mehmood, M.; Ahmed, F. Experimental Modeling of Dam Break Flood Wave Depth Propagation on a Fixed Bed. *Tech. J. UET Taxila* **2018**, *23*, 1–4.
103. Hamid, H.; Khan, F.A.; Khan, M.; Ajmal, M.; Mahmood, M.; Aslam, M.S.; Tufail, M. Dam Break Wave Propagation on a Non-Erodible Bed–Comparison of Experimental and Numerical Results. *Int. J. Emerg. Trends Eng. Res.* **2021**, *9*, 733–740. [CrossRef]
104. Stolle, J.; Ghodoosipour, B.; Derschum, C.; Nistor, I.; Petriu, E.; Goseberg, N. Swing Gate Generated Dam-Break Waves. *J. Hydraul. Res.* **2018**, *57*, 675–687. [CrossRef]
105. von Häfen, H.; Goseberg, N.; Stolle, J.; Nistor, I. Gate-Opening Criteria for Generating Dam-Break Waves. *J. Hydraul. Eng.* **2019**, *145*, 04019002. [CrossRef]
106. Liu, W.; Wang, B.; Wang, H.; Zhang, J.; Chen, Y.; Peng, Y.; Liu, X.; Yang, S. Experimental and Numerical Modeling of Dam-Break Flows in Wet Downstream Conditions. In Proceedings of the 38th IAHR World Congress, Panama City, Panama, 1–6 September 2019. [CrossRef]
107. Melis, M.; Poggi, D.; Giovanni; Fasanella, O.D.; Cordero, S.; Katul, G.G. Resistance to Flow on a Sloping Channel Covered by Dense Vegetation Following a Dam Break. *Water Resour. Res.* **2019**, *55*, 1040–1058. [CrossRef]
108. Turhan, E.; Ozmen-Cagatay, H.; Tantekin, A. Modeling Flood Shock Wave Propagation with the Smoothed Particle Hydrodynamics (SPH) Method: An Experimental Comparison Study. *Appl. Ecol. Environ. Res.* **2019**, *17*, 3033–3047. [CrossRef]
109. Turhan, E.; Ozmen-Cagatay, H.; Kocaman, S. Experimental and Numerical Investigation of Shock Wave Propagation Due to Dam-Break Over a Wet Channel. *Pol. J. Environ. Stud.* **2019**, *28*, 2877–2898. [CrossRef]
110. Wang, B.; Zhang, J.; Chen, Y.; Peng, Y.; Liu, X.; Liu, W. Comparison of Measured Dam-Break Flood Waves in Triangular and Rectangular Channels. *J. Hydrol.* **2019**, *575*, 690–703. [CrossRef]
111. Wu, K.F.J.; Liu, Z.; Sun, J. Numerical Simulation of Undular Bore Using a Shock-Capturing Boussinesq Model. In Proceedings of the 29th International Ocean and Polar Engineering Conference, Honolulu, HI, USA, 16–21 June 2019; pp. 3568–3573. Available online: https://onepetro.org/ISOPEIOPEC/proceedings-abstract/ISOPE19/All-ISOPE19/ISOPE-I-19-003/20847?redirectedFrom=PDF (accessed on 27 June 2022).
112. Liu, W.; Wang, B.; Guo, Y.; Zhang, J.; Chen, Y. Experimental Investigation on the Effects of Bed Slope and Tailwater on Dam-Break Flows. *J. Hydrol.* **2020**, *590*, 125256. [CrossRef]
113. Oertel, M.; Süfke, F. Two-Dimensional Dam-Break Wave Analysis: Particle Image Velocimetry Versus Optical Flow. *J. Hydraul. Res.* **2020**, *58*, 326–334. [CrossRef]

114. Shugan, I.V.; Chen, Y.-Y.; Hsu, C.-J. Experimental and Theoretical Study on Flood Bore Propagation and Forerunner Generation in Dam-Break Flow. *Phys. Wave Phenom.* **2020**, *28*, 274–284. [CrossRef]
115. Vosoughi, F.; Rakhshandehroo, G.; Nikoo, M.R.; Sadegh, M. Experimental Study and Numerical Verification of Silted-Up Dam Break. *J. Hydrol.* **2020**, *590*, 125267. [CrossRef]
116. Vosoughi, F.; Nikoo, M.R.; Rakhshandehroo, G.; Gandomi, A.H. Experimental Videos in Studying the Influences of Dry- and Wet-Bed Downstream Conditions on Dam Break Multiphase Flood Waves in a Reservoir with 7.5 cm Sediment Depth (25% silted-up). Mendeley Data, V3. Available online: https://doi.org/10.17632/p6bsdz7xch.3 (accessed on 21 June 2022).
117. Vosoughi, F.; Nikoo, M.R.; Rakhshandehroo, G.; Gandomi, A.H. Experimental Dataset on Water Levels, Sediment Depths and Wave Front Celerity Values in the Study of Multiphase Shock Wave for Different Initial Up- and Down-Stream Conditions. *Data Brief* **2021**, *36*, 107082. [CrossRef]
118. Wang, B.; Liu, X.; Zhang, J.; Guo, Y.; Chen, Y.; Peng, Y.; Liu, W.; Yang, S.; Zhang, F. Analytical and Experimental Investigations of Dam-Break Flows in Triangular Channels with Wet-Bed Conditions. *J. Hydraul. Eng.* **2020**, *146*, 04020070. [CrossRef]
119. Wang, B.; Liu, W.; Wang, W.; Zhang, J.; Chen, Y.; Peng, Y.; Liu, X.; Yang, S. Experimental and numerical investigations of similarity for dam-break flows on wet bed. *J. Hydrol.* **2020**, *583*, 124598. [CrossRef]
120. Ahmadi, S.M.; Yamamoto, Y. A New Dam-Break Outflow-Rate Concept and Its Installation to a Hydro-Morphodynamics Simulation Model Based on FDM (An Example on Amagase Dam of Japan). *Water* **2021**, *13*, 1759. [CrossRef]
121. Ansari, A.; Khavasi, E.; Ghazanfarian, J. Experimental and SPH Studies of Reciprocal Wet-Bed Dam-Break Flow over Obstacles. *Int. J. Mod. Phys. C* **2021**, *32*, 2150098. [CrossRef]
122. Birnbaum, J.; Lev, E.; Llewellin, E.W. Rheology of Three-Phase Suspensions Determined via Dam-Break Experiments. *Proc. R. Soc. A* **2021**, *477*, 20210394. [CrossRef]
123. Espartel, L.; Manica, R. Experiments on Initial Stages of Development of Dam-Break Waves. *Rev. Bras. Recur. Hidr.* **2021**, *26*, e6. [CrossRef]
124. Kocaman, S.; Evangelista, S.; Guzel, H.; Dal, K.; Yilmaz, A.; Viccione, G. Experimental and Numerical Investigation of 3D Dam-Break Wave Propagation in an Enclosed Domain with Dry and Wet Bottom. *Appl. Sci.* **2021**, *11*, 5638. [CrossRef]
125. Nguyen-Thi, L.-Q.; Nguyen, V.-D.; Pierens, X.; Coorevits, P. An Experimental and Numerical Study of the Influence of Viscosity on the Behavior of Dam-Break Flow. *Theor. Comput. Fluid Dyn.* **2021**, *35*, 345–362. [CrossRef]
126. Takagi, H.; Furukawa, F. Stochastic Uncertainty in a Dam-Break Experiment with Varying Gate Speeds. *J. Mar. Sci. Eng.* **2021**, *9*, 67. [CrossRef]
127. Wang, B.; Zhang, F.; Liu, X.; Guo, Y.; Zhang, J.; Peng, Y. Approximate Analytical Solution and Laboratory Experiments for Dam-Break Wave Tip Region in Triangular Channels. *J. Hydraul. Eng.* **2021**, *147*, 06021015. [CrossRef]
128. Xu, B.; Zhang, S.; Nielsen, P.; Wüthrich, D. Measurements of Bed Shear Stresses Near the Tip of Dam-Break Waves on a Rough Bed. *Exp. Fluids* **2021**, *62*, 49. [CrossRef]
129. Ozmen-Cagatay, H.; Turhan, E.; Kocaman, S. An Experimental Investigation of Dam-Break Induced Flood Waves for Different Density Fluids. *Ocean Eng.* **2022**, *243*, 110227. [CrossRef]
130. Yang, S.; Yang, W.; Zhang, C.; Qin, S.; Wei, K.; Zhang, J. Experimental and Numerical Study on the Evolution of Wave Front Profile of Dam-Break Waves. *Ocean Eng.* **2022**, *247*, 110681. [CrossRef]
131. Yang, S.; Tan, Z.; Yang, W.; Imani, H.; Song, D.; Luo, J.; Zhang, J. Experimental Study on Hydrodynamic Interaction between Dam-Break Waves and Circular Pier. *Ocean Eng.* **2022**, *266*, 113093. [CrossRef]
132. Nielsen, P.; Xu, B.; Wüthrich, D.; Zhang, S. Friction Effects on Quasi-Steady Dam-Break Wave Propagation on Horizontal Beds. *J. Fluid Mech.* **2022**, *939*, A21. [CrossRef]
133. Zhang, F.; Wang, B.; Guo, Y. Experimental Study of the Dam-Break Waves in Triangular Channels with a Sloped Wet Bed. *Ocean Eng.* **2022**, *255*, 111399. [CrossRef]
134. Matsutomi, H. Numerical Computations of Two-Dimensional Inundation of Rapidly Varied Flows due to Breaking of Dams. In Proceedings of the 20th IAHR Congress, Moscow, Russia, 5–9 September 1983; Volume 2, pp. 479–493.
135. Martin, H. Dam-Break Wave in Horizontal Channels with Parallel and Divergent Side Walls. In Proceedings of the 20th IAHR Congress, Moscow, Russia, 5–9 September 1983; Volume 2, pp. 494–505.
136. Michouev, A.V.; Sladkevich, M. Écoulement Dans le Bief Aval Dans le Cas d'une Rupture Partielle d'un Barrage [Flow Downstream in the Event of a Partial Dam-Break]. In Proceedings of the 20th IAHR Congress, Moscow, Russia, 5–9 September 1983; Volume 2, pp. 512–519. (In French)
137. Miller, S.; Chaudhry, M.H. Dam-Break Flows in Curved Channel. *J. Hydraul. Eng.* **1989**, *115*, 1465–1478. [CrossRef]
138. Bell, S.W.; Elliot, R.C.; Chaudhry, M.H. Experimental Results of Two-Dimensional Dam-Break Flows. *J. Hydraul. Res.* **1992**, *30*, 225–252. [CrossRef]
139. Bellos, C.V.; Soulis, V.; Sakkas, J.G. Experimental Investigation of Two-Dimensional Dam-Break Induced Flows. *J. Hydraul. Res.* **1992**, *30*, 47–63. [CrossRef]
140. Četina, M.; Rajar, R. Two-Dimensional Dam-Break Flow Simulation in a Sudden Enlargement. In *Modelling of Flood Propagation Over Initially Dry Areas, Proceedings of the Specialty Conference Co-Sponsored by ASC-CNR/GNDCI-ENEL Spa, Milan, Italy, 29 June–1 July 1994*; Molinaro, P., Natale, L., Eds.; American Society of Civil Engineers: New York, NY, USA, 1994; pp. 268–282.

141. Aureli, F.; Mignosa, P.; Tomirotti, M. Dam-break flows in presence of abrupt bottom variations. In Proceedings of the 28th IAHR World Congress, Graz, Austria, 22–27 August 1999; Technical University Graz: Graz, Austria, 1999. Available online: https://www.iahr.org/library/infor?pid=13679 (accessed on 14 July 2022).
142. Soares-Frazão, S.; Zech, Y. Effects of a Sharp Bend on Dam-Break Flow. In Proceedings of the 28th IAHR World Congress, Graz, Austria, 22–27 August 1999; Technical University Graz: Graz, Austria, 1999. Available online: https://www.iahr.org/library/infor?pid=13631 (accessed on 17 February 2023).
143. Soares-Frazão, S.; Sillen, X.; Zech, Y. Dam-Break Flow through Sharp Bends Physical Model and 2D Boltzmann Model Validation. In Proceedings of the 1st CADAM Workshop, Wallingford, UK, 2–3 March 1998.
144. Aureli, F.; Mignosa, P.; Tomirotti, M. Numerical Simulation and Experimental Verification of Dam-Break Flows with Shocks. *J. Hydraul. Res.* **2000**, *38*, 197–206. [CrossRef]
145. Aureli, F.; Belicchi, M.; Maione, U.; Mignosa, P.; Tomirotti, M. Fenomeni di Moto Vario Conseguenti al Crollo di Opere di Ritenuta. Parte II: Indagini Sperimentali e Modellazione Numerica in Presenza di Onde di Shock [Dam-Break Flows. Part II: Experimental and Numerical Modelling in the Presence of Shocks]. *L'Acqua* **1998**, *5*, 27–36. (In Italian)
146. Bento Franco, A.; Betâmio de Almeida, A. Dam-break in a channel. In *Concerted Action on Dam Break Modelling: Objectives, Project, Report, Test Cases, Meeting Proceedings*; Soares Frazão, S., Morris, M., Zech, Y., Eds.; Université Catholique de Louvain: Louvain-la-Neuve, Belgium, 2000.
147. Viseu, T.; Bento Franco, A.; Betâmio de Almeida, A. Numerical and Computational Results of the 2D BIPLAN Model. In Proceedings of the 1st CADAM Workshop, Wallingford, UK, 2–3 March 1998.
148. Hiver, J. Adverse-Slope and Slope (Bump). In *Concerted Action on Dam Break Modelling: Objectives, Project, Report, Test Cases, Meeting Proceedings*; Soares Frazão, S., Morris, M., Zech, Y., Eds.; Université Catholique de Louvain: Louvain-la-Neuve, Belgium, 2000.
149. Soares-Frazão, S.; de Bueger, C.; Dourson, V.; Zech, Y. Dam-Break Wave Over a Triangular Bottom Sill. In *River Flow 2002, Proceedings of the International Conference on Fluvial Hydraulics, Louvain-la-Neuve, Belgium, 4–6 September 2002*; Bousmar, D., Zech, Y., Eds.; Balkema: Lisse, The Netherlands, 2002; Volume 1, pp. 437–442.
150. Soares-Frazão, S. Experiments of Dam-Break Wave Over a Triangular Bottom Sill. *J. Hydraul. Res.* **2007**, *45* (Suppl. 1), 19–26. [CrossRef]
151. Soares-Frazão, S.; Zech, Y. Dam Break in Channels with 90° Bend. *J. Hydraul. Eng.* **2002**, *128*, 956–968. [CrossRef]
152. Bukreev, V.I. Water Impingement on a Vertical Wall Due to Discontinuity Decay Above a Drop. *J. Appl. Mech. Tech. Phys.* **2003**, *44*, 59–63. [CrossRef]
153. Bukreev, V.I.; Gusev, A.V. Gravity Waves Due to Discontinuity Decay Over an Open-Channel Bottom Drop. *J. Appl. Mech. Tech. Phys.* **2003**, *44*, 506–515. [CrossRef]
154. Soares-Frazão, S.; Lories, D.; Taminiau, D.; Zech, Y. Dam-Break Flow in a Channel with a Sudden Enlargement. In Proceedings of the 30th IAHR Congress, Thessaloniki, Greece, 25–27 August 2003.
155. Bukreev, V.I.; Gusev, A.V.; Malysheva, A.A.; Malysheva, I.A. Experimental Verification of the Gas-Hydraulic Analogy with Reference to the Dam-Break Problem. *Fluid Dyn.* **2004**, *39*, 801–809. [CrossRef]
156. Bellos, C. Experimental Measurements of Flood Wave Created by a Dam Break. *Eur. Water* **2004**, *7*, 3–15.
157. Natale, L.; Petaccia, G.; Savi, F. Mathematical Simulation of the Effects of Bridges and Structures on Flood Waves Propagation. In *River Flow 2004, Proceedings of the International Conference on Fluvial Hydraulics, Naples, Italy, 23–25 June 2004*; Greco, M., Carravetta, A., Della Morte, R., Eds.; Balkema: Lisse, The Netherlands, 2004; Volume 2, pp. 895–901.
158. Bukreev, V.I. On the Water Depth in the Breach during a Partial Dam Break. *Fluid Dyn.* **2005**, *40*, 769–776. [CrossRef]
159. Bukreev, V.I. On the discharge characteristic at the dam site after dam break. *J. Appl. Mech. Tech. Phys.* **2006**, *47*, 679–687. [CrossRef]
160. Gusev, A.V.; Ostapenko, V.V.; Malysheva, A.A.; Malysheva, I.A. Open-Channel Waves Generated by Propagation of a Discontinuous Wave over a Bottom Step. *J. Appl. Mech. Tech. Phys.* **2008**, *49*, 23–33. [CrossRef]
161. Bukreev, V.I.; Degtyarev, V.V.; Chebotnikov, A.V. Experimental Verification of Methods for Calculating Partial Dam-Break Waves. *J. Appl. Mech. Tech. Phys.* **2008**, *49*, 754–761. [CrossRef]
162. Evangelista, S.; Di Cristo, C.; De Marinis, G. Experiments and Simulations of Dam Break over Fixed and Granular Beds. In Proceedings of the 34th IAHR World Congress, Brisbane, Australia, 26 June–1 July 2011; pp. 3450–3457. Available online: https://www.researchgate.net/publication/273060021_Experiments_and_simulations_of_dam_break_over_fixed_and_granular_beds#fullTextFileContent (accessed on 23 December 2022).
163. Evangelista, S. Esperimenti e Simulazioni Numeriche di Dam Break su Letto Fisso e Mobile [Experiments and Numerical Simulations of Dam Break on Fixed and Movable Beds]. *L'Acqua* **2014**, *3*, 9–21. (In Italian)
164. Ozmen-Cagatay, H.; Kocaman, S. Dam-Break Flow in the Presence of Obstacle: Experiment and CFD Simulation. *Eng. Appl. Comput. Fluid Mech.* **2011**, *5*, 541–552. [CrossRef]
165. Ozmen-Cagatay, H.; Kocaman, S. Investigation of Dam-Break Flow Over Abruptly Contracting Channel with Trapezoidal-Shaped Lateral Obstacles. *J. Fluids Eng.* **2012**, *134*, 081204. [CrossRef]
166. Kocaman, S.; Ozmen-Cagatay, H. The Effect of Lateral Channel Contraction on Dam Break Flows: Laboratory Experiment. *J. Hydrol.* **2012**, *432–433*, 145–153. [CrossRef]
167. Ozmen-Cagatay, H.; Kocaman, S.; Guzel, H. Investigation of Dam-Break Flood Waves in a Dry Channel with a Hump. *J. Hydro-Environ. Res.* **2014**, *8*, 304–315. [CrossRef]

168. Degtyarev, V.V.; Ostapenko, V.V.; Kovyrkina, O.A.; Zolotykh, A.V. Comparison of Theory and Experiment in Simulation of Dam Break in a Rectangular Channel with a Sudden Change in Cross-Sectional Area. *J. Appl. Mech. Tech. Phys.* **2014**, *55*, 999–1004. [CrossRef]
169. Wood, A.; Wang, K.H. Modeling Dam-Break Flows in Channels with 90 Degree Bend Using an Alternating-Direction Implicit Based Curvilinear Hydrodynamic Solver. *Comput. Fluids* **2015**, *114*, 254–264. [CrossRef]
170. Kikkert, G.A.; Liyanage, T.; Shang, C. Dam-Break Generated Flow from an Infinite Reservoir into a Positively Inclined Channel of Limited Width. *J. Hydro-Environ. Res.* **2015**, *9*, 519–531. [CrossRef]
171. Chen, S.; Li, Y.; Tian, Z.; Fan, Q. On Dam-Break Flow Routing in Confluent Channels. *Int. J. Environ. Res. Public Health* **2019**, *16*, 4384. [CrossRef] [PubMed]
172. Kobayashi, D.; Uchida, T.; Kawahara, Y. The Characteristics of Dam Break Flows in a Meandering Channel. In Proceedings of the 38th IAHR World Congress, Panama City, Panama, 1–6 September 2019. [CrossRef]
173. Kavand, R.; Ghomeshi, M.; Daryaee, M. Experimental Study of the Effect of Bed Roughness on Wave Characteristics Resulting from Dam Break in Curve Channel. *J. Hydraul.* **2020**, *14*, 111–122. (In Arabic) [CrossRef]
174. Kocaman, S.; Güzel, H.; Evangelista, S.; Ozmen-Cagatay, H.; Viccione, G. Experimental and Numerical Analysis of a Dam-Break Flow through Different Contraction Geometries of the Channel. *Water* **2020**, *12*, 1124. [CrossRef]
175. Ismail, H.; Larocque, L.A.; Bastianon, E.; Chaudhry, M.H.; Imran, J. Propagation of Tributary Dam-Break Flows through a Channel Junction. *J. Hydraul. Res.* **2021**, *59*, 214–223. [CrossRef]
176. Gamero, P.; Cantero-Chinchilla, F.N.; Bergillos, R.J.; Castro-Orgaz, O.; Dey, S. Shallow-Water Lee-Side Waves at Obstacles: Experimental Characterization and Turbulent Non-Hydrostatic Modeling Using Weighted-Averaged Residual Equations. *Environ. Model. Softw.* **2022**, *155*, 105422. [CrossRef]
177. Kobayashi, D.; Uchida, T. Experimental and Numerical Investigation of Breaking Bores in Straight and Meandering Channels with Different Froude Numbers. *Coast. Eng. J.* **2022**, *64*, 442–457. [CrossRef]
178. Vosoughi, F.; Nikoo, M.R.; Rakhshandehroo, G.; Adamowski, J.F.; Gandomi, A.H. Downstream Semi-Circular Obstacles' Influence on Floods Arising from the Failure of Dams with Different Levels of Reservoir Silting. *Phys. Fluids* **2022**, *34*, 013312. [CrossRef]
179. Vosoughi, F.; Nikoo, M.R.; Rakhshandehroo, G.; Alamdari, N.; Gandomi, A.H.; Al-Wardy, M. The Application of Bayesian Model Averaging Based on Artificial Intelligent Models in Estimating Multiphase Shock Flood Waves. *Neural Comput. Appl.* **2022**, *34*, 20411–20429. [CrossRef]
180. Greenspan, H.P.; Young, R.E. Flow Over a Containment Dyke. *J. Fluid Mech.* **1978**, *87*, 179–192. [CrossRef]
181. Sicard, J.; Nicollet, G. Effets d'une onde de rupture sur un barrage aval [Effects of a dam-break wave on a downstream dam]. In Proceedings of the 20th IAHR Congress, Moscow, Russia, 5–9 September 1983; Volume 2, pp. 564–570.
182. Ramsden, J.D. Forces on a Vertical Wall Due to Long Waves, Bores, and Dry-Bed Surges. *J. Waterw. Port Coast. Ocean. Eng.* **1996**, *122*, 134–141. [CrossRef]
183. Liu, P.L.-F.; Lin, P.; Chang, K.-A.; Sakakiyama, T. Numerical Modeling of Wave Interaction with Porous Structures. *J. Waterw. Port Coast. Ocean Eng.* **1999**, *125*, 322–330. [CrossRef]
184. Barakhnin, V.B.; Krasnoshchekova, T.V.; Potapov, I.N. Reflection of a Dam–Break Wave at a Vertical Wall. Numerical Modeling and Experiment. *J. Appl. Mech. Tech. Phys.* **2001**, *42*, 269–275. [CrossRef]
185. Soares-Frazão, S.; Zech, Y. Dam Break Flow Experiment: The Isolated Building Test Case. In Proceedings of the 2nd IMPACT Workshop, Mo i Rana, Norway, 12–13 September 2002.
186. Soares-Frazão, S.; Zech, Y. Experimental Study of Dam-Break Flow against an Isolated Obstacle. *J. Hydraul. Res.* **2007**, *45* (Suppl. 1), 27–36. [CrossRef]
187. Brufau, P.; Garcia-Navarro, P.; Vásquez-Cendón, M.E.; Méndez, A.; Puertas, J. Numerical Model Validation with Experimental Data on Dam Break Problems Involving Wetting/Drying Fronts over Initially Dry Bed Adverse Slopes. In *River Flow 2002, Proceedings of the International Conference on Fluvial Hydraulics, Louvain-la-Neuve, Belgium, 4–6 September 2002*; Bousmar, D., Zech, Y., Eds.; Balkema: Lisse, The Netherlands, 2002; Volume 1, pp. 487–494.
188. Méndez, A.; Pena, L.; Brufau, P.; Puertas, J. An Experimental Approach to the Dam Break Problem. Real Data to Check Numerical Models. In Proceedings of the 29th Congress of International Association for Hydraulic Research, Beijing, China, 16–21 September 2001; Li, G., Ed.; Tsinghua University Press: Beijing, China, 2001; Theme C; pp. 184–189.
189. Ciobotaru, R.M.; Bidoae, R.; Raad, P.E. Interaction of a Single Large Wave with a Tall Fixed Structure: A Numerical Study. In Proceedings of the FEDSM'03, 4th ASME-JSME Joint Fluids Engineering Conference, Honolulu, HI, USA, 6–10 July 2003; pp. 437–442. [CrossRef]
190. Trivellato, F. Experimental and Numerical Investigation of Bore Impact on a Wall. *WIT Trans. Built Environ.* **2003**, *71*, 3–12. [CrossRef]
191. Bertolazzi, E.; Trivellato, F. *Numerical Modeling of Clear Water Bore Impact*; University of Trento: Trento, Italy, 2003. Available online: https://e.bertolazzi.dii.unitn.it/files/2002-DIMS-18.pdf (accessed on 19 October 2022).
192. Campisano, A.; Creaco, E.; Modica, C. Experimental and Numerical Analysis of the Scouring Effects of Flushing Waves on Sediment Deposits. *J. Hydrol.* **2004**, *299*, 324–334. [CrossRef]
193. Hu, C.; Kashiwagi, M. A CIP-based method for numerical simulations of violent free-surface flows. *J. Mar. Sci. Technol.* **2004**, *9*, 143–157. [CrossRef]

194. Raad, P.E.; Bidoae, R. The Three-Dimensional Eulerian–Lagrangian Marker and Micro Cell Method for the Simulation of Free Surface Flows. *J. Comput. Phys.* **2005**, *203*, 668–699. [CrossRef]
195. Arnason, H. Interactions between an Incident Bore and a Free-Standing Coastal Structure. Ph.D. Thesis, University of Washington, Seattle, WA, USA, 2005.
196. Kleefsman, K.M.T.; Fekken, G.; Veldman, A.E.P.; Iwanowski, B.; Buchner, B. A Volume-of-Fluid Based Simulation Method for Wave Impact Problems. *J. Comput. Phys.* **2005**, *206*, 363–393. [CrossRef]
197. Issa, R.; Violeau, D. 3D Dambreaking-Test-Case 2. EDF-Ercoftac-SPH European Research Interest Community SIG. 2006. Available online: https://docplayer.net/63169198-Ercoftac-test-case-2-3d-dambreaking-release-1-1-march-reza-issa-and-damien-violeau-electricite-de-france.html (accessed on 31 January 2023).
198. Larese, A.; Rossi, R.; Oñate, E.; Idelsohn, S.R. Validation of the Particle Finite Element Method (PFEM) for Simulation of Free Surface Flows. *Eng. Comput.* **2008**, *25*, 385–425. [CrossRef]
199. Liang, D.; Falconer, R.A.; Jiang, C.; Wang, X. Numerical Simulation of Flood Flows Due to Levee Breaches. In Proceedings of the 32nd IAHR Congress, Venice, Italy, 1–6 July 2007; CORILA: Venice, Italy, 2007. Available online: https://www.iahr.org/library/infor?pid=15794 (accessed on 31 January 2023).
200. Nouri, Y. The Impact of Hydraulic Bores and Debris on Free Standing Structures. Master's Thesis, University of Ottawa, Ottawa, ON, Canada, 2008.
201. Nistor, I.; Nouri, Y.; Palermo, D.; Cornett, A. Experimental Investigation of the Impact of a Tsunami-Induced Bore on Structures. In *Coastal Engineering 2008, Proceedings of the 31st International Conference, Hamburg, Germany, 31 August–5 September 2008*; McKee Smith, J., Ed.; World Scientific Publishing: Singapore, 2008; pp. 3324–3336. [CrossRef]
202. Nouri, Y.; Nistor, I.; Palermo, D.; Cornett, A. Experimental Investigation of Tsunami Impact on Free Standing Structures. *Coast. Eng. J.* **2010**, *52*, 43–70. [CrossRef]
203. Bukreev, V.I.; Zykov, V.V. Bore Impact on a Vertical Plate. *J. Appl. Mech. Tech. Phys.* **2008**, *49*, 926–933. [CrossRef]
204. Arnason, H.; Petroff, C.; Yeh, H. Tsunami bore impingement onto a vertical column. *J. Disaster Res.* **2009**, *4*, 391–403. [CrossRef]
205. Cruchaga, M.A.; Celentano, D.J.; Tezduyar, T.E. Computational modeling of the collapse of a liquid column over an obstacle and experimental validation. *J. Appl. Mech.* **2009**, *76*, 021202. [CrossRef]
206. Hu, C.; Sueyoshi, M. Numerical Simulation and Experiment on Dam Break Problem. *J. Mar. Sci. Appl.* **2010**, *9*, 109–114. [CrossRef]
207. Aureli, F.; Maranzoni, A.; Mignosa, P.; Ziveri, C. An Image Processing Technique for Measuring Free Surface of Dam-Break Flows. *Exp. Fluids* **2011**, *50*, 665–675. [CrossRef]
208. Al-Faesly, T.; Palermo, D.; Nistor, I.; Cornett, A. Experimental Modeling of Extreme Hydrodynamic Forces on Structural Models. *Int. J. Prot. Struct.* **2012**, *3*, 477–505. [CrossRef]
209. Lara, J.L.; del Jesus, M.; Losada, I.J. Three-Dimensional Interaction of Waves and Porous Coastal Structures: Part II: Experimental Validation. *Coast. Eng.* **2012**, *64*, 26–46. [CrossRef]
210. Triatmadja, R.; Nurhasanah, A. Tsunami Force on Buildings with Openings and Protection. *J. Earthq. Tsunami* **2012**, *6*, 1250024. [CrossRef]
211. Aguíñiga, F.; Jaiswal, M.; Sai, J.O.; Cox, D.T.; Gupta, R.; van de Lindt, J.W. Experimental Study of Tsunami Forces on Structures. In *Coastal Hazards*; Huang, W., Wang, K., Cehng, Q.J., Eds.; American Society of Civil Engineers: Resto, VA, USA, 2013; pp. 111–118. [CrossRef]
212. Nakao, H.; Zhang, G.; Sumimura, T.; Hoshikuma, J. Numerical Assessment of Tsunami-Induced Effect on Bridge Behavior. In Proceedings of the 29th US–Japan Bridge Engineering Workshop, Tsukuba, Japan, 11–13 November 2013. Available online: https://www.pwri.go.jp/eng/ujnr/tc/g/pdf/29/29-1-3_Nakao.pdf (accessed on 1 February 2023).
213. Lobovský, L.; Botia-Vera, E.; Castellana, F.; Mas-Soler, J.; Souto-Iglesias, A. Experimental Investigation of Dynamic Pressure Loads During Dam Break. *J. Fluids Struct.* **2014**, *48*, 407–434. [CrossRef]
214. Ratia, H.; Murillo, J.; García-Navarro, P. Numerical Modelling of Bridges in 2D Shallow Water Flow Simulations. *Int. J. Numer. Methods Fluids* **2014**, *75*, 250–272. [CrossRef]
215. Aureli, F.; Dazzi, S.; Maranzoni, A.; Mignosa, P.; Vacondio, R. Experimental and Numerical Evaluation of the Force Due to the Impact of a Dam-Break Wave on a Structure. *Adv. Water Resour.* **2015**, *76*, 29–42. [CrossRef]
216. Kocaman, S.; Ozmen-Cagatay, H. Investigation of Dam-Break Induced Shock Waves Impact on a Vertical Wall. *J. Hydrol.* **2015**, *525*, 1–12. [CrossRef]
217. Liao, K.; Hu, C.; Sueyoshi, M. Free Surface Flow Impacting on an Elastic Structure: Experiment versus Numerical Simulation. *Appl. Ocean Res.* **2015**, *50*, 192–208. [CrossRef]
218. Liang, Q.; Chen, K.-C.; Hou, J.; Xiong, Y.; Wang, G.; Qiang, J. Hydrodynamic Modelling of Flow Impact on Structures under Extreme Flow Conditions. *J. Hydrodynam. B* **2016**, *28*, 267–274. [CrossRef]
219. Mohd, N.; Kamra, M.M.; Sueyoshi, M.; Hu, C. Lattice Boltzmann Method for Free Surface Impacting on Vertical Cylinder: A Comparison with Experimental Data. *Evergreen* **2017**, *4*, 28–37. [CrossRef]
220. Kamra, M.M.; Mohd, N.; Liu, C.; Sueyoshi, M.; Hu, C. Numerical and Experimental Investigation of Three-Dimensionality in the Dam-Break Flow Against a Vertical Wall. *J. Hydrodyn.* **2018**, *30*, 682–693. [CrossRef]
221. Liu, L.; Sun, J.; Lin, B.; Lu, L. Building Performance in Dam-Break Flow–An Experimental Study. *Urban Water J.* **2018**, *15*, 251–258. [CrossRef]

222. Martínez-Aranda, S.; Fernández-Pato, J.; Caviedes-Voullième, D.; García-Palacín, I.; García-Navarro, P. Towards Transient Experimental Water Surfaces: A New Benchmark Dataset for 2D Shallow Water Solvers. *Adv. Water Resour.* **2018**, *121*, 130–149. [CrossRef]
223. Stamataki, I.; Zang, J.; Buldakov, E.; Kjeldsen, T.; Stagonas, D. Study of Dam Break Flow Interaction with Urban Settlements over a Sloping Channel. *E3S Web Conf.* **2018**, *40*, 06006. [CrossRef]
224. Tinh, N.X.; Mitobe, Y.; Tanaka, H. Laboratory Experiment Study on the Building Relative Angle against Tsunami Waves. *Tohoku J. Nat. Disaster Sci.* **2018**, *54*, 7–12.
225. Demir, A.; Dincer, A.E.; Bozkus, Z.; Tijsseling, A.S. Numerical and Experimental Investigation of Damping in a Dam-Break Problem with Fluid-Structure Interaction. *J. Zhejiang Univ. Sci. A* **2019**, *20*, 258–271. [CrossRef]
226. Ghodoosipour, B.; Stolle, J.; Nistor, I.; Mohammadian, A.; Goseberg, N. Experimental Study on Extreme Hydrodynamic Loading on Pipelines. Part 1: Flow Hydrodynamics. *J. Mar. Sci. Eng.* **2019**, *7*, 251. [CrossRef]
227. Ghodoosipour, B.; Stolle, J.; Nistor, I.; Mohammadian, A.; Goseberg, N. Experimental Study on Extreme Hydrodynamic Loading on Pipelines Part 2: Induced Force Analysis. *J. Mar. Sci. Eng.* **2019**, *7*, 262. [CrossRef]
228. Kamra, M.M.; Al Salami, J.; Sueyoshi, M.; Hu, C. Experimental Study of the Interaction of Dambreak with a Vertical Cylinder. *J. Fluids Struct.* **2019**, *86*, 185–199. [CrossRef]
229. Mokhtar, Z.A.; Mohammed, T.A.; Yusuf, B.; Lau, T.L. Experimental Investigation of Tsunami Bore Impact Pressure on a Perforated Seawall. *Appl. Ocean Res.* **2019**, *84*, 291–301. [CrossRef]
230. Dutta, D.; Kumar, L.; Saud Afzal, M.; Rathore, P. Hydrodynamic Study of the Flows Caused by Dam Break Around a Rectangular Obstacle. In Proceeding of ICRACEM 2020, 1st Online International Conference on Recent Advances in Computational and Experimental Mechanics, Kharagpur, India, 4–6 September 2020; SM-20-046.
231. Dutta, D.; Kumar, L.; Saud Afzal, M.; Rathore, P. Hydrodynamic Study of the Flows Caused by Dam Break Around a Rectangular Obstacle. In *Recent Advances in Computational and Experimental Mechanics, Vol II. Lecture Notes in Mechanical Engineering*; Springer: Singapore, 2022; pp. 159–169. [CrossRef]
232. Farahmandpour, O.; Marsono, A.K.; Forouzani, P.; Tap, M.M.; Abu Bakar, S. Experimental Simulation of Tsunami Surge and Its Interaction with Coastal Structure. *Int. J. Prot. Struct.* **2020**, *11*, 258–280. [CrossRef]
233. Kocaman, S.; Evangelista, S.; Viccione, G.; Güzel, H. Experimental and Numerical Analysis of 3D Dam-Break Waves in an Enclosed Domain with a Single Oriented Obstacle. *Environ. Sci. Proc.* **2020**, *2*, 35. [CrossRef]
234. Pratiwi, V.; Kusuma, M.S.B.; Kardhana, H.; Farid, M. Experimental Study of Dam Break Flow Generated by the Flap Gate in Horizontal Channel. *Int. J. GEOMATE* **2020**, *19*, 19–26. [CrossRef]
235. Shen, J.; Wei, L.; Wu, D.; Liu, H.; Huangfu, J. Spatiotemporal Characteristics of the Dam-Break Induced Surge Pressure on a Vertical Wall. *Coast. Eng. J.* **2020**, *62*, 566–581. [CrossRef]
236. Memarzadeh, R.; Sheybanifard, H.; Zounemat-Kermani, M. Numerical and Experimental Study of Abrupt Wave Interaction with Vertical and Inclined Rectangular Obstacles. *J. Appl. Fluid Mech.* **2021**, *14*, 921–933. [CrossRef]
237. Del Gaudio, A.; De Paola, F.; Di Cristo, C.; La Forgia, G.; Leopardi, A.; Vacca, A. Experimental Investigation and Numerical Evaluation of the Free Surface of a Dam Break Wave in the Presence of an Obstacle. *Environ. Sci. Proc.* **2022**, *21*, 23. [CrossRef]
238. Fang, Q.; Liu, S.; Zhong, G.; Liang, J.; Zhen, Y. Experimental Investigation of Extreme Flood Loading on Buildings Considering the Shadowing Effect of the Front Building. *J. Hydraul. Eng.* **2022**, *148*, 04022007. [CrossRef]
239. Garoosi, F.; Mellado-Cusicahua, A.N.; Shademani, M.; Shakibaeinia, A. Experimental and Numerical Investigations of Dam Break Flow over Dry and Wet Beds. *Int. J. Mech. Sci.* **2022**, *215*, 106946. [CrossRef]
240. Lin, J.-H.; Chang, Y.-W.; Chen, G.-Y. Boulder Transportation on the Flat Bed by Dam Break. *J. Earthq. Tsunami* **2022**, *16*, 2241002. [CrossRef]
241. Liu, S.; Nistor, I.; Mohammadian, A.; Azimi, A.H. Experimental Investigation on the Impact of Dam-Break Induced Surges on a Vertical Wall. *Fluids* **2022**, *7*, 258. [CrossRef]
242. Wang, S.; Garlock, M.; Deike, L.; Glisic, B. Feasibility of Kinetic Umbrellas as Deployable Flood Barriers During Landfalling Hurricanes. *J. Struct. Eng.* **2022**, *148*, 04022047. [CrossRef]
243. Xie, W.; Shimozono, T. Water Surge Impingement onto a Vertical Wall: Laboratory Experiments and Stochastic Analysis on Impact Pressure. *Ocean Eng.* **2022**, *248*, 110422. [CrossRef]
244. Soares-Frazão, S.; Spinewine, B.; Duthoit, A.; Deswijsen, J.F.; Zech, Y. Dam-Break Flow Experiments in Simplified City Layouts. In *River Flow 2006, Proceedings of the International Conference on Fluvial Hydraulics, Lisbon, Portugal, 6–8 September 2006*; Ferreira, R., Alves, E., Leal, J., Cardoso, A., Eds.; Taylor & Francis: London, UK, 2006; Volume 1, pp. 513–521.
245. Soares-Frazão, S.; Zech, Y. Dam-Break Flow Through an Idealised City. *J. Hydraul. Res.* **2008**, *46*, 648–658. [CrossRef]
246. Szydłowski, M.; Twaróg, B. Numerical Investigation of Flooding of Real-Topography Developed Areas Following River Embankment Failure. *Task Q.* **2006**, *10*, 321–338.
247. Yoon, K. *Experimental Study on Flood Inundation Considering Urban Characteristics (FFC06-05)*; Urban Flood Disaster Management Research Center: Seoul, Korea, 2007.
248. Kim, B.; Sanders, B.F.; Famiglietti, J.S.; Guinot, V. Urban Flood Modeling with Porous Shallow-Water Equations: A Case Study of Model Errors in the Presence of Anisotropic Porosity. *J. Hydrol.* **2015**, *523*, 680–692. [CrossRef]
249. Albano, R.; Sole, A.; Mirauda, D.; Adamowski, J. Modelling Large Floating Bodies in Urban Area Flash-Floods via a Smoothed Particle Hydrodynamics Model. *J. Hydrol.* **2016**, *541*, 344–358. [CrossRef]

250. Norin, S.V.; Belikov, V.V.; Aleksyuk, A.I. Simulating Flood Waves in Residential Areas. *Power Technol. Eng.* **2017**, *51*, 52–57. [CrossRef]
251. Guinot, V.; Soares-Frazão, S.; Delenne, C. Experimental Validation of Transient Source Term in Porosity-Based Shallow Water Models. *E3S Web Conf.* **2018**, *40*, 06033. [CrossRef]
252. Guinot, V.; Delenne, C.; Soares-Frazão, S. Self-Similar Solutions of Shallow Water Equations with Porosity. *J. Hydraul. Res.* **2022**, *61*, 109–119. [CrossRef]
253. Kusuma, M.S.B.; Setiawati, T.; Farid, M. Experimental Model of Dam Break Flow Around Several Blockages Configurations. *Int. J. GEOMATE* **2019**, *16*, 26–32. [CrossRef]
254. Chumchan, C.; Rattanadecho, P. Experimental and Numerical Investigation of Dam Break Flow Propagation Passed through Complex Obstacles Using LES Model Based on FVM and LBM. *Songklanakarin J. Sci. Technol.* **2020**, *42*, 564–572. [CrossRef]
255. Dong, B.; Xia, J.; Zhou, M.; Deng, S.; Ahmadian, R.; Falconer, R.A. Experimental and Numerical Model Studies on Flash Flood Inundation Processes Over a Typical Urban Street. *Adv. Water Resour.* **2021**, *147*, 103824. [CrossRef]
256. Yeh, H.H.; Ghazali, A. On Bore Collapse. *J. Geophys. Res. Atmos.* **1988**, *93*, 6930–6936. [CrossRef]
257. Yeh, H.H.; Ghazali, A.; Marton, I. Experimental Study of Bore Run-Up. *J. Fluid Mech.* **1989**, *206*, 563–578. [CrossRef]
258. Petroff, C.M.; Moore, A.L.; Arnason, H. Particle Advection by Turbulent Bores–Orientation Effects. In Proceedings of the International Tsunami Symposium, Seattle, WA, 7–10 August 2001; NOAA/PMEL: Seattle, WA, USA, 2001; pp. 897–904.
259. Anh, V.M. Reduction of Wave Overtopping by Vetiver Grass. Master's Thesis, Delft University, Delft, The Netherlands, 2007.
260. Barnes, M.P.; O'Donoghue, T.; Alsina, J.M.; Baldock, T.E. Direct Bed Shear Stress Measurements in Bore-Driven Swash. *Coast. Eng.* **2009**, *56*, 853–867. [CrossRef]
261. De Leffe, M.; Le Touzé, D.; Alessandrini, B. SPH Modeling of Shallow-Water Coastal Flows. *J. Hydraul. Res.* **2010**, *48* (Suppl. S1), 118–125. [CrossRef]
262. O'Donoghue, T.; Pokrajac, D.; Hondebrink, L.J. Laboratory and Numerical Study of Dambreak-Generated Swash on Impermeable Slopes. *Coast. Eng.* **2010**, *57*, 513–530. [CrossRef]
263. Kikkert, G.A.; O'Donoghue, T.; Pokrajac, D.; Dodd, N. Experimental Study of Bore-Driven Swash Hydrodynamics on Impermeable Rough Slopes. *Coast. Eng.* **2012**, *60*, 149–166. [CrossRef]
264. Adegoke, P.B.; Atherton, W.; Al Khaddar, R.M. A Novel Simple Method for Measuring the Velocity of Dam-Break Flow. *WIT Trans. Ecol. Environ.* **2014**, *184*, 23–34. [CrossRef]
265. Rahman, S.; Akib, S.; Khan, M.T.R.; Shirazi, S.M. Experimental Study on Tsunami Risk Reduction on Coastal Building Fronted by Sea Wall. *Sci. World J.* **2014**, *2014*, 729357. [CrossRef]
266. Hartana; Murakami, K. Numerical and Experimental Simulation of Two-Phase Tsunami Flow Through Buildings with Openings. *J. Earthq. Tsunami* **2015**, *9*, 1550007. [CrossRef]
267. Chen, B.-T.; Kikkert, G.A.; Pokrajac, D.; Dai, H.-J. Experimental Study of Bore-Driven Swash–Swash Interactions on an Impermeable Rough Slope. *Coast. Eng.* **2016**, *108*, 10–24. [CrossRef]
268. Chen, C.; Melville, B.W.; Nandasena, N.A.K.; Shamseldin, A.Y.; Wotherspoon, L. Experimental Study of Uplift Loads Due to Tsunami Bore Impact on a Wharf Model. *Coast. Eng.* **2016**, *117*, 126–137. [CrossRef]
269. Chen, C.; Melville, B.W.; Nandasena, N.A.K.; Shamseldin, A.Y.; Wotherspoon, L. Mitigation Effect of Vertical Walls on a Wharf Model Subjected to Tsunami Bores. *J. Earthq. Tsunami* **2017**, *11*, 1750004. [CrossRef]
270. Esteban, M.; Glasbergen, T.; Takabatake, T.; Hofland, B.; Nishizaki, S.; Nishida, Y.; Stolle, J.; Nistor, I.; Bricker, J.; Takagi, H.; et al. Overtopping of Coastal Structures by Tsunami Waves. *Geosciences* **2017**, *7*, 121. [CrossRef]
271. Dai, H.-J.; Kikkert, G.A.; Chen, B.-T.; Pokrajac, D. Entrained Air in Bore-Driven Swash on an Impermeable Rough Slope. *Coast. Eng.* **2017**, *121*, 26–43. [CrossRef]
272. Tar, T.; Kato, N.; Suzuki, H.; Nagai, Y.; Ohnishi, K.; Okubayashi, T. Experimental and Numerical Study on the Reduction of Tsunami Flow Using Multiple Flexible Pipes. *J. Loss Prev. Process Ind.* **2017**, *50*, 364–385. [CrossRef]
273. Chen, C.; Melville, B.W.; Nandasena, N.A.K. Investigations of reduction Effect of Vertical Wall on Dam-Break-Simulated Tsunami Surge Exerted on Wharf Piles. *J. Earthq. Tsunami* **2018**, *12*, 1840006. [CrossRef]
274. Chen, C.; Melville, B.W.; Nandasena, N.A.K.; Farvizi, F. An Experimental Investigation of Tsunami Bore Impacts on a Coastal Bridge Model with Different Contraction Ratios. *J. Coast. Res.* **2018**, *34*, 460–469. [CrossRef]
275. Ishii, H.; Shibayama, T.; Stolles, J. Physical and Numerical Modelling of the Flow Structure behind Structure in Tsunami-like Flow. *Coast. Eng. Proc.* **2018**, *1*, currents17. [CrossRef]
276. Lu, S.; Liu, H.; Deng, X. An Experimental Study of the Run-Up Process of Breaking Bores Generated by Dam-Break under Dry- and Wet-Bed Conditions. *J. Earthq. Tsunami* **2018**, *12*, 1840005. [CrossRef]
277. Chen, C.; Wang, F.; Lin, H. Experimental Study on Dam-Break-Like Tsunami Surge Impacts on Small Balls Climbing on Different Slopes. *J. Earthq. Tsunami* **2020**, *14*, 2050022. [CrossRef]
278. Chen, C.; Chen, J.; Lin, P.; Chen, C.; Chen, H. Experimental Study of Dam-Break-Like Tsunami Bore Impact Mechanism on a Container Model. *Pol. Marit. Res.* **2020**, *27*, 53–59. [CrossRef]
279. Elsheikh, N.; Azimi, A.H.; Nistor, I.; Mohammadian, A. Experimental Investigations of Hydraulic Surges Passing over a Rectangular Canal. *J. Earthq. Tsunami* **2020**, *14*, 2040004. [CrossRef]
280. Elsheikh, N.; Nistor, I.; Azimi, A.H.; Mohammadian, A. Tsunami-Induced Bore Propagating over a Canal—Part 1: Laboratory Experiments and Numerical Validation. *Fluids* **2022**, *7*, 213. [CrossRef]

281. Barranco, I.; Liu, P.L.-F. Run-Up and Inundation Generated by Non-Decaying Dam-Break Bores on a Planar Beach. *J. Fluid Mech.* **2021**, *915*, A81. [CrossRef]
282. Chen, C.; Wang, F. An Experimental Study of Energy Dissipation of Sea Grass in a Dam Break Flume. *Glob. NEST J.* **2022**, *24*, 129–134. [CrossRef]
283. Liu, S.; Nistor, I.; Mohammadian, A.; Azimi, A. Experimental Investigation of Beach Slope Effects on the Kinematic Behaviors of Dam Break Flow. In Proceedings of the 39th IAHR World Congress, Granada, Spain, 19–24 June 2022; Ortega-Sánchez, M., Ed.; IAHR: Madrid, Spain, 2022; pp. 6194–6202. [CrossRef]
284. Liu, S.; Nistor, I.; Mohammadian, A.; Azimi, A.H. Experimental and Numerical Investigation of Beach Slope Effects on the Hydrodynamic Loading of Tsunami-like Surges on a Vertical Wall. *J. Mar. Sci. Eng.* **2022**, *10*, 1580. [CrossRef]
285. Rajaie, M.; Azimi, A.H.; Nistor, I.; Rennie, C.D. Experimental Investigations on Hydrodynamic Characteristics of Tsunami-Like Hydraulic Bores Impacting a Square Structure. *J. Hydraul. Eng.* **2022**, *148*, 04021061. [CrossRef]
286. von Häfen, H.; Krautwald, C.; Bihs, H.; Goseberg, N. Dam-Break Waves' Hydrodynamics on Composite Bathymetry. *Front. Built Environ.* **2022**, *8*, 877378. [CrossRef]
287. Buchner, B. Green Water on Ship-Type Offshore Structures. Ph.D. Thesis, Delft University of Technology, Delft, The Netherlands, 2002. Available online: https://repository.tudelft.nl/islandora/object/uuid:e383a7ef-43b5-4137-93d1-d5ab8fc75568/datastream/OBJ/download (accessed on 8 February 2023).
288. Hernández-Fontes, J.V.; Vitola, M.A.; Silva, M.C.; Esperança, P.D.T.T.; Sphaier, S.H. Use of Wet Dam-Break to Study Green Water Problem. In Proceedings of the 36th International Conference on Offshore Mechanics and Arctic Engineering, Trondheim, Norway, 25–30 June 2017; American Society of Mechanical Engineers: New York, NY, USA, 2017; OMAE2017-62113, V07AT06A065. [CrossRef]
289. Hernández-Fontes, J.V.; Vitola, M.A.; Silva, M.C.; Esperança, P.D.T.T.; Sphaier, S.H. On the Generation of Isolated Green Water Events Using Wet Dam-Break. *J. Offshore Mech. Arct. Eng.* **2018**, *140*, 051101. [CrossRef]
290. Hernández-Fontes, J.V.; Vitola, M.A.; Esperança, P.D.T.T.; Sphaier, S.H. Assessing Shipping Water Vertical Loads on a Fixed Structure by Convolution Model and Wet Dam-Break Tests. *Appl. Ocean Res.* **2019**, *82*, 63–73. [CrossRef]
291. Hernández-Fontes, J.V.; Vitola, M.A.; Esperança, P.D.T.T.; Sphaier, S.H.; Silva, R. Patterns and Vertical Loads in Water Shipping in Systematic Wet Dam-Break Experiments. *Ocean Eng.* **2020**, *197*, 106891. [CrossRef]
292. Hernández-Fontes, J.V.; Esperança, P.D.T.T.; Silva, R.; Mendoza, E.; Sphaier, S.H. Violent Water-Structure Interaction: Overtopping Features and Vertical Loads on a Fixed Structure Due to Broken Incident Flows. *Mar. Struct.* **2020**, *74*, 102816. [CrossRef]
293. Hernández-Fontes, J.V.; Hernández, I.D.; Silva, R.; Mendoza, E.; Esperança, P.D.T.T. A Simplified and Open-Source Approach for Multiple-Valued Water Surface Measurements in 2D Hydrodynamic Experiments. *J. Braz. Soc. Mech. Sci. Eng.* **2020**, *42*, 623. [CrossRef]
294. Wang, D.; Dong, S. Experimental Investigation on the Interactions Between Dam-Break Flow and a Floating Box. *J. Ocean Univ. China* **2022**, *21*, 633–646. [CrossRef]
295. Chanson, H.; Coussot, P.; Jarny, S.; Tocquer, L. *A Study of Dam Break Wave of Thixotropic Fluid: Bentonite Surges Down an Inclined Plane*; Rep. No. CH54/04; Department of Civil Engineering, The University of Queensland: Brisbane, Australia, 2004. Available online: https://espace.library.uq.edu.au/view/UQ:9437 (accessed on 12 December 2022).
296. Komatina, D.; Đorđević, D. Numerical Simulation of Hyper-Concentrated Flows. In *River Flow 2004, Proceedings of the International Conference on Fluvial Hydraulics, Naples, Italy, 23–25 June 2004*; Greco, M., Carravetta, A., Della Morte, R., Eds.; Balkema: Lisse, The Netherlands, 2004; Volume 2, pp. 1111–1120.
297. Cochard, S.; Ancey, C. Accurate Measurements of Free-Surface in the Dam-Break Problem. In *River Flow 2006, Proceedings of the International Conference on Fluvial Hydraulics, Lisbon, Portugal, 6–8 September 2006*; Ferreira, R., Alves, E., Leal, J., Cardoso, A., Eds.; Taylor & Francis: London, UK, 2006; Volume 2, pp. 1863–1872.
298. Cochard, S. Measurements of Time-Dependent, Free-Surface Viscoplastic Flows Down Steep Slopes. Ph.D. Thesis, École Polytechnique Fédéral de Lausanne, Lausanne, Switzerland, 2007.
299. Cochard, S.; Ancey, C. Tracking The Free Surface of Time-Dependent Flows: Image Processing for the Dam-Break Problem. *Exp. Fluids* **2008**, *44*, 59–71. [CrossRef]
300. Chanson, H.; Jarny, S.; Coussot, P. Dam Break Wave of Thixotropic Fluid. *J. Hydraul. Eng.* **2006**, *132*, 280–293. [CrossRef]
301. Balmforth, N.J.; Craster, R.V.; Perona, P.; Rust, A.C.; Sassi, R. Viscoplastic Dam Breaks and the Bostwick Consistometer. *J. Non-Newton. Fluid Mech.* **2007**, *142*, 63–78. [CrossRef]
302. Ancey, C.; Cochard, S. The Dam-Break Problem for Herschel–Bulkley Viscoplastic Fluids Down Steep Flumes. *J. Non-Newton. Fluid Mech.* **2009**, *158*, 18–35. [CrossRef]
303. Cochard, S.; Ancey, C. Experimental Investigation of the Spreading of Viscoplastic Fluids on Inclined Planes. *J. Non-Newton. Fluid Mech.* **2009**, *158*, 73–84. [CrossRef]
304. Brondani Minussi, R.; de Freitas Maciel, G. Numerical Experimental Comparison of Dam Break Flows with Non-Newtonian Fluids. *J. Braz. Soc. Mech. Sci. Eng.* **2012**, *34*, 167–178. [CrossRef]
305. Bates, B.M.; Ancey, C. The Dam-Break Problem for Eroding Viscoplastic Fluids. *J. Non-Newton. Fluid Mech.* **2017**, *243*, 64–78. [CrossRef]
306. Jing, X.; Chen, Y.; Xie, D.; Williams, D.J.; Wu, S.; Wang, W.; Yin, T. The Effect of Grain Size on the Hydrodynamics of Mudflow Surge from a Tailings Dam-Break. *Appl. Sci.* **2019**, *9*, 2474. [CrossRef]

307. Modolo, A.V.F.; Loureiro, B.V.; Soares, E.J.; Thompson, R.L. Influence of the Plastic Number on the Evolution of a Yield Stress Material Subjected to a Dam Break. *J. Appl. Fluid Mech.* **2019**, *12*, 1967–1978. [CrossRef]
308. Tang, J.B.; Lin, P.Z.; Cui, P. Depth-Resolved Numerical Model of Dam Break Mud Flows with Herschel-Bulkley Rheology. *J. Mt. Sci.* **2022**, *19*, 1001–1017. [CrossRef]
309. Xue, Y.; Xu, W.-L.; Luo, S.-J.; Chen, H.-Y.; Li, N.-W.; Xu, L.-J. Experimental Study of Dam-Break Flow in Cascade Reservoirs with Steep Bottom Slope. *J. Hydrodyn.* **2011**, *23*, 491–497. [CrossRef]
310. Chen, H.Y.; Xu, W.L.; Deng, J.; Xue, Y.; Li, J. Experimental Investigation of Pressure Load Exerted on a Downstream Dam by Dam-Break Flow. *J. Hydraul. Eng.* **2014**, *140*, 199–207. [CrossRef]
311. Liu, H.J.; Li, Y.; Wang, X.G.; Xuan, G.X.; Zhu, L. Experimental Study of the Flood Superposition Effect Due to Cascade Dam Break. In Proceedings of the 37th IAHR World Congress, Kuala Lumpur, Malaysia, 13–18 August 2017; Ghani, A.A., Chan, N.W., Ariffin, J., Wahab, A.K.A., Harun, S., Kassim, A.H.M., Karim, O.A., Eds.; IAHR: Madrid, Spain, 2017; pp. 2299–2306.
312. Zhang, Y.; Xu, W. Retarding Effects of an Intermediate Intact Dam on the Dam-Break Flow in Cascade Reservoirs. *J. Hydraul. Res.* **2017**, *55*, 438–444. [CrossRef]
313. Luo, J.; Xu, W.; Tian, Z.; Chen, H. Numerical Simulation of Cascaded Dam-Break Flow in Downstream Reservoir. *Proc. Inst. Civ. Eng.–Water Manag.* **2019**, *172*, 55–67. [CrossRef]
314. Kocaman, S.; Dal, K. A New Experimental Study and SPH Comparison for the Sequential Dam-Break Problem. *J. Mar. Sci. Eng.* **2020**, *8*, 905. [CrossRef]
315. Bechteler, W.; Kulisch, H.; Nujic, M. 2-D Dam-Break Flooding Waves – Comparison Between Experimental and Calculated Results. In *Floods and Flood Management*; Saul, A.J., Ed.; Springer: Dordrecht, The Netherlands, 1992; Volume 15, pp. 247–260. [CrossRef]
316. Liem, R.; Köngeter, J. The Influence of Initial Flow Conditions on the Propagation of Dam Break Wave. In Proceedings of the 28th IAHR World Congress, Graz, Austria, 22–27 August 1999. Available online: https://www.iahr.org/library/infor?pid=13676 (accessed on 3 October 2022).
317. Aureli, F.; Mignosa, P. Rapidly Varying Flows Due to Levee-Breaking. In *River Flow 2002, Proceedings of the International Conference on Fluvial Hydraulics, Louvain-la-Neuve, Belgium, 4–6 September 2002*; Bousmar, D., Zech, Y., Eds.; Balkema: Lisse, The Netherlands, 2002; Volume 1, pp. 459–466.
318. Aureli, F.; Mignosa, P. Comparison Between Experimental and Numerical Results of 2D Flows Due to Levee Breaking. In Proceedings of the 29th IAHR World Congress, Beijing, China, 16–21 September 2001; Li, G., Ed.; Tsinghua University Press: Beijing, China, 2001; Theme C, pp. 252–258.
319. Sarma, A.K.; Das, M.M. Analytical Solution of a Flood Wave Resulting from Dike Failure. *Proc. Inst. Civ. Eng.—Water Marit. Eng.* **2003**, *156*, 41–45. [CrossRef]
320. Briechle, S.; Joeppen, A.; Köngeter, J. Physical Model Tests for Dike-Break Induced, Two-Dimensional Flood Wave Propagation. In *River Flow 2004, Proceedings of the International Conference on Fluvial Hydraulics, Naples, Italy, 23–25 June 2004*; Greco, M., Carravetta, A., Della Morte, R., Eds.; Balkema: Lisse, The Netherlands, 2004; Volume 2, pp. 959–966.
321. Briechle, S.R. Die flachenhafte Ausbreitung der Flutwellenach Versagen von Hochwasserschutzeinrichtungen an Fliesgewassern [Flood Wave Generated by the Collapse of a Flood Protection]. Ph.D. Thesis, University of Aachen, Aachen, Germany, 2006. Available online: https://d-nb.info/98060897x/34 (accessed on 19 October 2022). (In German)
322. Harms, M.; Briechle, S.; Köngeter, J.; Schwanenberg, D. Dike-Break Induced Flow: Validation of Numerical Simulations and Case Study. In *River Flow 2004, Proceedings of the International Conference on Fluvial Hydraulics, Naples, Italy, 23–25 June 2004*; Greco, M., Carravetta, A., Della Morte, R., Eds.; Balkema: Lisse, The Netherlands, 2004; Volume 2, pp. 937–944.
323. Oertel, M.; Schlenkhoff, A. Flood Wave Propagation and Flooding of Underground Facilities. In *River Flow 2008, Proceedings of the International Conference on Fluvial Hydraulics, Çeşme, Izmir, Turkey, 3–5 September 2008*; Altinakar, M.S., Kokpinar, M.A., Aydin, I., Cokgor, S., Kirkgoz, S., Eds.; Kubaba Congress Department and Travel Services: Ankara, Turkey, 2008; Volume 1, pp. 595–600.
324. Oertel, M. Analyse der Flutung Unterirdischer Bauwerke in Flussnahen Urbanen Regionen Nach Versagen von Hochwasserschutzeinrichtungen [Analyzing Flooding Processes of Underground Facilities in Urban River Areas after Malfunction of Flood Protection Measures]. Ph.D. Thesis, University of Wuppertal, Wuppertal, Germany, 2008. Available online: https://www.hydro.uni-wuppertal.de/fileadmin/bauing/hydro/berichte/Nr.15_Oertel.pdf (accessed on 19 October 2022). (In German)
325. Roger, S.; Dewals, B.J.; Erpicum, S.; Schwanenberg, D.; Schüttrumpf, H.; Köngeter, J.; Pirotton, M. Experimental and Numerical Investigations of Dike-Break Induced Flows. *J. Hydraul. Res.* **2009**, *47*, 349–359. [CrossRef]
326. Sun, J.; Lu, L.; Lin, B.; Liu, L. Processes of Dike-Break Induced Flows: A Combined Experimental and Numerical Model Study. *Int. J. Sediment Res.* **2017**, *32*, 465–471. [CrossRef]
327. Al-Hafidh, I.A.I.; Calamak, M.; LaRocque, L.A.; Chaudhry, M.H.; Imran, J. Experimental Investigation of Flood Management by an Instantaneous Levee Breach. *J. Hydraul. Eng.* **2022**, *148*, 04021056. [CrossRef]
328. Yoon, K.S.; Rehman, K.; Yoo, H.J.; Lee, S.O.; Hong, S.H. Large Scale Laboratory Experiment: The Impact of the Hydraulic Characteristics of Flood Waves Caused by Gradual Levee Failure on Inundation Areas. *Water* **2022**, *14*, 1446. [CrossRef]
329. Greenspan, H.P.; Johansson, A.V. An Experimental Study of Flow over an Impounding Dike. *Stud. Appl. Math.* **1981**, *64*, 211–223. [CrossRef]
330. Sharifi, T. An Experimental Study of Catastrophic Failure of Liquid Storage Tanks. Ph.D. Thesis, Imperial College of Science and Technology, University of London, London, UK, 1987. Available online: https://spiral.imperial.ac.uk/bitstream/10044/1/46527/2/Sharifi-T-1987-PhD-Thesis.pdf (accessed on 7 February 2023).

331. Maschek, W.; Roth, A.; Kirstahler, M.; Meyer, L. *Simulation Experiments for Centralized Liquid Sloshing Motions*; Report KfK-5090; Kernforschungszentrum Karlsruhe: Karlsruhe, Germany, 1992. Available online: https://core.ac.uk/download/pdf/197569152.pdf (accessed on 7 February 2023).
332. Cleaver, R.P.; Cronin, P.S.; Evans, J.A.; Hirst, I.L. An Experimental Study of Spreading Liquid Pools. In *Institution of Chemical Engineers Symposium Series No. 148*; Institution of Chemical Engineers: Yarraville, Australia, 2001; pp. 167–179. Available online: https://www.icheme.org/media/10158/xvi-paper-13.pdf (accessed on 7 February 2023).
333. Cronin, P.S.; Evans, J.A. *A Series of Experiments to Study the Spreading of Liquid Pools with Different Bund Arrangements*; Contract Research Report 405/2002; Advantica Technologies Limited for the Health and Safety Executive: Leicestershire, UK, 2002. Available online: https://www.hse.gov.uk/research/crr_pdf/2002/crr02405.pdf (accessed on 7 February 2023).
334. Atherton, W. *An Experimental Investigation of Bund Wall Overtopping and Dynamic Pressures on the Bund Wall Following Catastrophic Failure of a Storage Vessel*; Research Report 333; Liverpool John Moores University for the Health and Safety Executive: Liverpool, UK, 2005.
335. Atherton, W. An Empirical Investigation of Catastrophic and Partial Failures of Bulk Storage Vessels and Subsequent Bund Wall Overtopping and Dynamic Pressures. Ph.D. Thesis, Liverpool John Moores University, Liverpool, UK, 2008. Available online: https://researchonline.ljmu.ac.uk/id/eprint/5866/1/446356.pdf (accessed on 7 February 2023).
336. Zhang, B.; Liu, Y.; Zhu, W.; Gopalaswami, N.; Mannan, M.S. Experimental Study of Bund Overtopping Caused by a Catastrophic Failure of Tanks. *Ind. Eng. Chem. Res.* **2017**, *56*, 12227–12235. [CrossRef]
337. Megdiche, I. Evaluation of the Mechanical Strength of Bund Walls under the Catastrophic Failure of Storage Tanks via Fluid Structure Interaction. Ph.D. Thesis, Liverpool John Moores University, Liverpool, UK, 2018. Available online: https://researchonline.ljmu.ac.uk/id/eprint/10217/7/2019MegdichePhD.pdf (accessed on 7 February 2023).
338. Zhao, S.; Huo, J.; Xu, R.; Liu, Y.; Jing, M.; Zhang, B. Prevention of Bund Overtopping after a Catastrophic Tank Failure Accident: Effects of Bund Design, Liquids and Scale-Up. *Process Saf. Environ. Prot.* **2022**, *166*, 41–56. [CrossRef]
339. Ritter, A. Die Fortpflanzung der Wasserwellen [Propagation of Water Waves]. *Z. Ver. Dtsch. Ing.* **1892**, *36*, 947–954. (In German)
340. Stoker, J.J. *Water Waves: The Mathematical Theory with Applications*; Wiley: New York, NY, USA, 1957.
341. Mignot, E.; Dewals, B. Hydraulic Modelling of Inland Urban Flooding: Recent Advances. *J. Hydrol.* **2022**, *609*, 127763. [CrossRef]
342. Mignot, E.; Li, X.; Dewals, B. Experimental Modelling of Urban Flooding: A Review. *J. Hydrol.* **2019**, *568*, 334–342. [CrossRef]
343. Buchner, B. The Impact of Green Water on FPSO Design. In *OTC 95, Proceedings of the 27th Offshore Technology Conference, Houston, Texas, 1–4 May 1995*; OTC 7698; OnePetro: Richardson, TX, USA, 1995; Volume 2, pp. 45–57. [CrossRef]
344. Schønberg, T.; Rainey, R.T.C. A Hydrodynamic Model of Green Water Incidents. *Appl. Ocean Res.* **2002**, *24*, 299–307. [CrossRef]
345. Chuang, W.-L.; Chang, K.-A.; Mercier, R. Review of Experimental Modeling of Green Water in Laboratories. In *ISOPE 2019, Proceedings of the 29th International Ocean and Polar Engineering Conference, Honolulu, HI, USA, 16–21 June 2019*; Chung, J.S., Akselsen, O.M., Jin, H.W., Kawai, H., Lee, Y., Matskevitch, D., Van, S.H., Wan, D., Wang, A.M., Yamaguchi, S., Eds.; International Society of Ocean and Polar Engineers: Cupertino, CA, USA, 2019; Volume 3, pp. 2466–2472.
346. Henderson, F.M. *Open Channel Flow*; Macmillan: New York, NY, USA, 1966; pp. 491–493.
347. Heller, V. Scale Effects in Physical Hydraulic Engineering Models. *J. Hydraul. Res.* **2011**, *49*, 293–306. [CrossRef]
348. Ye, Z.; Zhao, X.; Deng, Z. Numerical Investigation of the Gate Motion Effect on a Dam Break Flow. *J. Mar. Sci. Technol.* **2016**, *21*, 579–591. [CrossRef]
349. FEMA. *Federal Guidelines for Inundation Mapping of Flood Risks Associated with Dam Incidents and Failures*; FEMA P-946; U.S. Department of Homeland Security: Washington, DC, USA, 2013. Available online: https://www.fema.gov/sites/default/files/2020-08/fema_dam-safety_inundation-mapping-flood-risks.pdf (accessed on 23 January 2023).
350. NZSOLD. *New Zealand Dam Safety Guidelines*; New Zealand Society on Large Dams (NZSOLD): Wellington, New Zealand, 2015. Available online: https://nzsold.org.nz/wp-content/uploads/2019/10/nzsold_dam_safety_guidelines-may-2015-1.pdf (accessed on 23 January 2023).
351. Vischer, D.L.; Hager, W.H. *Dam Hydraulics*; Wiley: Chichester, UK, 1998; pp. 287–288.
352. Tan, T.; Ma, Y.; Zhang, J.; Niu, X.; Chang, K.-A. Experimental Study on Flow Kinematics of Dam-Break Induced Surge Impacting onto a Vertical Wall. *Phys. Fluids* **2023**, *35*, 025127. [CrossRef]
353. De Marchi, G. Sull'Onda di Piena che Seguirebbe al Crollo della Diga di Cancano. Prove su Modello per il Tronco Fluviale dalla Diga a Ponte Cepina–Calcolo per il Tronco da Ponte Cepina a Tirano [On the Dam-Break Wave Resulting from the Collapse of the Cancano Dam. Physical Model for the River Reach from the Dam to Ponte Cepina–Numerical Model for the River Reach from Ponte Cepina to Tirano]. *L'Energia Elettr.* **1945**, *22*, 319–340. (In Italian)
354. FLOW-3D Modeling Capabilities. Hybrid Shallow Water/3D Flow. Available online: https://www.flow3d.com/modeling-capabilities/hybrid-shallow-water-3d-flow/ (accessed on 10 March 2023).
355. FLOW-3D Modeling Capabilities. Moving Objects. Available online: https://www.flow3d.com/modeling-capabilities/moving-objects/ (accessed on 10 March 2023).